AD-A082 167 AIR FORCE INST OF TECH WRIGHT-PATTERSON AFB OH SCHOO--ETC F/G 20/4
A DIAGNOSTIC STUDY OF FLOW IN THE WAKE OF A CIRCULAR DISK USING--ETC(U)
MAR 80 S L MORRIS
UNCLASSIFIED AFIT/GAE/AA/79D-12 NL

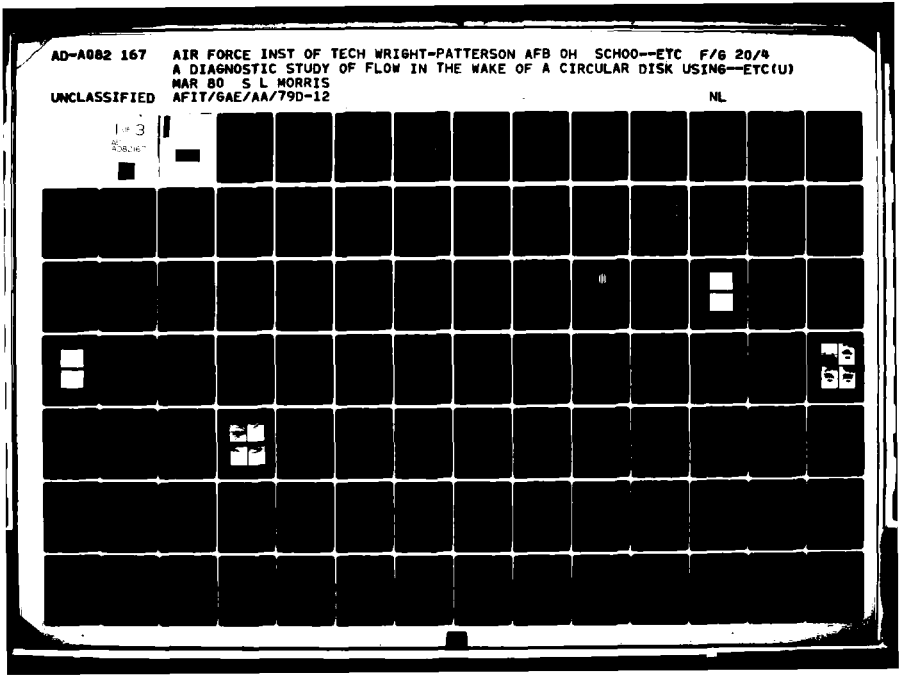

AFIT/GAE/AA/79D-12

A DIAGNOSTIC STUDY OF FLOW IN THE WAKE OF A CIRCULAR DISK USING A PHOTON CORRELATION LASER VELOCIMETER.

THESIS

AFIT/GAE/AA/79D-12 Steven L. Morris
Captain USAF

AFIT/GAE/AA/79D-12

A DIAGNOSTIC STUDY OF FLOW IN THE WAKE OF A CIRCULAR DISK USING A PHOTON CORRELATION LASER VELOCIMETER

THESIS

Presented to the Faculty of the School of Engineering
of the Air Force Institute of Technology
Air University
in Partial Fulfillment of the Requirements
for the Degree of Master of Science

by
Steven L. Morris
Captain USAF
Graduate Aeronautical Engineering
March 1980

Preface

This study was conceived to experimentally investigate flow in the wake of a circular disk. This was accomplished utilizing schlieren photography and a photon correlation laser velocimeter system. The unique capability of the laser velocimeter to determine flow direction, when used in conjunction with a phase modulator, was employed in establishing the bounds of the recirculation zone in the near wake of the disk. Mean velocity and turbulence intensity profiles were obtained at various stream-wise locations in the wake region with the laser velocimeter system. A comparison is made between the results obtained with the schlieren and those obtained with the laser velocimeter system. Similar comparisons of results are made with other experimental data and theoretical predictions whenever possible.

I would like to express my sincere appreciation to Dr. Harold E. Wright, my thesis advisor, for his continual support, encouragement, patience and invaluable suggestions during the course of this study. I would like to thank Dr. William Elrod, Dr. James Hitchcock, and Capt. (Dr.) George Catalano for their valuable assistance. Mr. William Baker and Mr. Harold "Leroy" Cannon should also be commended for their ceaseless efforts in ensuring that the test apparatus was always operational. The AFIT workshops provided me a

quick response in the fabrication and modification of the test hardware. Finally, I want to thank my wife, Jacqueline, for her faithful support during some difficult times.

Steven L. Morris

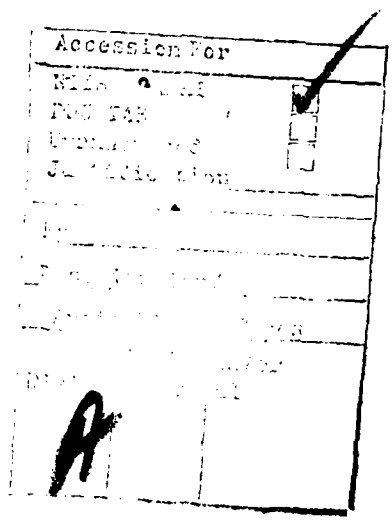

Contents

Contents

List of Figures

List of Tables

List of Symbols

Symbol	Description	Units
A	Jet cross sectional area	ft^2
A*	Nozzle cross-sectional area	ft^2
a	Constant	
d	Orifice Plate Diameter	in
d*	Combustor Inlet Diameter	in
D	Jet Diameter	in
D	Beam Separation	cm
D	Combustor Diameter	in
f_d	Doppler Frequency Shift	HZ
f_d*	Doppler Frequency Shift with Phase Modulation	HZ
Δf	Frequency shift	KHZ
h	Step Height in Combustor	in
k	Metering Orifice Flow Coefficient	
L	Combustor Length	in
L´	Recirculation Zone Length	in
L	Lens Focal Length	cm
M	Mach number	
$\dot{m}$	Mass Flow Rate	lbm/sec
P_L	Supply Line Pressure	in Hg
P_o	Calming Chamber Pressure	in Hg
ΔP	Orifice Pressure Differential	in Hg
PATM	Atmospheric Pressure	in Hg
R	Disk Radius	in

Symbol	Description	Units
R_o	Jet Radius	in
R	Dimensionless Value of Auto-correlation Function	
r_o	Radius ($1/e^2$) of Laser Beam	mm
S	Fringe Spacing	μm
T_o	Total Temperature	°R
TATM	Room Temperature	°F
U	Mean Velocity	ft/sec
U_o	Jet Exit Velocity	ft/sec
U*	Apparent Mean Velocity	ft/sec
U_p	Phase Modulator Induced Velocity	ft/sec
U_{cen}	Centerline Velocity	ft/sec
u´	Velocity Fluctuations in X-direction	ft/sec
X	Axial Coordinate from Jet Plane in Downstream Direction	in
x	Distance Downstream of Disk Along X-axis	in
Y	Coordinate Axis in Horizontal Plane Normal to X-axis	in
Y	Expansion Factor Ratio	
$Y_{½}$	Distance from Centerline of Jet where $U = ½U_{cen}$	in
Z	Coordinate Axis in Vertical Plane Normal to X-axis	in
λ	Wavelength of Laser Light	m
θ	Convergence Half Angle of the Laser Beams	degrees

Symbol	Description	Units
η	Turbulence Intensity	%
μ	Index of Refraction	

Abstract

The present investigation involves a diagnostic study of flow in the wake of a circular disk utilizing schlieren photography and a photon correlation laser velocimeter system (LDV). The schlieren system was used to examine the basic flow pattern over a 2.0 inch diameter disk and to establish the bounds of the recirculation zone. In all tests, the flow originated from a 1.5 inch diameter axially symmetric free jet with an exit Mach number of 0.35. The disk was positioned in the flow 12 jet diameters downstream of the exit. Mean velocity and turbulence intensity profiles were measured at selected locations in the near wake region of the 2.0 and a 1.5 inch diameter disk with the LDV system. This was accomplished without particle seeding of the flow. A free jet survey was conducted for comparison with theoretical predictions to analyze the quality of the LDV data.

The schlieren system produced high quality photographs from which the dimensions of the recirculation zone were obtained. Mean velocity and turbulence intensity profiles were acquired at the varied stream-wise locations behind each disk with the LDV system. The laser velocimeter system, when used in conjunction with a phase modulator, clearly identified the flow direction. Bounds of the recirculation zone found from the LDV study agreed with the results of the schlieren study.

A DIAGNOSTIC STUDY OF FLOW IN THE WAKE OF A CIRCULAR DISK USING A PHOTON CORRELATION LASER VELOCIMETER

I. Introduction

Zones of recirculating flow are quite common occurrences in aerodynamic flow over a structure. Until the advent of the laser doppler velocimeter system (LDV), classical flow measurement techniques have been deficient in determining whether flow is in the positive or negative direction. While magnitudes of velocities and turbulence intensities can be determined with a high degree of accuracy and confidence with the hot wire anemometer, it is inept in ascertaining flow direction without the aid of multi-wire systems. Therefore, recirculation zones are indistinguishable from the downstream flow unless the observer knows beforehand the exact dimensions of the reversed flow region, which is seldom the case. The photon correlation laser velocimeter system of this study provides the capability to measure velocity magnitudes and turbulence intensities as well as the ability to determine the flow direction. Ability to completely analyze flow over a body and observe the nature of reversed flow regions in a nonintrusive way is a great advancement in the field of Aeronautical Research.

Previous Studies

Two recent studies were conducted involving the use and the checkout of the photon correlation laser velocimeter system which was used in the present investigation (Refs 9 and 21). Neither study was concerned with flow direction determination since they were operating in conditions with only downstream flow. Their studies evaluated the accuracy and limitations of the LDV system. This was accomplished through a comparison of results obtained with the LDV system to data obtained from other methods such as the hot wire anemometer system, pitot-static tube measurements, and theoretical predictions when possible. The study described in Ref 9 examined locations along the axes of a free jet at different Mach numbers. Mean velocity and turbulence intensity profiles were compared to those obtained with the hot wire anemometer system and with theory. The investigation revealed a good correlation between the mean velocity profiles, while some of the turbulence intensity data was erratic. The second study involved the measurement of air velocity and turbulence intensities across the inside diameter of a duct and a comparison with hot wire anemometer and pitot-static tube data (Ref 21). A good correlation existed between all three methods of mean velocity determination. The turbulence intensities revealed a close agreement among turbulence levels between 2% and 30%.

Another study encountered involved a completely different laser doppler anemometer system which required particle "seeding" (Ref 4). This was of particular interest since it examined the wake behind a bluff body and made measurements in and outside of the recirculation zone in both hot and cold flow. While the test conditions were very different from those employed in the present investigation, the system produced good results and allowed for velocity sign determination.

Present Study

The present investigation is a continuation of a joint research effort of AFWAL/FIMM and AFIT involving the capabilities of the photon correlation laser velocimeter system. This study proposes to use the LDV system to examine jet flow over a circular disk. A jet exit Mach number of 0.35 was chosen for the testing. The objectives of this study were as follows:

1. To use schlieren photography in observing recirculation zone dimensions.

2. To demonstrate that with the use of a laser velocimeter system and phase modulator flow direction can be determined.

3. To map out mean velocity and turbulence intensity profiles at various locations in the wake of a circular disk.

4. To compare the results of the laser velocimeter system to observations made with the schlieren system.

5. To accomplish the laser velocimeter phase of the study without seeding the flow.

Scope

In this study, flow over a circular disk originating from a 1.5 inch diameter axially symmetric jet was examined. For each test, a circular disk was mounted 18 inches (12 jet diameters) from the jet plane on the centerline of the jet. A 2.0 inch diameter disk was examined with schlieren photography to assist in determining recirculation zone size. The laser velocimeter system was used to examine flow, under the same conditions, over the 2.0 inch and a 1.5 inch diameter disk. All distances were nondimensionalized by the disk radius in order to allow for comparisons between the data obtained for each disk. The recirculation zone size defined by the LDV system was compared with that observed in the schlieren photographs. The department compressed air system was used to supply the flow and no artificial seeding of the air was employed. A complete description of the test apparatus is provided in Section II.

II. Test Apparatus

From an instrumentation veiwpoint, two different apparatus set-ups were used during this investigation. Since the testing was divided into two phases, the schlieren observations and the laser velocimeter study, two sets of equipment were utilized. With the schlieren system, use of a vertical calming chamber arrangement was convenient. The set-up of a horizontal calming chamber was accomplished in order to adapt to an existing traversing mechanism for the laser velocimeter system. For the range of velocities and small temperature changes buoyancy effects were ruled out. Also due to the small height changes in the flow, gravity effects were neglected.

The model utilized throughout this investigation consisted of a circular disk with four support and mounting brackets to adapt to a standard calming chamber. The disk model is shown in Fig 1. Two such models were constructed of steel with disk diameters of 1.5 and 2.0 inches, each with a thickness of 0.5 inch. The models were fabricated and machined with a 0.125 inch diameter port entering the side of the disk and opening on the top center. At the side entrance of the port, a copper tube was adjoined and sealed with epoxy and attached along the outside of one of the support brackets (see Fig 1). This provided a means of injecting helium directly into the flow behind the circular

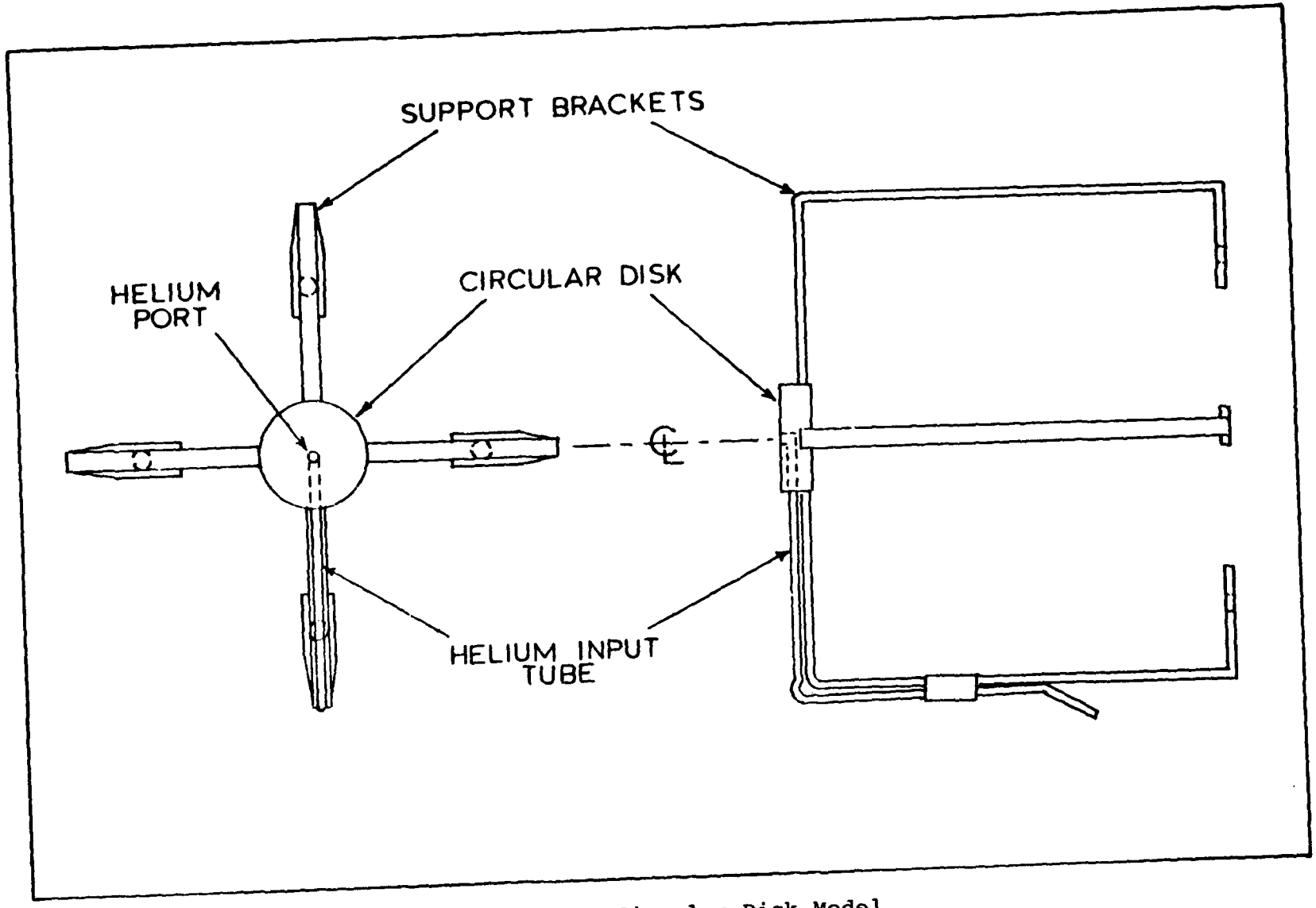

Fig 1. Circular Disk Model

disk. This was to provide the necessary density gradients in the recirculation zone for observation with the schlieren system. Each leg support was 0.125 inch thick and 0.25 inch wide. These dimensions were kept as small as possible to avoid excessive flow disturbances, while at the same time maintaining structural integrity and keeping disk vibrations to a minimum.

The axially symmetric jet attached to the calming chamber consisted of a plexiglass nozzle with a 1.5 inch diameter. For all phases of the testing, the models were located such that the disks were 18.0 inches, or 12 jet diameters, from the jet exit. The disks were positioned in each case, parallel to the jet exit plane or normal to the flow. Alignment was accomplished insuring that the center-lines of both the jet and the disk were along a common line. This was done optically utilizing the laser beam as a reference point.

The apparatus arrangement for the schlieren phase of the investigation is shown in Fig 2. The model was attached to the vertical calming chamber such that it was in the view of the schlieren system. Fine alignment was accomplished on the schlieren system by adjustment of the concave mirrors, light source, and camera unit such that the desired flow region was observed. Helium was then pumped into the disk under pressure from a nearby bottle with a control valve. An ASME standard square edged orifice plate with flange taps

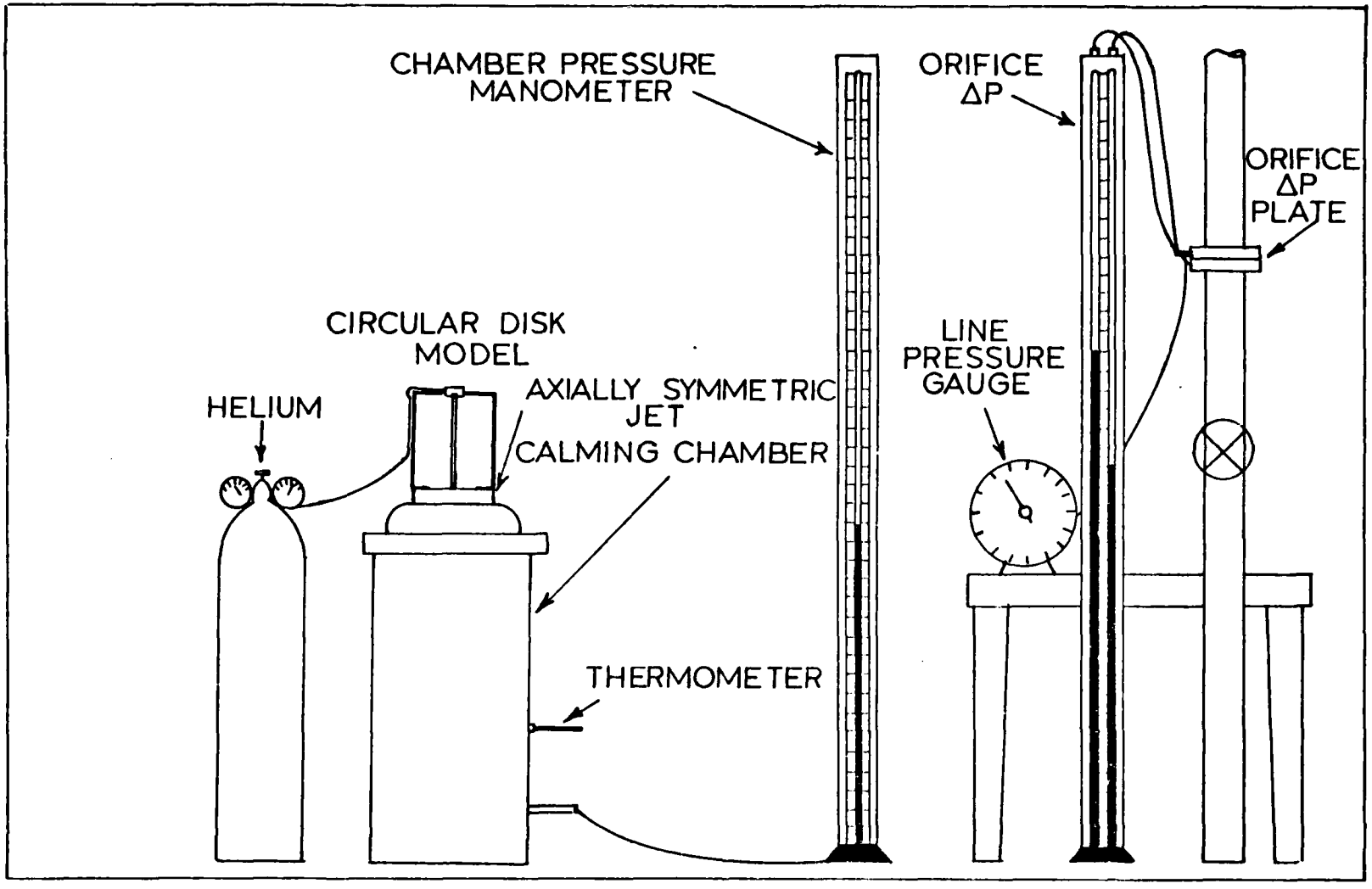

Fig 2. Apparatus Set-up for Schlieren Testing

was installed in the air supply for use in calculating mass flow rate. A pressure gauge was used to observe line pressure prior to the orifice and a 50 inch mercury U-tube manometer measured the pressure differential across the orifice plate. Calming chamber pressure was monitored with a mercury manometer and temperature was determined with a mercury themometer mounted in the chamber. A thermometer and barometer present in the room provided atmospheric temperature and pressure.

The laser velocimeter system set-up for the second phase of the testing is shown in Fig 3. The horizontal calming chamber arrangement was used to accommodate the laser velocimeter system with only a minimum amount of modifications required to an existing stand. Once the LDV system was mounted and focused on the optical bench and traversing mechanism, it could be indexed along a line at a desired distance behind the disk, while maintaining a constant alignment of the optical train. This eliminated the necessity of realigning the optical system for each data point taken. However, in order to examine the flow at different distances behind the disk, the entire traversing mechanism had to be moved in the stream-wise direction. Massflow rate and other flow condition measurements were obtained in the same manner as in the first phase of the testing.

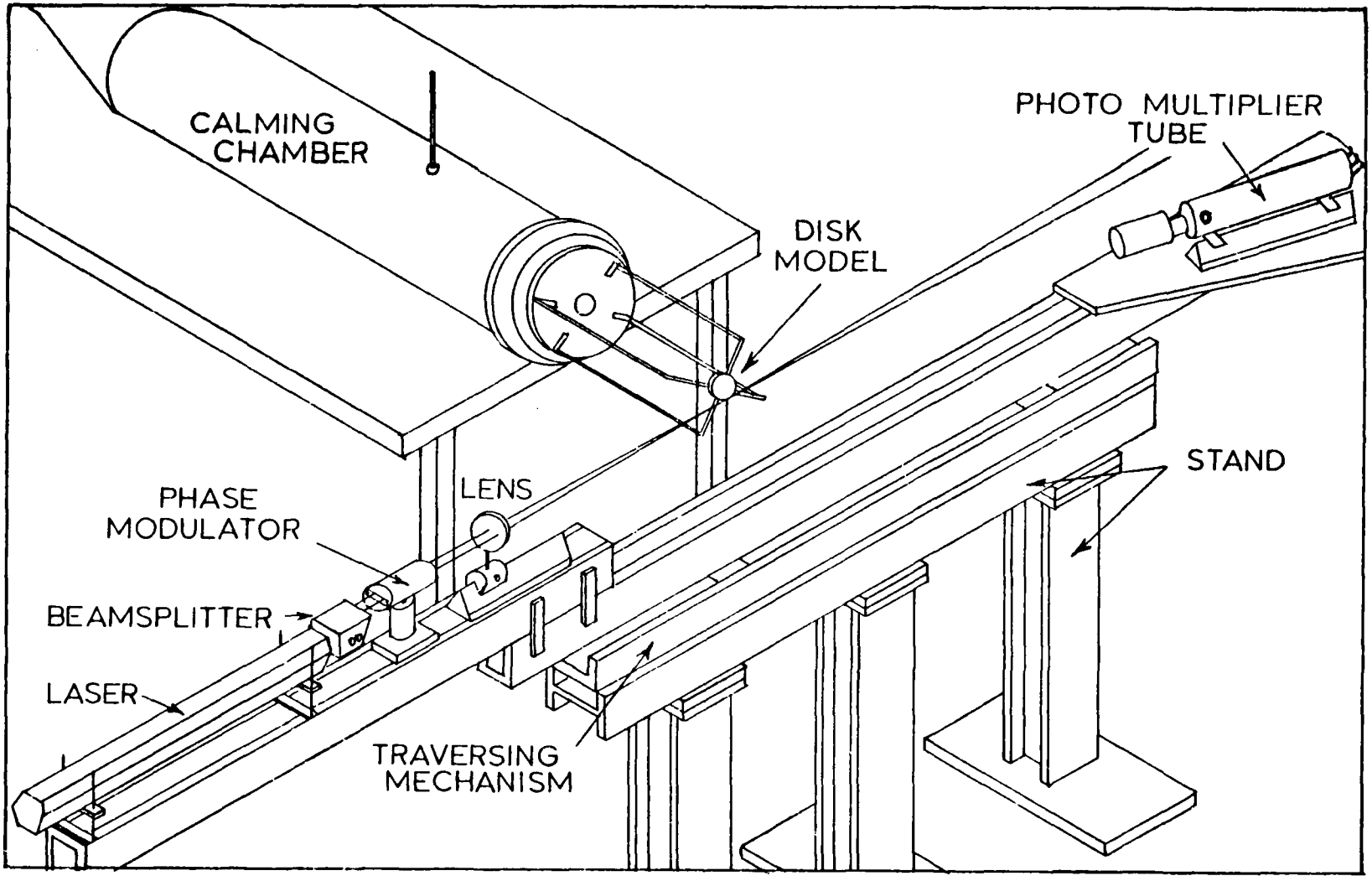

Fig 3. Laser Velocimeter System Set-up

III. Instrumentation

During the course of this investigation, two major sets of instrumentation were used, namely the schlieren system and the photon correlation laser velocimeter system. A description of each of the two systems and their components are provided.

Schlieren System

Figure 4 is a schematic of the schlieren system utilized in this study. It consists of two large concave mirrors, either a continuous light source or a spark lamp, a knife edge, and a camera assembly with a variable speed shutter.

Mirrors. Two 16-inch diameter concave mirrors, with focal lengths of 75 inches, were used in this system and positioned as shown in Fig 4. They were mounted on optical stands with a vertical adjustment for proper positioning. A small mirror was inserted into the optical path to allow the use of the continuous light source.

Light sources. Two types of light sources were used. A continuous light source was required in aligning the system. This consisted of a high intensity lamp which was reflected off a small mirror onto the large concave mirrors. This could also be used to observe an averaged flow pattern at real time with the use of a viewing screen on the camera assembly.

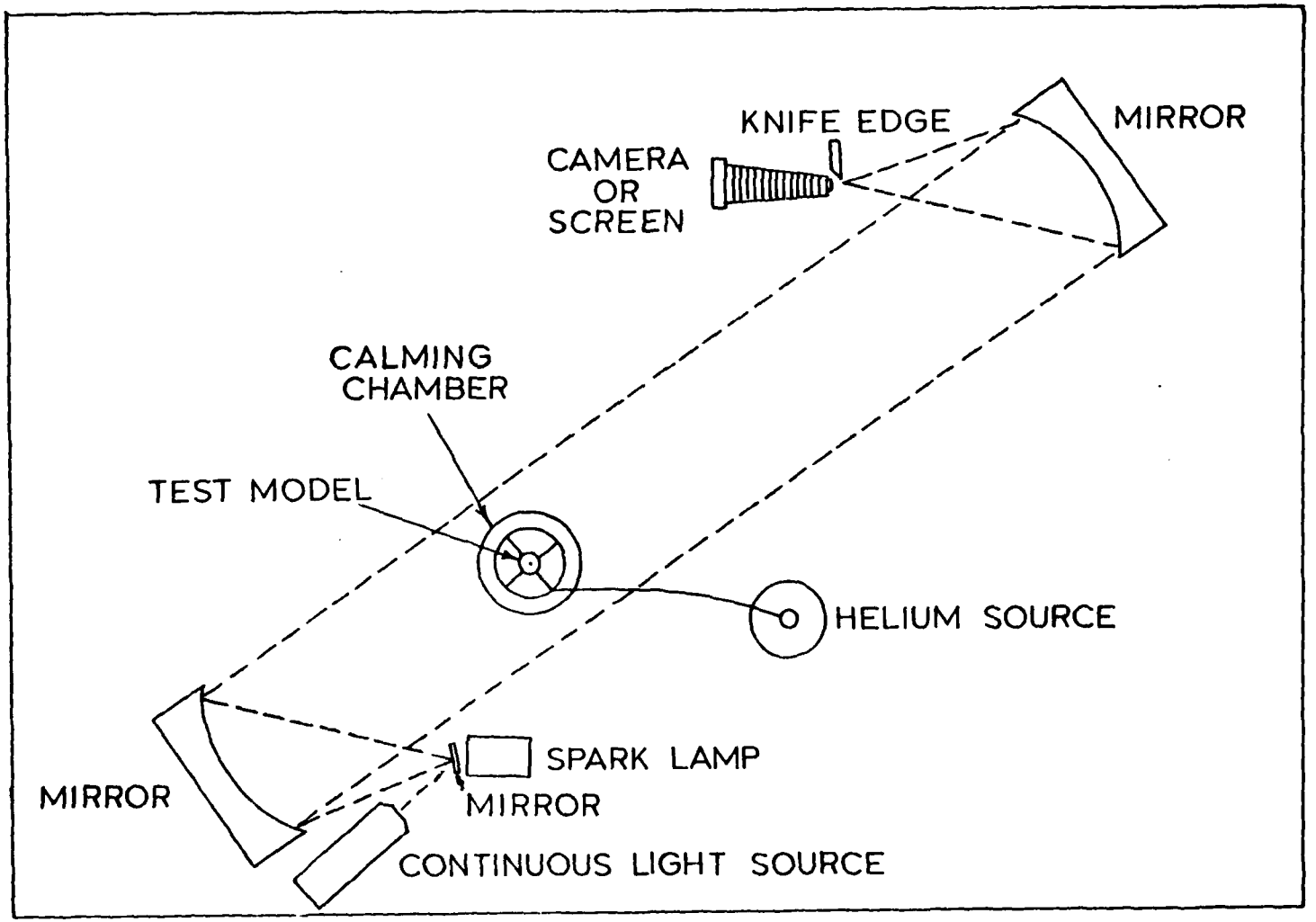

Fig 4. Schlieren System Arrangement

The second light source employed was a high intensity spark lamp with a flash duration of approximately a microsecond. Switching from the continuous light source to the spark lamp required only the removal of the small mirror from the optical path. The spark lamp provided the capability of "freezing" the flow due to the short flash duration. The spark lamp is therefore invaluable in high speed photography.

Knife edge. The knife edge utilized in this system allowed for both vertical and horizontal positioning as well as the ability to be rotated to any angle. The knife edge was mounted on a stand in front of the camera assembly with the capability for fine adjustments.

Camera assembly. The camera assembly consisted of a camera bellows with a variable speed shutter and a polaroid camera back assembly. The polaroid camera could be replaced by a frosted glass screen for viewing purposes. The entire camera assembly was positioned such that it was on the focal plane of the mirrors. The camera shutter was used in conjunction with the continuous light source providing the capability to stop and photograph the flow up to approximately 1/200 second.

Laser Velocimeter System

The laser velocimeter system consisted of a 15mW helium-neon laser, a beamsplitter, a phase modulator, a 762mm focal length lens, a 200mm telephoto lens, a

photomultiplier tube, a digital correlator and storage unit and a frequency counter. Figures 3 and 5 show the optical set-up and Fig 6 illustrates the processing equipment.

Laser. A 15mW Spectra Physics helium-neon laser, Model 124A, and a Model 255DC exciter was employed as the laser in this system. This laser emits a 1.1mm diameter beam.

Beamsplitter. The Malvern RF307 transmitter beamsplitter and polarization unit split the 1.1mm diameter beam leaving the laser into two 1.1mm beams of nearly equal intensity. The beamsplitter was equipped to be attached directly into the output end of the laser. Control knobs allowed the exit beam separation and the beam crossover, or focus point, to be varied. The front knob controlled the crossover point and the rear knob allowed the outgoing beam separation to be changed. The focus point could be varied from 15cm ahead of the beamsplitter to many meters to achieve the desired fringe spacing which will be discussed later in Appendix B. The beams could be spaced up to about 20mm apart.

Phase modulator unit. A Malvern K9023 phase modulator and drive unit was required in all of the present testing in order to establish flow direction. It also extends the capability of the laser velocimeter system in obtaining velocity and turbulence intensity data in high speed or highly turbulent flow. With it in the system, data points

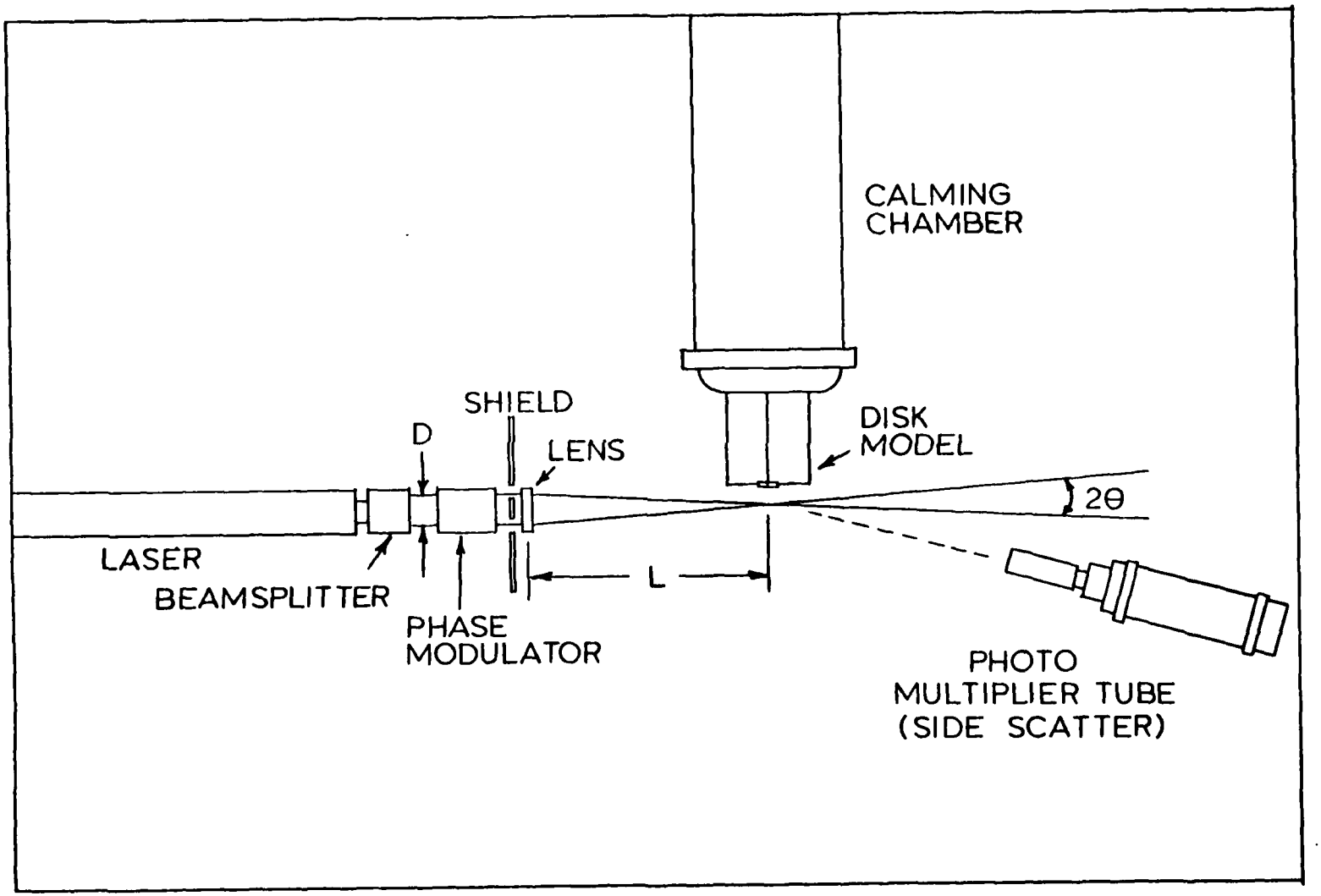

Fig 5. Laser Velocimeter System Optical Set-up

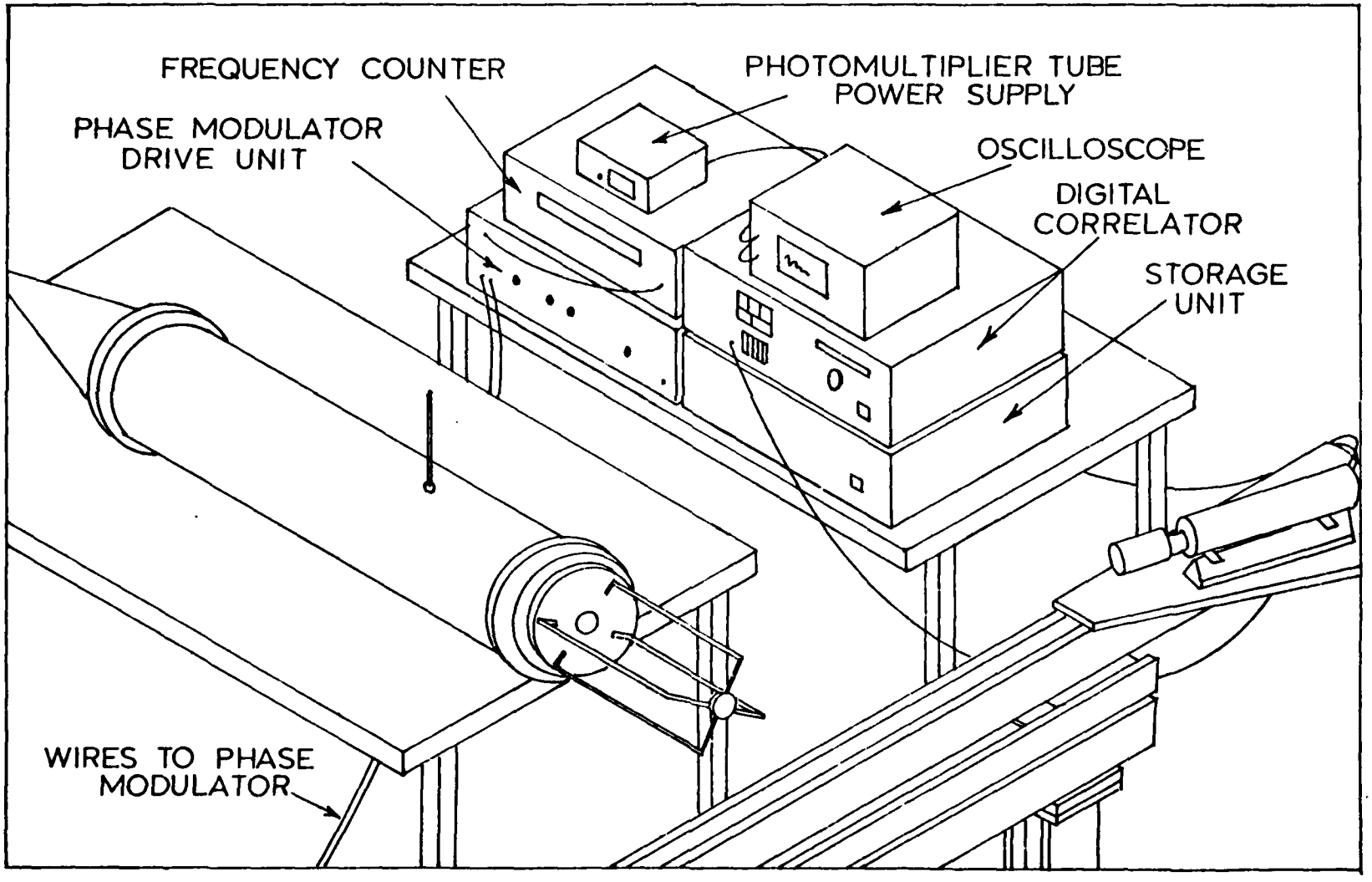

Fig 6. Laser Velocimeter Instrumentation Set-up

which are normally unobtainable may be acquired. The operation of the phase modulator will be discussed in Section IV. The phase modulator requires that the two laser beams be parallel and approximately 20mm apart (a slightly smaller spacing is tolerable). The two beams must enter one end of the phase modulator, pass through the two crystals, and exit the output end as two sharp distinct beams. Figure 7 shows the proper relationship between the beamsplitter and phase modulator and how it should look when properly aligned. Adjustment knobs on the phase modulator mounting stand permit fine alignment of the device.

Since the laser beams must be parallel as they pass through the phase modulator, a lens must be used to focus them at the desired crossover point, forming the test rhombus. The crossover point is the focal length of the lens, so the flow conditions influence the proper lens selection. For the present study, a 762mm focal length lens was used. A Hewlett-Packard 5325B Universal Counter was employed to determine the precise frequency shift inputted by the drive unit to the phase modulator.

Photomultiplier tube. A Malvern EMI 9863 Model KE/100 photomultiplier tube was used in this system. A 200mm Soligor telephoto lens with two spacers (giving a total spacing of 9.0cm) was installed on the front of the photomultiplier tube to collect the light scattered due to the flow at the test rhombus and focus it onto the pinhole

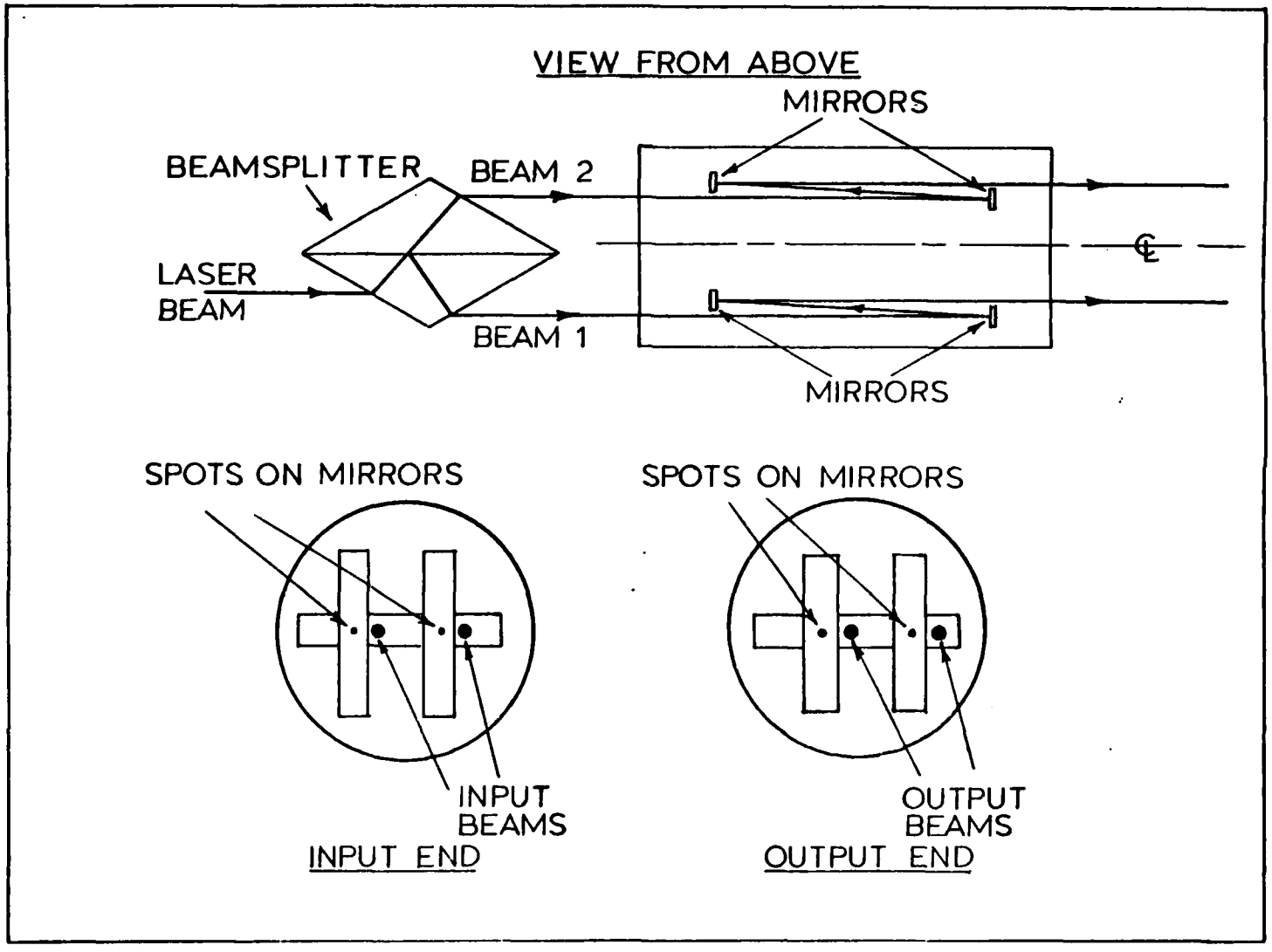

Fig 7. Proper Alignment of Beamsplitter and Phase Modulator

aperture system. A 400μm pinhole was used resulting in a flow control volume diameter of 0.72mm being observed (Ref 18). 1850 volts were supplied to the photomultiplier tube by an EMI power supply when in the operating mode. A standby mode on the power supply allowed the photomultiplier tube to not be in operation while room lights were on, avoiding any damage to it.

Digital correlation. Data processing was accomplished by the Malvern digital correlator type K7023. This unit receives data from the photomultiplier tube, stores and processes it, and develops the autocorrelation function which is displayed on the oscilloscope. As long as the system is in operation, the autocorrelation function is continually being updated. When placed in the stop mode, the autocorrelation function is frozen at some time "t" permitting the maximum and minimum values of function to be obtained. These values are used in calculating the velocity and turbulence intensity. When the system is reset, the data gathering and processing is started anew.

Oscilloscope. A Tektronics oscilloscope was used to display the autocorrelation function developed by the digital correlation. This in turn was used in the interrogation of the channels of the digital correlator.

IV. Principle of Operation

The schlieren set-up used in this study, shown in Fig 4, is a standard system with its principle of operation described in Refs 17, 22, and 23. A detailed presentation of the laser velocimeter system is provided in Refs 9, 18, and 21. The purpose of this section is to provide an in-depth examination of the phase modulator.

Phase Modulator

In the determination of flow direction, the phase modulator is an essential component in the optical train of the laser velocimeter system. Without the phase modulator in the system, the two laser beams are focused such that they intersect at a point in the flow field forming a pattern of light and dark fringes (Fig 8). As the particles in the flow pass through this fringe pattern, a doppler frequency shift, f_D , results from the photons scattered in the control volume. This fringe pattern is stationary, with the mean flow velocity, U , related to the doppler frequency shift by

$$f_D = \frac{U}{S} \qquad (1)$$

where S = the fringe spacing, μm . The fringe spacing is calculated according to Eq (11) of Appendix B. Since the fringe spacing is constant for a given geometry, the

doppler frequency shift is linearly related to the velocity.

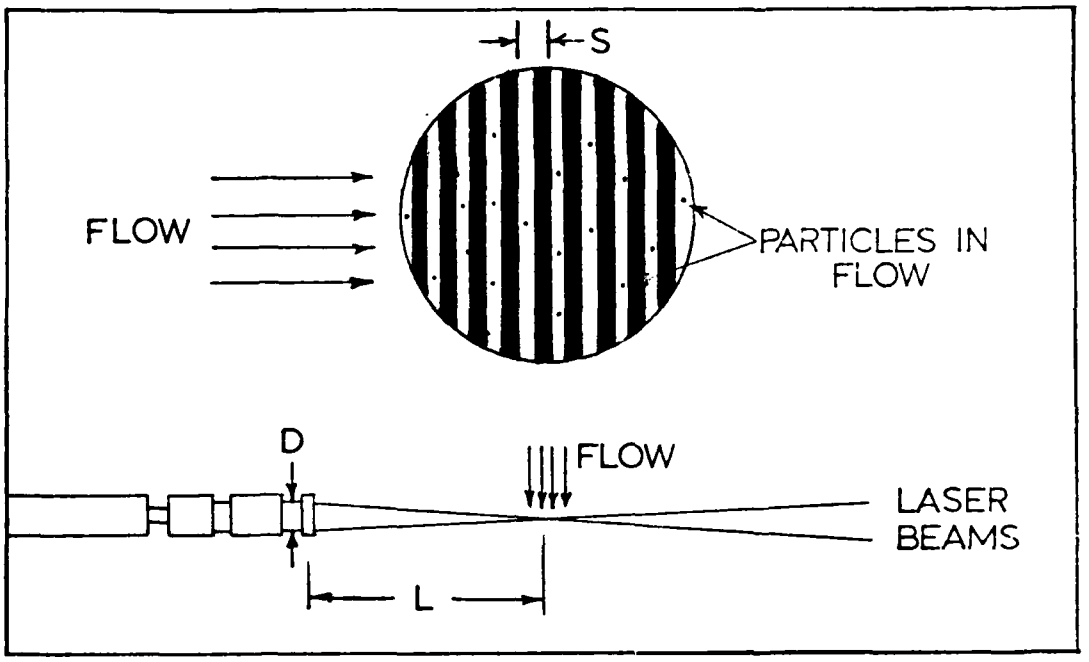

Fig 8. Laser Beam Focal Point and Fringe Spacing

The phase modulator provides a method of artificially shifting this frequency for use in directional determination. The two nearly equal intensity laser beams emitted from the beamsplitter enter into the phase modulator as seen in Fig 7. Each beam passes through an electro-optical crystal and out the opposite end. A lens is used to focus the resulting two parallel beams onto a point in the flow. When the phase modulator is in the "off" position, the same previously mentioned stationary fringe pattern is created. When the phase modulator is "on", a certain saw tooth voltage is applied to the crystals causing the phase of one beam to be

retarded and the phase of the other beam to be advanced. This causes the fringe pattern created at the intersection point to move linearly in space at a rate depending on the size of the applied voltage. The positioning of the mode switch on the drive unit determines which beam will be retarded and which will be advanced, and hence the direction of the fringe line movements. In the drive mode, they will translate in one direction, in the center position they will remain stationary, and in the inverted mode they will move in the opposite direction. The rate of movement is determined by the magnitude of the frequency imparted by the drive unit. The unit in this study provided a frequency shift varying from 0 to about 1 megahertz. In the absence of any flow, the modulator will result in an autocorrelation function as seen in Fig 9. Therefore, an artificial velocity, U_p , has been created such that

$$U_p = (\Delta f)(S) \qquad (2)$$

where Δf is the frequency shift of the phase modulator.

In flow conditions, the U_p created by the phase modulator will be either added or subtracted to the true mean velocity of the flow to achieve the apparent velocity displayed on the oscilloscope. If the fringe pattern is moving against the flow, the particles will pass through quicker resulting in an increase in the apparent velocity and therefore the frequency of the autocorrelation function

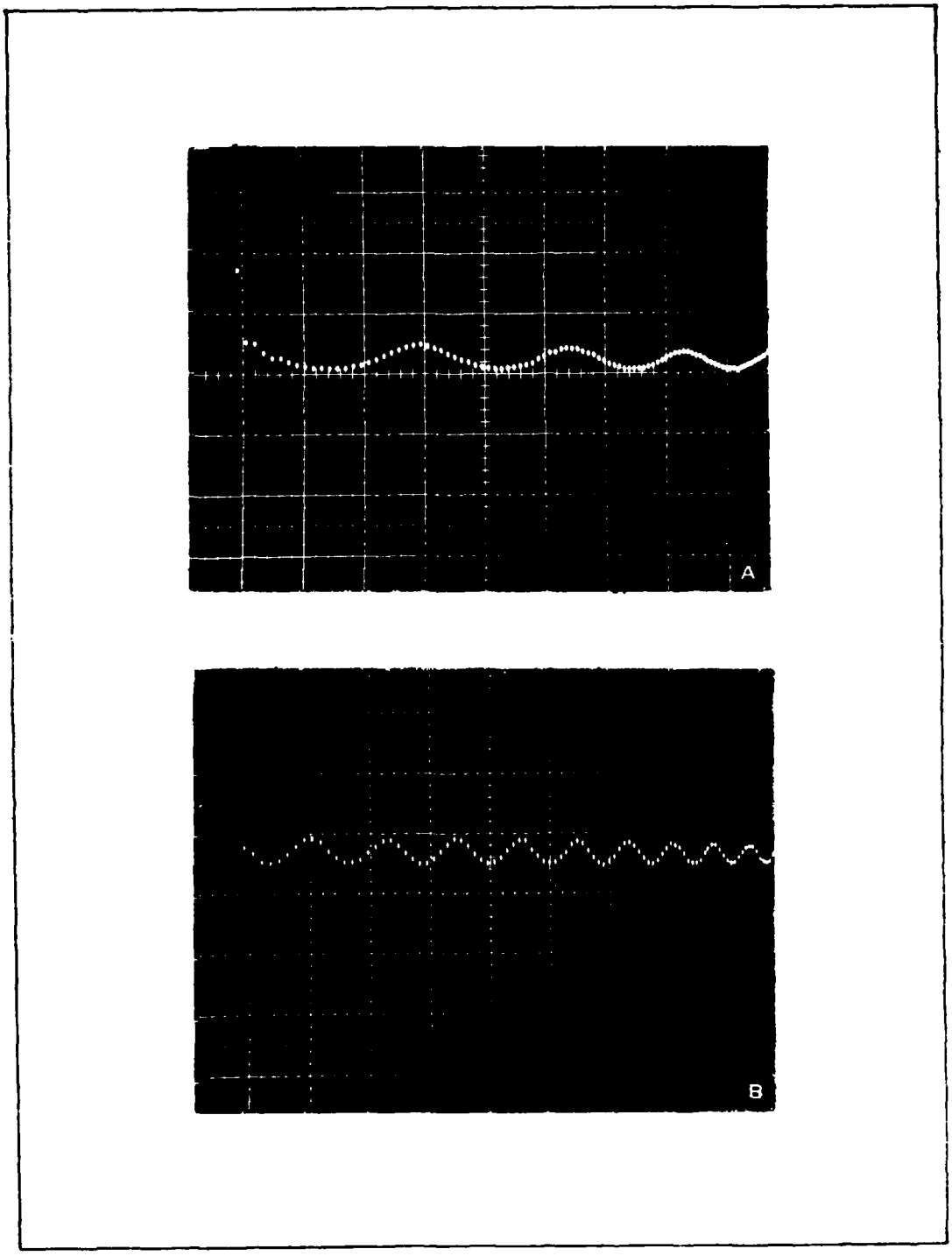

Fig 9. Autocorrelation Functions Due to Phase Modulator Only at 200×10^{-9} Second Sample Time at a) 204.0 KHZ b) 512.0 KHZ

will be increased. Conversely, if the fringes move with the flow, the apparent velocity will be less as will be the frequency of the autocorrelation function. This is shown in Figure 10. Of course in actuality the true velocity of the air will be the same.

Using the above concepts, flow direction can be determined as follows. First, look at a flow condition in which the direction is known to see how the frequency shifts affect the autocorrelation function. For example, if the frequency of the autocorrelation function and therefore the apparent velocity increases when the switch is moved from the off to the inverted position (or decreased when moved from the off to drive mode), the fringes must be moving against the flow. The direction of the flow will be the same anywhere in the flow field where a similar relation between the mode switching and autocorrelation function frequency exists. However, if a point in the field is encountered where the frequency is decreased when switching from the off to the inverted mode (or increased when switching from off to the drive mode), the flow must now be in the same direction as the fringe movement indicating that the flow has reversed direction. Therefore, flow direction can be determined strictly from observing trends on the oscilloscope. Figure 11 shows two autocorrelation functions, with and without phase modulation, at the same point in the flow field at high turbulence intensities.

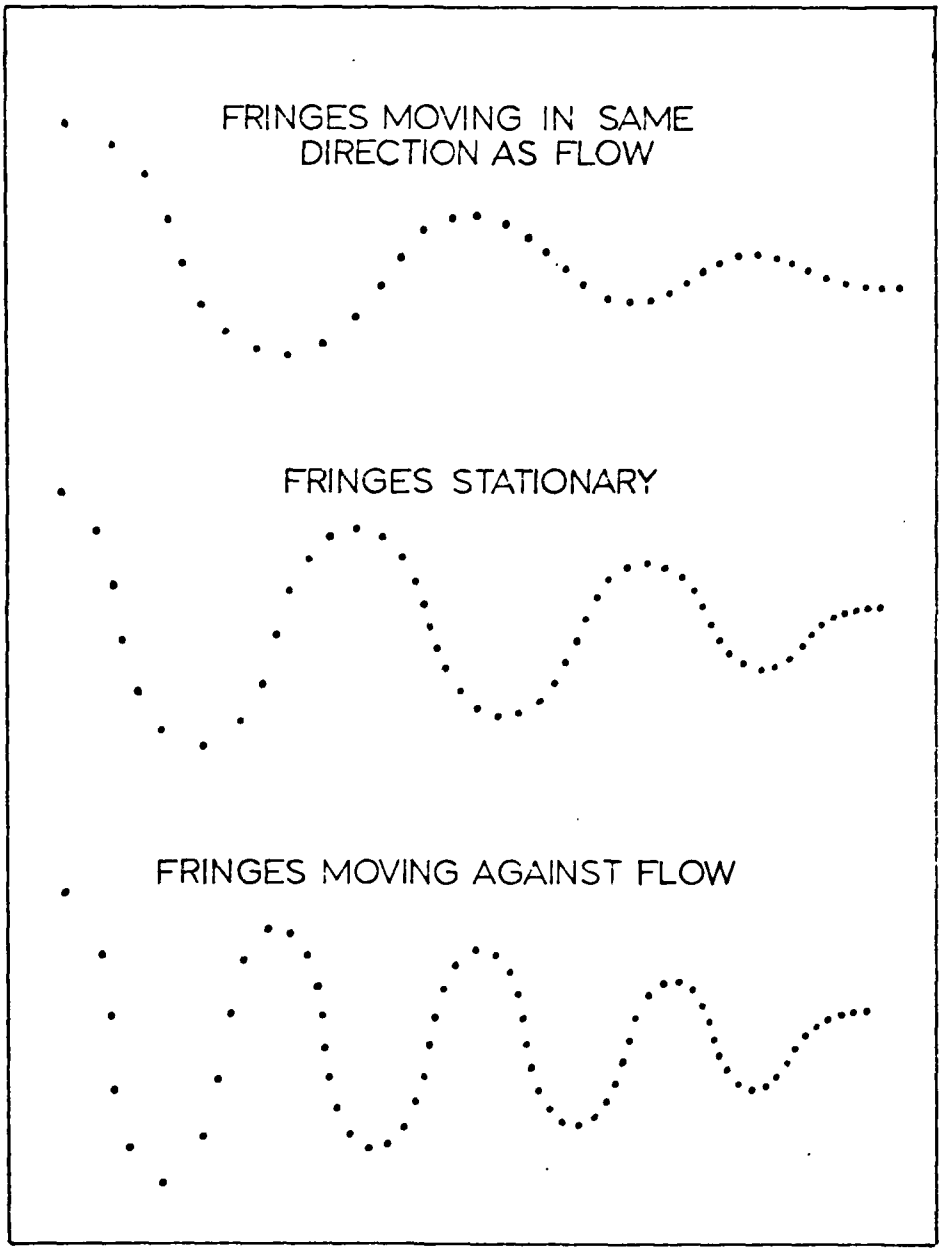

Fig 10. Autocorrelation Function Changes Due to Phase Modulation

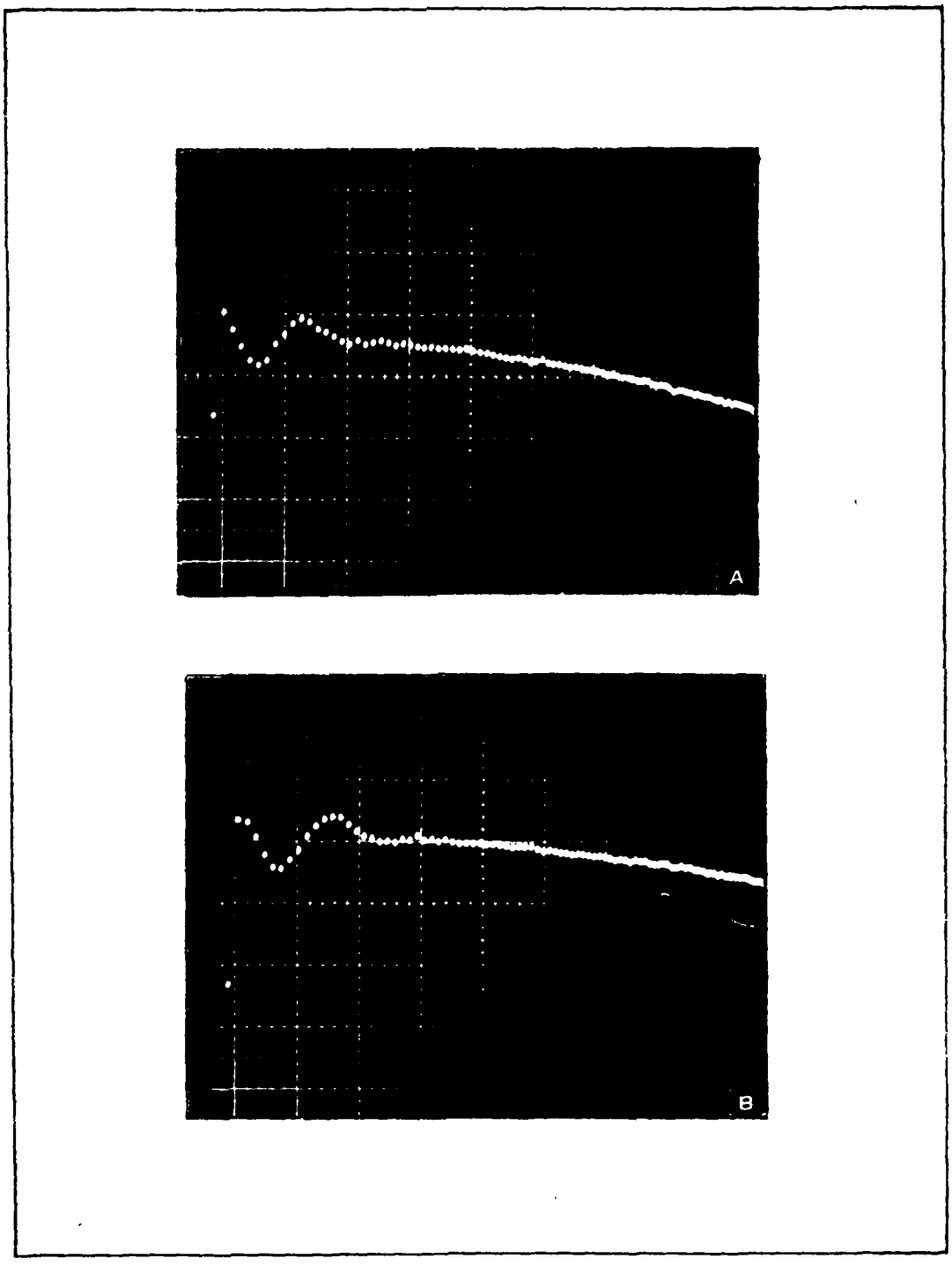

Fig 11. Oscilloscope Display at Same Flow Point a) With and b) Without Phase Modulation

The phase modulator is also very important since it extends the capability of the laser velocimeter in very high or very low speed flow, as well as in high turbulence intensities. In low speed flow, the fringe movement can be set such that it is in the opposite direction of the flow allowing particles to pass quicker and scatter more light increasing the resolution of the photomultiplier tube. The opposite is true in high speed flows where the fringe movement can be set in the same direction as the flow "slowing" the apparent velocity down and giving better resolution. Turbulence levels can also "appear" to be reduced permitting easier determination of the required maximum and minimum points used in computing turbulence intensities. The appropriate data reduction equations are presented in Appendix B.

A limit does exist on the capabilities of the phase modulator in investigating certain flow regimes. This is dependent upon the flow field being examined and the maximum frequency shift that can be obtained with the phase modulator. In very high speed flow, with a corresponding high doppler frequency shift, a large frequency shift is required of the phase modulator in order to achieve an observable change in the autocorrelation function's frequency. If the phase modulator is not capable of producing a large enough frequency shift, then the flow direction cannot be established. A similar limit to the capabilities of the phase modulator exists in high turbulence levels.

In such cases, there is an overlapping between the doppler frequency spectrum of the flow and a zero frequency spectrum created by the large velocity fluctuations. When this occurs, the resulting probability density function cannot be deciphered and flow information is unobtainable. By shifting the frequency with the phase modulator, these spectrums can be separated resulting in a decipherable function. The amount of shifting required depends upon the turbulence levels. As the turbulence intensities increase, the frequency spectrums become broader causing the overlap to increase. Therefore, the phase modulator must be capable of providing a sufficient frequency shift for the given condition or the separation cannot be achieved. In such cases, a phase modulator with a large maximum frequency shift is a necessity in producing satisfactory results.

V. Experimental Procedure

The experimental procedure employed in this study was divided into two phases. The first utilized a schlieren system to visualize flow patterns over a 2.0 inch diameter disk in an effort to determine recirculation zone dimensions. The second phase mapped out the velocity and turbulence intensity profiles at various locations behind the 2.0 and later a 1.5 inch diameter disk. Both phases used a disk and free jet arrangement as shown in Fig 12. This method of testing was chosen over wind tunnel testing to preclude the use of windows. Windows can cause a problem with the optics of the laser velocimeter system possibly producing erroneous results. Since one of the objectives of this study was to determine the capability of the laser velocimeter system in determining flow direction without seeding, any unnecessary source of error was avoided.

Test Conditions

The combination of jet diameter, disk diameter, and disk location was initially determined with the schlieren. The three parameters were varied, in addition to massflow rate, until the circular disk was completely immersed in the jet flow. The schlieren provided a means for making this observation. If the disk was too large or too close to the jet or the diameter of the jet was too small, the disk acted like an infinite flat plate rather than a bluff

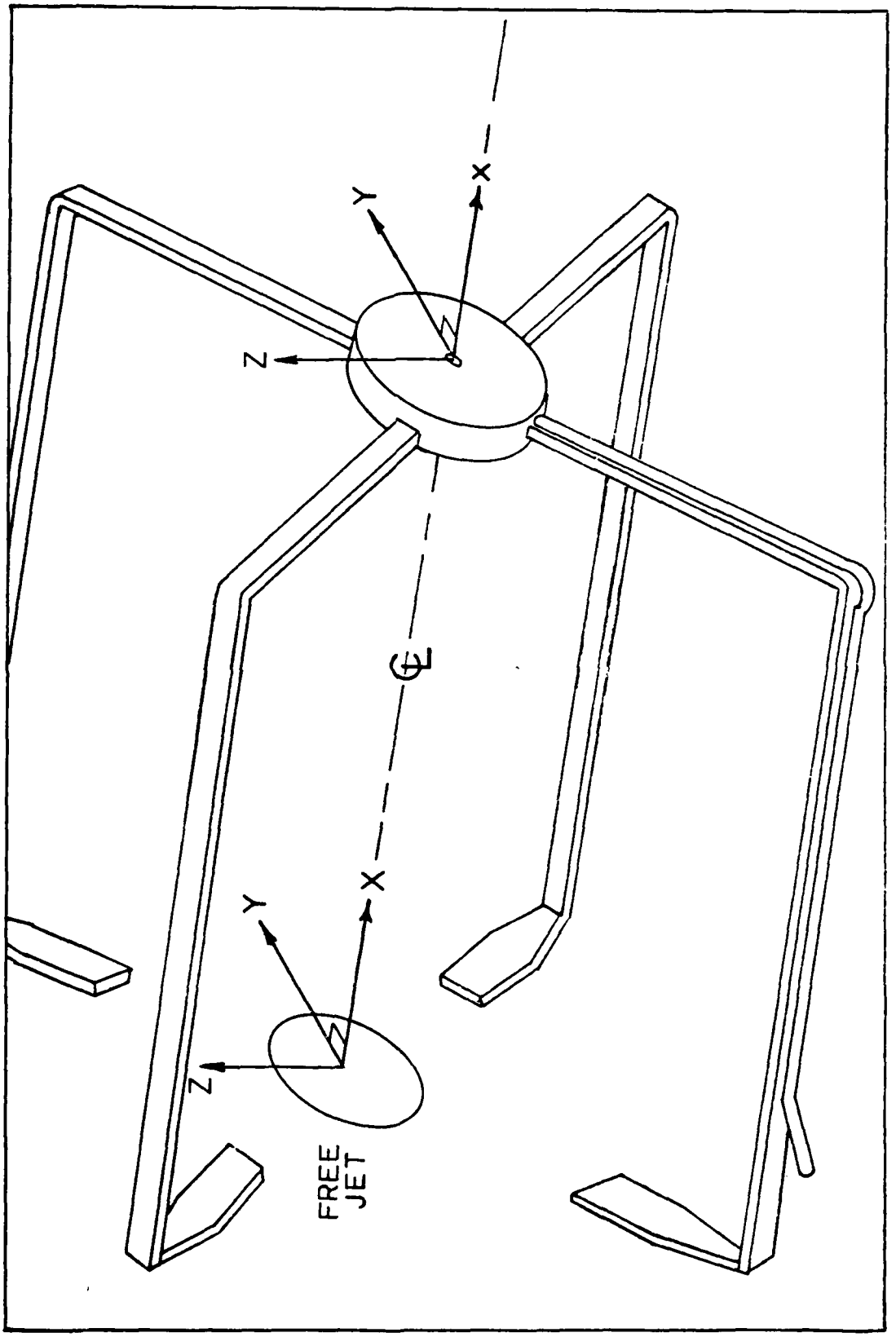

Fig 12. Free Jet and Disk Reference Frame

body engulfed in the flow. The desired flow condition, insuring flow immersement, was achieved with a 2.0 inch diameter disk, a 1.5 inch diameter jet and a downstream disk location of 18.0 inches (12 jet diameters). A jet exit Mach number of 0.35 was used for all testing.

The massflow rate and ultimately the Mach number was determined with an ASME standard square edged orifice plate with flange taps. The massflow rate equation used is given below:

$$\dot{m} = .5250 k Y d^2 \sqrt{\frac{.6515\ P_L}{T_o}\ \Delta P} \qquad (3)$$

where $\dot{m}$ = the mass flow rate, $\frac{lbm}{sec}$

d = orifice plate diameter = 1.5 inches for schlieren and 1.0 inches for LDV system arrangement

k = metering orifice flow coefficient

P_L = supply line pressure, inches Hg

ΔP = orifice differential pressure, inches Hg

Y = expansion factor ratio.

Reference 14 provides the methods used in determining proper values of k and Y. The Mach number could then be computed with the equation

$$\frac{\dot{m}}{A} = .162 \frac{P_o}{\sqrt{T_o}} \frac{M}{(1+.2M^2)^3} \qquad \text{(for air)} \qquad (4)$$

where P_o = calming chamber pressure, $\frac{lbf}{ft^2}$

T_o = calming chamber total pressure, R

A = cross sectional area of jet exit, ft^2

M = Mach number at jet exit.

A constant massflow rate and calming chamber pressure was maintained for each test, by adjusting the compressed air by-pass valve. The pressure gauges were monitored to avoid fluctuations in the flow rate.

Schlieren Testing

The apparatus and schlieren arrangement were previously illustrated in Figs 2 and 4. For each test a constant flow rate was established by the above means Helium was then injected into the flow through the port in the disk center. With the use of the frosted viewing screen, in place of the Land camera back, and the continuous light source, the resulting flow was observed. This observation represented an averaged flow pattern since variations in the flow occurring over very short durations cannot be seen in real time with the human eye. Once the proper knife edge setting was made, photographs were taken with a shutter speed of approximately 1/200 second. Photographs were also taken of the flow pattern utilizing the spark lamp with a flash duration on the order of a microsecond. Throughout the testing, the helium input pressure was varied until the best

photographs were obtained. A pressure reading of 30 lbf/in^2 on the helium gauge provided the best flow visualization.

Laser Velocimeter Tests

A much more detailed diagnostic study of the nature of the flow was undertaken with the laser velocimeter system.

Equipment set-up. The buildup and alignment of the laser velocimeter system was accomplished according to the directions in Ref 18 and Appendix A of Ref 21. Figures 3 and 6 show the location of the optical bench and traversing mechanism relative to the flow, the arrangement of the optical train, and the set-up of the data processing instrumentation.

Proper alignment of the system was one of the most critical requirements in obtaining high quality data. Continual checking of the following items helped to insure that the proper alignment was always maintained:

1. Two sharp distinct parallel laser beams of near equal intensity should exit from the output end of the phase modulator.

2. The beam intersection point should occur at the desired point in the flow. This was obtained by placing a piece of white paper at the focal point of the beams such that one sharp dot was observed. Then the traversing mechanism was used to position the focal volume at the desired point.

3. The focal volume should be focused on the pinhole-aperture in the photomultiplier tube. This was accomplished by positioning the photomultiplier tube such that the image of the focal point on the paper was visible in the polaroid window. The telephoto lens was then focused on this point. Final adjustments were made by rotating the reflex mirror such that the image could be viewed with the x10 magnification eyepiece and centered on the pinhole. Careful adherence to the above usually resulted in a good autocorrelation function.

One further test which was accomplished periodically to insure proper alignment, involved the phase modulator. In a no flow condition, a certain frequency shift, Δf , was imparted to the phase modulator which corresponded to a velocity

$$U_p = (\Delta f)(S) \qquad (2)$$

where S is the fringe spacing. The phase modulator resulted in an autocorrelation function being displayed on the oscilloscope. From this display a velocity could be obtained just as it is in flow conditions. A good alignment of the system resulted in a sharp high quality autocorrelation function with the observed velocity from the display being very close to the expected U_p . When a problem existed in the alignment, the autocorrelation function was of much lower quality with the observed velocity differing

somewhat from the calculated U_p . Data points should not be considered as unobtainable due to high turbulence intensities until the alignment of the system has been checked.

Reference frame. Figure 12 illustrates the coordinate system used in this study. X is the distance from the jet exit plane in the downstream direction. Y is the distance from the common centerline of the jet and disk in the radial direction, parallel to the traverse of the laser beams. x is the distance behind the circular disk in the downstream direction. The mean velocity values, U , acquired in this investigation are the velocity components in the x direction. Turbulence intensity data presented is defined as

$$\eta = \sqrt{\left(\frac{u'}{U}\right)^2} \qquad (5)$$

where u' = velocity fluctuation in the x direction

η = turbulence intensity.

The diameter of the jet will be referred to as D and the disk radius as R .

From Fig 12 it is seen that the laser beam propagates in the Y direction, intersecting the X-axis at $z = 0$. The disk model was also oriented such that the laser beam focal volume would not be "looking" at flow in the wake of the support brackets.

Data acquisition. The first test conducted was a survey of the free jet 18 inches from the exit (X/D = 12.0). Two data points were taken at each position (one with and one without the phase modulator) to establish a relationship between the mode settings on the phase modulator drive unit and the changes in the frequency of the autocorrelation function in a known flow direction. The traverses were made at 0.25 inch intervals across the width of the flow.

The remainder of the testing examined flow at various distances downstream from the circular disk. Disks of 2.0 and 1.5 inch diameters were used in the investigation. Table I summarizes the test runs which were conducted with the laser velocimeter system.

TABLE I

Laser Velocimeter Test Runs

2.0 Inch Diameter Disk		1.5 Inch Diameter Disk	
x (Inches)	$\frac{x}{R}$	x (Inches)	$\frac{x}{R}$
0.375	0.375		
0.75	0.75	0.5625	0.75
1.5	1.5	1.125	1.5
2.25	2.25	1.6875	2.25
3.0	3.0	2.25	3.0
3.75	3.75	2.3125	3.75
5.5	5.5	4.125	5.5

All tests were conducted with a disk location 12.0 jet diameters from the jet plane with an exit Mach number of 0.35. Traverses were made from one side of the flow field to the other with data points taken at every 0.25 inch interval. This usually resulted in only a 6.0 to 6.5 inch span due to an inability to obtain data further out in the -Y or Y direction as a result of the high turbulence intensities. Just as in the jet survey, two data points were recorded at each flow position in order to establish flow direction. The results obtained in this study are presented in the following section.

VI. Results and Discussion of Results

Schlieren Results

The primary objective of the schlieren phase of the study was to obtain quality photographs of jet flow over a circular disk in order to determine the bounds of the recirculation zone. Observations were made with both a continuous light source and shutter combination and a spark lamp. All testing was performed with a circular disk placed 18 inches (12 jet diameters) downstream of a 1.5 inch diameter axially symmetric jet. The Mach number of the jet exit was 0.35. In all photographs presented in this section, flow is moving from bottom to top.

Figure 13 is photographs taken at the above conditions, corresponding to a jet exit velocity of 396 feet per second, with a continuous light source and a shutter speed of 1/200 second. The 2.0 inch disk serves as a reference point for recirculation zone measurements.

Figure 13a illustrates the flow over the disk without the injection of helium. In the photograph, a faint heart-shaped light area is visible on the downstream side of the disk. The light lines originate at the edges of the disk and extend outward and downstream until they reach a point where they appear to loop around and join at the centerline. At this junction, the light areas tend to form an arrow pointing toward the center of the disk. It is

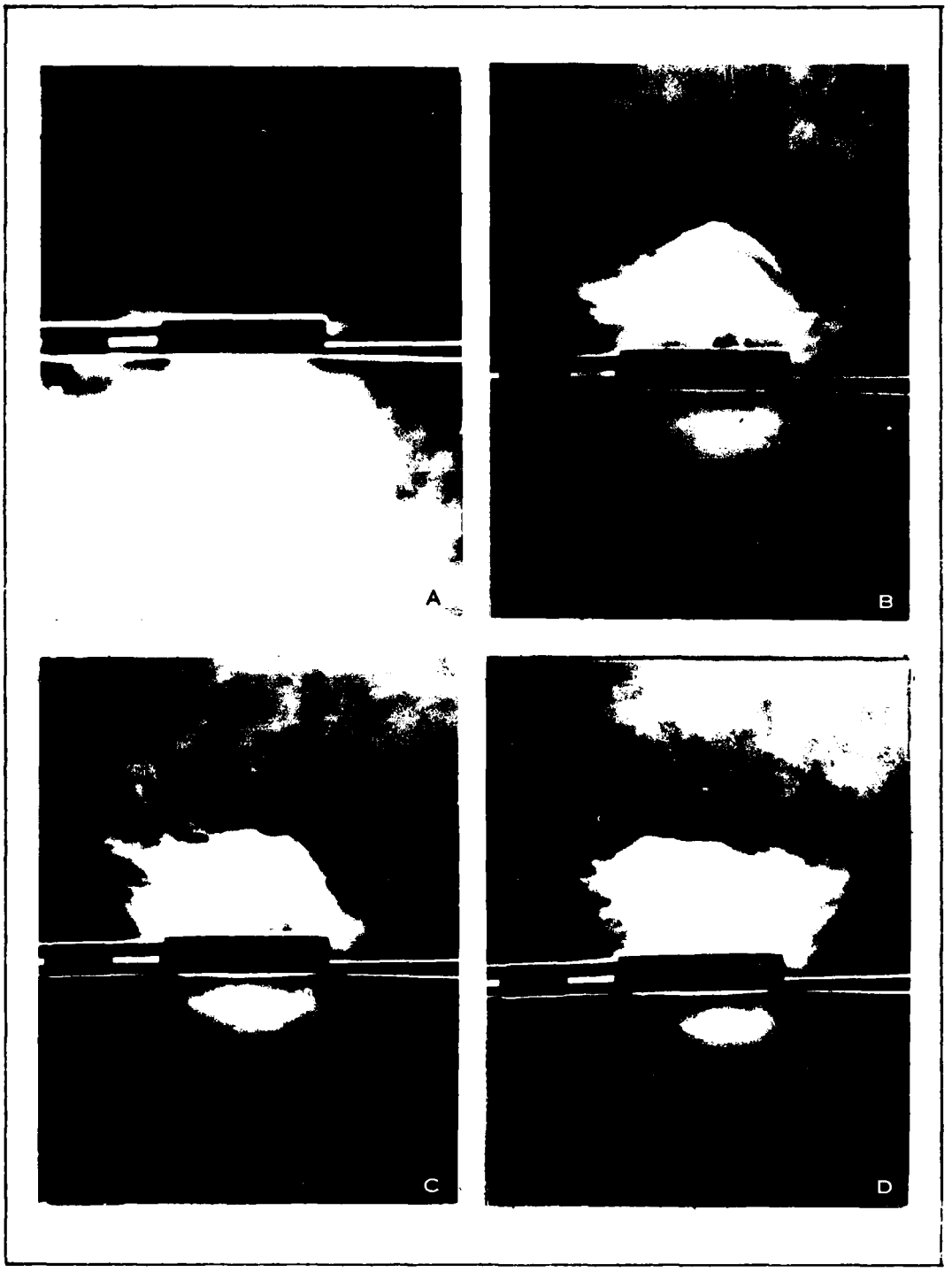

Fig 13. Schlieren Photographs With 1/200 Second Shutter Speed

believed this pattern represents the boundary of the recirculation zone. Figure 13b, c, and d are at the same flow conditions with helium being injected into the flow under 30 psi of pressure. The brightly illuminated region immediately behind the disk might be thought of as the entire reversed flow region; however, in reality it is the helium which is entrained by the reversed flow. The helium zone extends out to a point where the pressure of the reversed flow exceeds the pressure of the helium. This results in the top of the entrained helium being rounded with helium escaping out the sides. The escaping helium tends to move outward and downstream before curving around and joining along the centerline. As in the flow without helium, a valley is observed to be pointing toward the disk along the centerline. By taking measurements from these photographs, an approximate recirculation zone size is obtained. The width of the zone reaches a maximum of approximately 1.5 disk diameters at about one diameter behind the disk. This corresponds to a $Y/R = 1.5$ at $x/R = 1.0$. The length of the zones appears to be somewhere between $x/R = 3.0$ and $x/R = 4.0$.

These results agree well with information reported in Ref 5. The immediate wake behind the disk is described as being "surrounded by a thin 'vortex layer' which wavers and thickens under turbulence." The underpressure in this region results in the flow being sucked in toward the axis

of the disk. The zone is broken up in a few disk diameters as the pressure recovers. Figure 14 gives a pictorial view of this description.

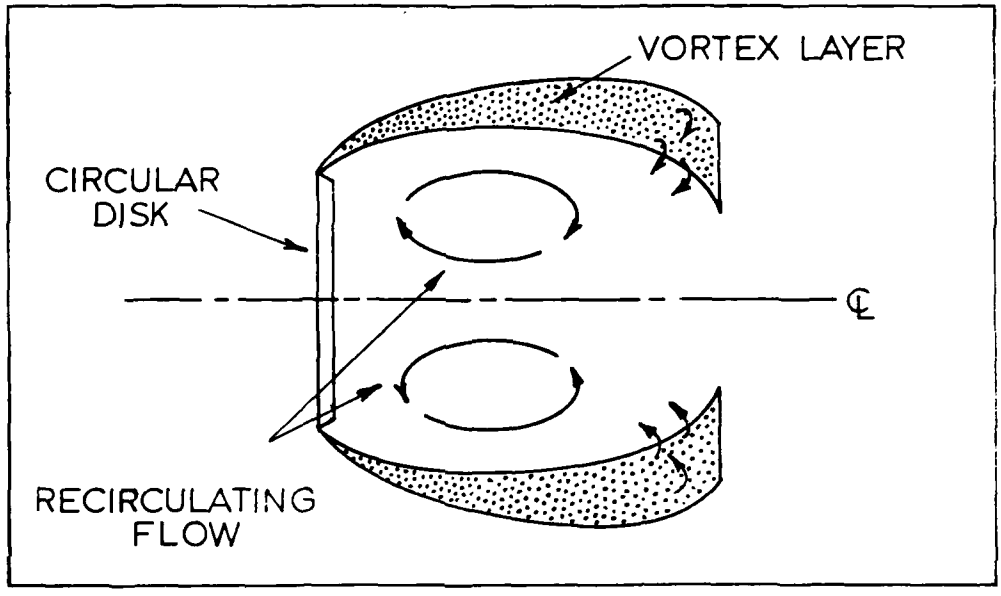

Fig 14. Recirculation Zone Behind A Circular Disk

Reference 24 provides results which further support the schlieren observations. The test set-up was different from the one used in this study, consisting of a circular disk mounted in a wind tunnel test section. The ratio of the disk diameter to the diameter of the test section varied from 0.2 to 0.47, and the flow velocity ranged from about 16.5 feet per second to 164 feet per second. The results revealed an average recriculation zone length of approximately two disk diameters. Very little change in the

recirculation zone's length was attributed to the different initial flow velocities. The width of the recirculation zone was found to vary from about 1.4 to 1.5 disk diameters. Despite the differences in the experimental arrangement, the boundary of the recirculation zone obtained in the present study agrees well with the data presented in Ref 24.

The second series of photographs in Fig 15 were taken with a spark lamp with a flash duration of about a microsecond (about 1/5000 the speed of the shutter arrangement). These photographs present a slightly different picture. Rather than illustrating a defined recirculation zone, they focus more on the helium entrainment region. Several interesting observations are made. From Fig 15b, c, and d, the helium region varies in location from photograph to photograph. This indicates that the flow is more complex in the recirculation zone than it initially appeared to be in the photographs made with a 1/200 second shutter speed. While the photographs only give a two-dimensional representation, the variance in the helium core is a three-dimensional occurence. The flow is most likely oscillating about the centerline of the disk as well as recirculating in the stream-wise direction. Helium is shed as the core oscillates from side to side. The series of photographs in Fig 15 illustrate that the previous series employing a 1/200 second shutter speed, presented an averaged flow

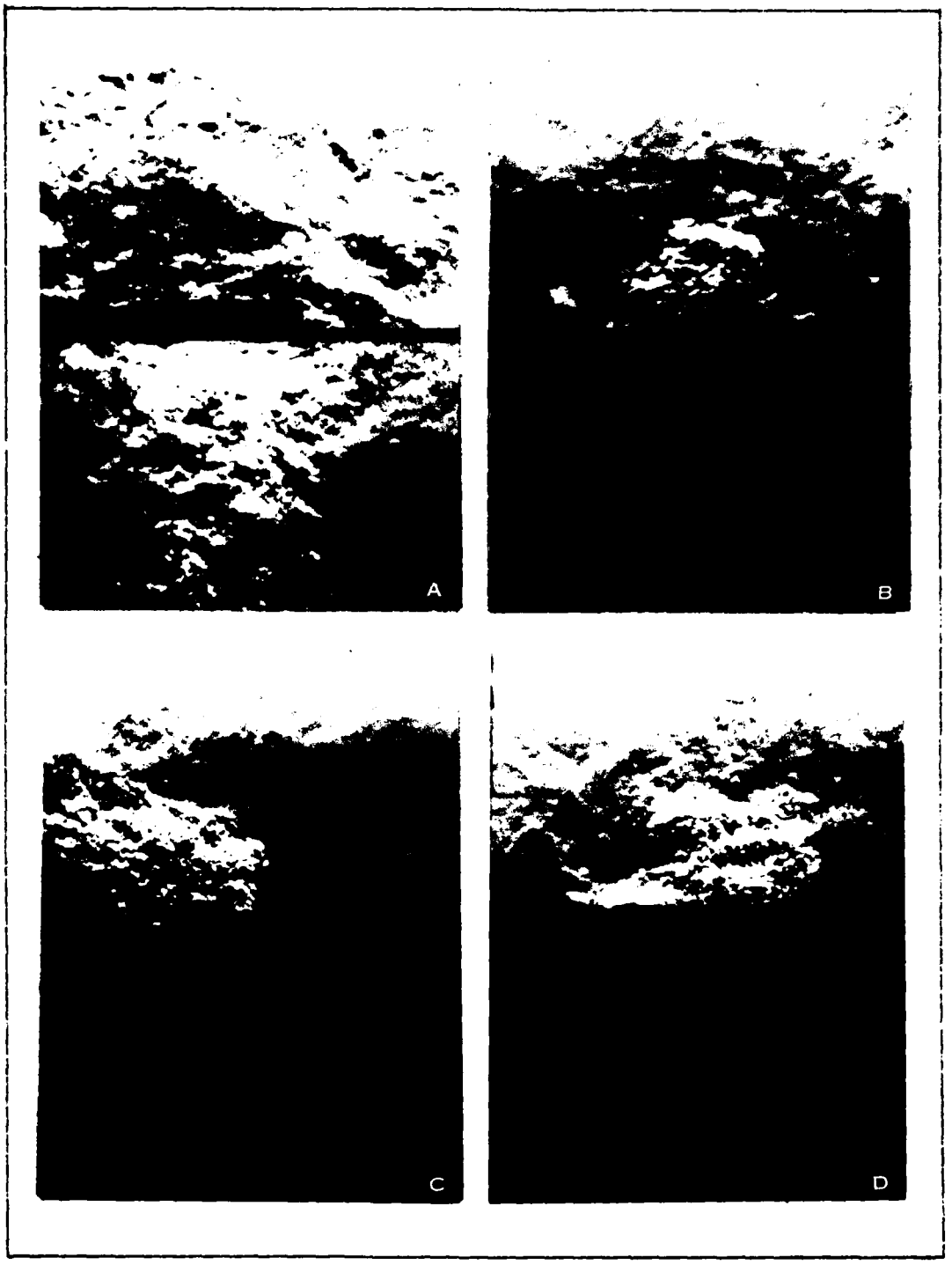

Fig 15. Schlieren Photographs With Spark Lamp

pattern, superimposing each location of the helium core as it oscillated onto the same picture. The flow therefore is a very dynamic process.

Laser Velocimeter Results

The laser velocimeter system investigation was accomplished in three parts. Initially, a survey of the free jet was taken 18.0 inches (12 jet diameters) from the exit plane. The near wake behind a 2.0 inch diameter disk was then evaluated at seven stream-wise locations. Finally, the above procedure was repeated for a 1.5 inch diameter disk obtaining measurements at six stream-wise positions. All test runs with the circular disks were conducted under the same flow conditions as in the schlieren study (D = 1.5 inches, X/D = 12.0, and M = 0.35).

Free jet survey. The purpose of obtaining a free jet survey was twofold. First, it provided the flow conditions at the downstream location where the disk would later be placed. Second, it allowed for a comparison with theoretical predictions and other experimental data. Figure 16 is the velocity profile obtained from the free jet survey. A similarity profile was developed by dividing each velocity by the centerline velocity, U_{cen}, and each location by the value of Y where the velocity had decayed to half its centerline value. Therefore,

$$\frac{U}{U_{cen}} = 0.5 \quad \text{at} \quad \frac{Y}{Y_{\frac{1}{2}}} = 1.0 \qquad (6)$$

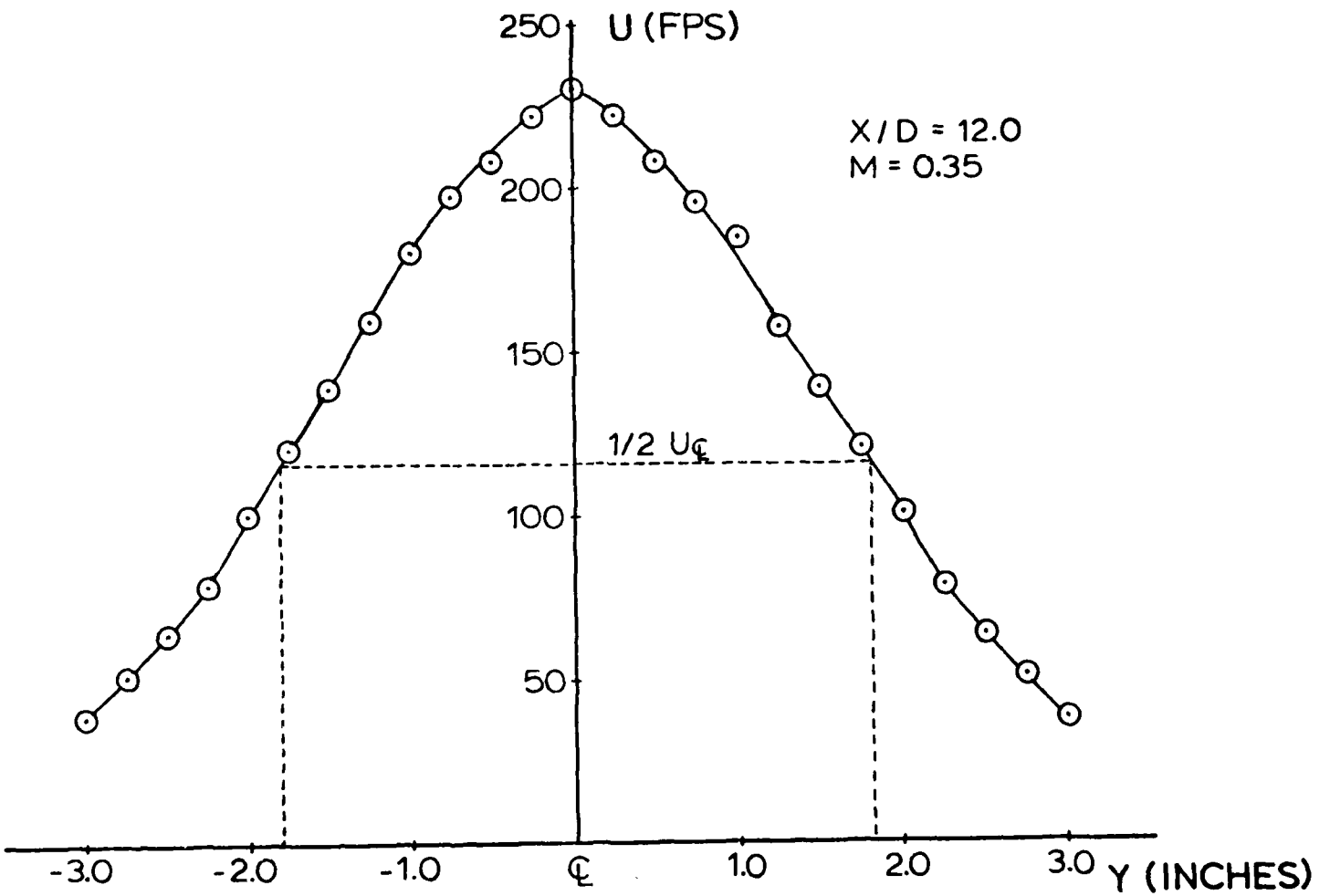

Fig 16. Free Jet Mean Velocity Profile

This is compared to the similarity profiles obtained from Refs 2 and 19 as seen in Fig 17. The correlation between the Tollmien and Gortler curves and the present data is very good.

Another source of comparison is the relationship between downstream position, X , and $Y_{\frac{1}{2}}$. From Ref 19

$$\frac{Y_{\frac{1}{2}}}{X} = 0.097$$

for axially symmetric jets. Reference 22 gives a slightly different value of

$$\frac{Y_{\frac{1}{2}}}{X} = 0.085$$

The present study found

$$\frac{Y_{\frac{1}{2}}}{X} = 0.10$$

The results found with the laser velocimeter system therefore are in good agreement with those presented in Refs 19 and 22 with a difference ranging between 3% and 16%. The results are exceptionally good considering that similarity profiles are not established until approximately 10 jet diameters downstream of the exit and the present study is only at 12 jet diameters where there is still room for a spread in the data.

Another parameter for comparison is the axial velocity decay along the centerline of the jet. Reference 19

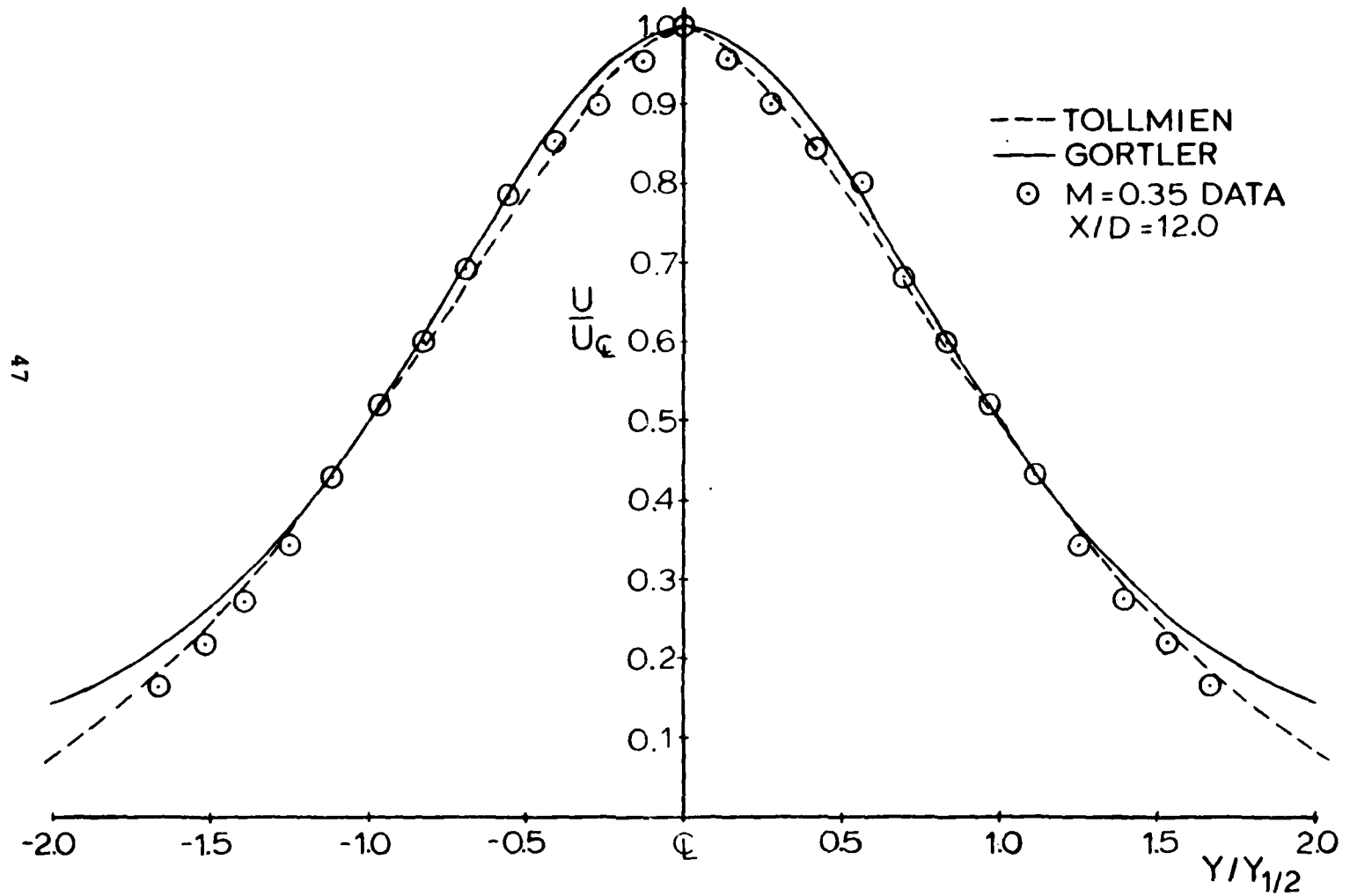

Fig 17. Free Jet Similarity Profiles

presents an equation for axial velocity decay, good between 10 and 30 jet diameters from the exit. The equation is

$$\frac{U_{cen}}{U_o} \approx 6.5 \frac{D}{X} \qquad (7)$$

where U_o = the velocity at the jet exit. For the present testing U_o = 396.7 feet per second found with the equation

$$U_o = 49M\sqrt{T_o}$$

where T_o = calming chamber total temperature

M = Mach number at jet exit = 0.35

Reference 2 presents the Tollmien solution for axial velocity decay which is

$$\frac{U_{cen}}{U_o} = \frac{0.96}{\frac{aX}{R_o} + 0.29} \qquad (8)$$

where R_o = jet radius = 0.75 inch

a = constant (approximately 0.66)

The results are shown in Fig 18. The data obtained with the laser velocimeter system is relatively good in comparison with the theoretical predictions.

From both the mean velocity profile and the axial velocity decay comparisons, the data obtained with the LDV is very good. This serves to further increase the confidence level in the LDV data and indicates that the system was functioning well.

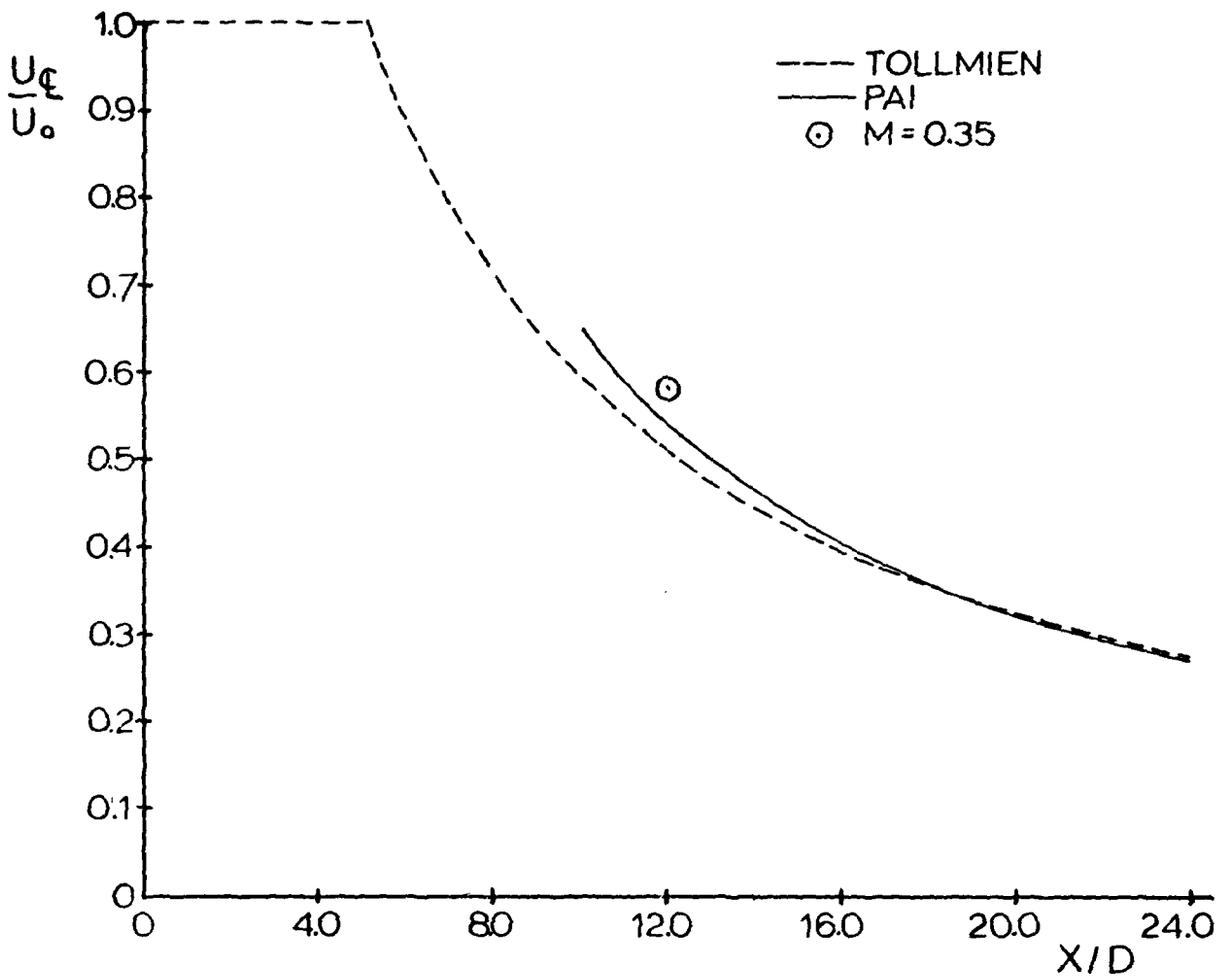

Fig 18. Axial Velocity Decay for Axially Symmetric Free Jet

Turbulence intensity data is presented in Fig 19. While Ref 19 concludes that a kinematic similarity of turbulence intensities is not established until an X/D of at least 20, the trends in present data resemble trends in the experimental data compiled by Corrsin. Reference 18 indicates that the turbulence intensity calculation is only good up to 20%, while Ref 21 found good correlation with hot wire anemometer results between 2% and 30%. Considering the above, turbulence intensity values obtained in this study above 20% should be viewed as "in the neighborhood of" the respective value.

2.0 inch diameter disk. This section presents data obtained with the laser velocimeter system of flow in the near wake of a 2.0 inch diameter circular disk. Table I presents the downstream locations at which traverses were made.

The data presented in this section must be viewed with the following ideas in mind. The data points were connected with lines in order to depict trends in the flow, and, as such, the lines are only approximations. This is especially true in the regions over which the flow was changing directions and high turbulence intensities prohibited a suitable autocorrelation junction from which data could be obtained.

Throughout the results, the graphs are labeled with or without modulation. This is to indicate the

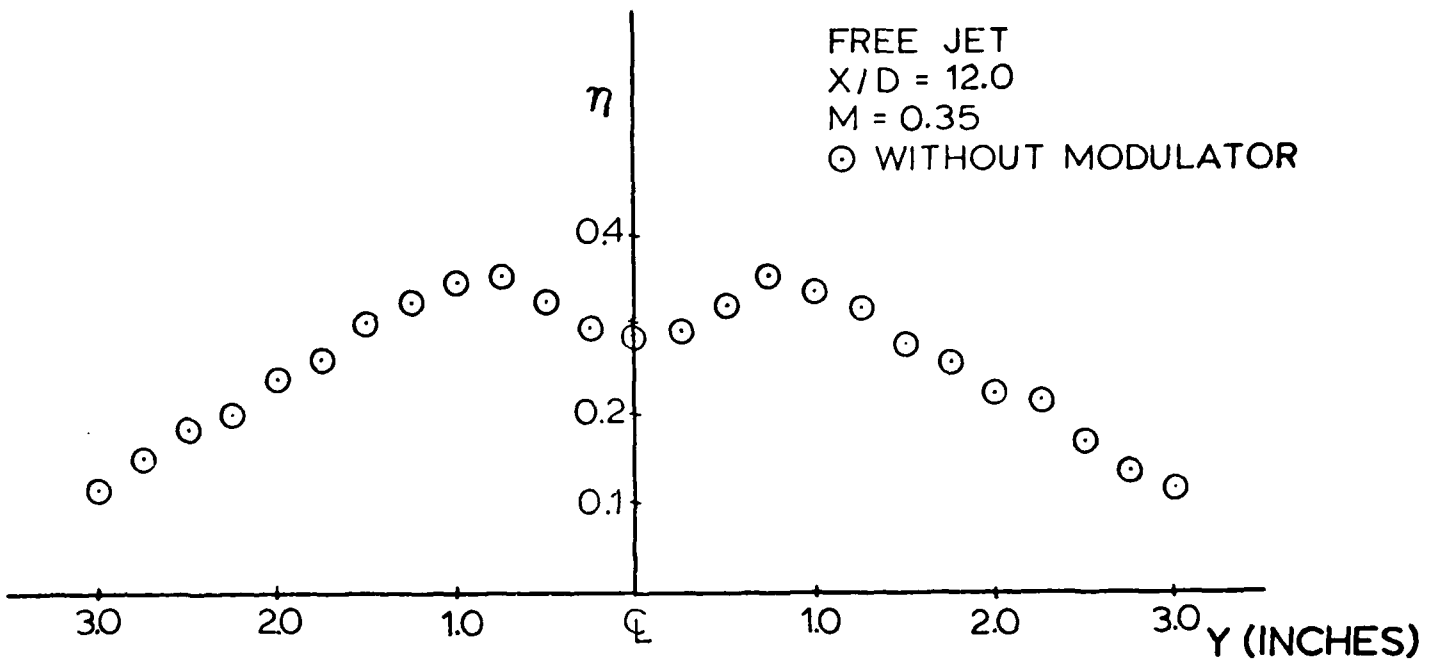

Fig 19. Free Jet Turbulence Intensity Profile

autocorrelation function from which the data was computed at each point, even though the phase modulator was always required in determining flow direction. Both the with and without phase modulation curves are presented for comparison purposes.

Figures 20 through 33 present the mean velocity profiles obtained at the respective locations downstream of the disk. Attempts were made to develop a similarity profile from the mean velocity curves, as was done for the free jet; however, one was not obtained from this study. The ordinate of the graphs is the mean velocity in feet per second and the abscissa is the Y position, nondimensionalized by the disk radius, R . Figures 34 and 35 were taken from the without modulation graphs to summarize the results for comparison purposes.

The mean velocity profiles presented in this study are found to be symmetrical about the disk centerline. This indicates that the disk was properly aligned normal to the flow on a common centerline with the free jet. It also lends credibility to the data since theoretically the wake flow should be symmetrical behind the body.

The mean velocity values obtained from the with and without phase modulation autocorrelation functions are very close. Theoretically, their values should be identical, but due to the interpolation required in obtaining the exact fraction of the channel where the peak occurred, variances

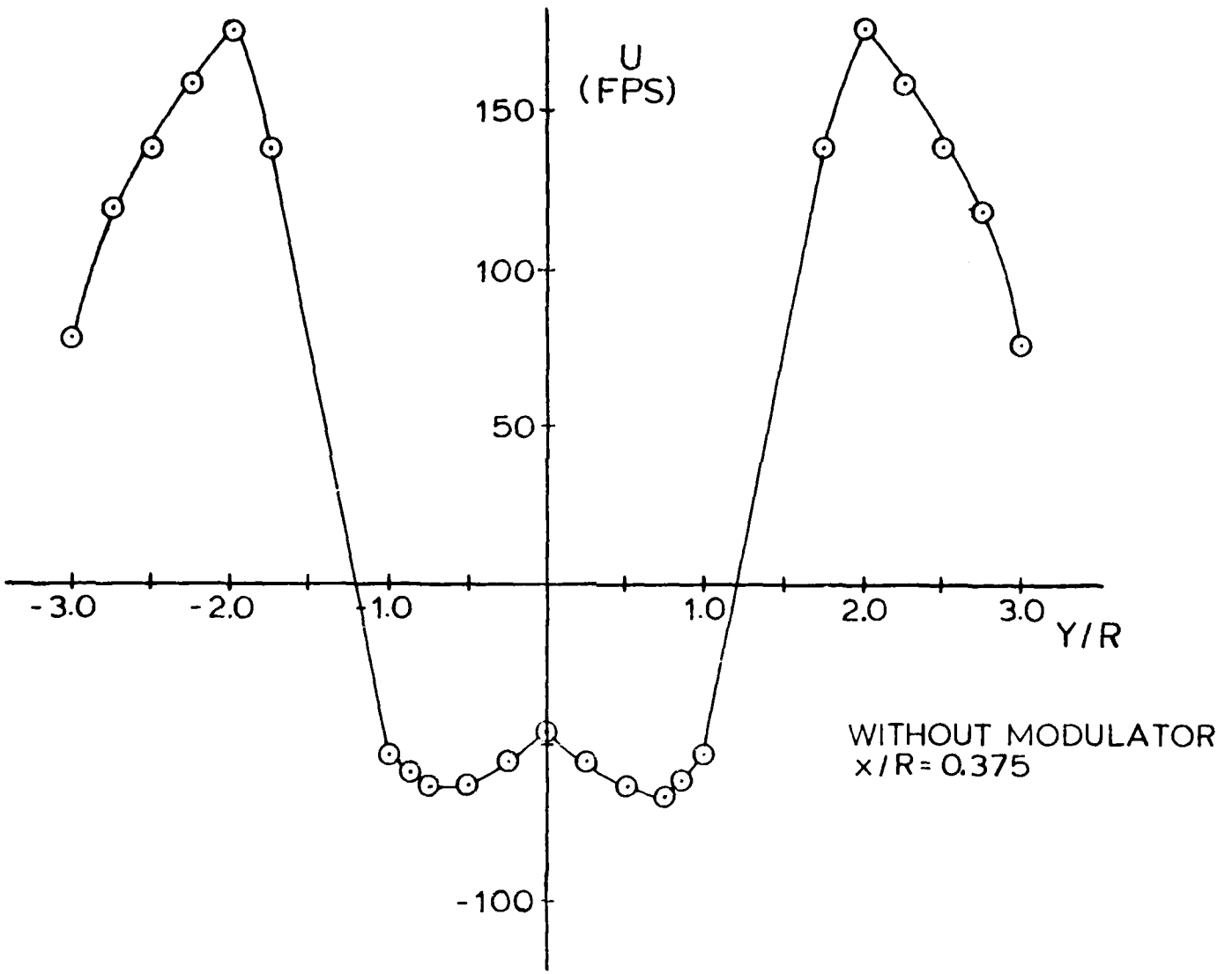

Fig 20. Mean Velocity Profile, 2.0 Inch Diameter Disk

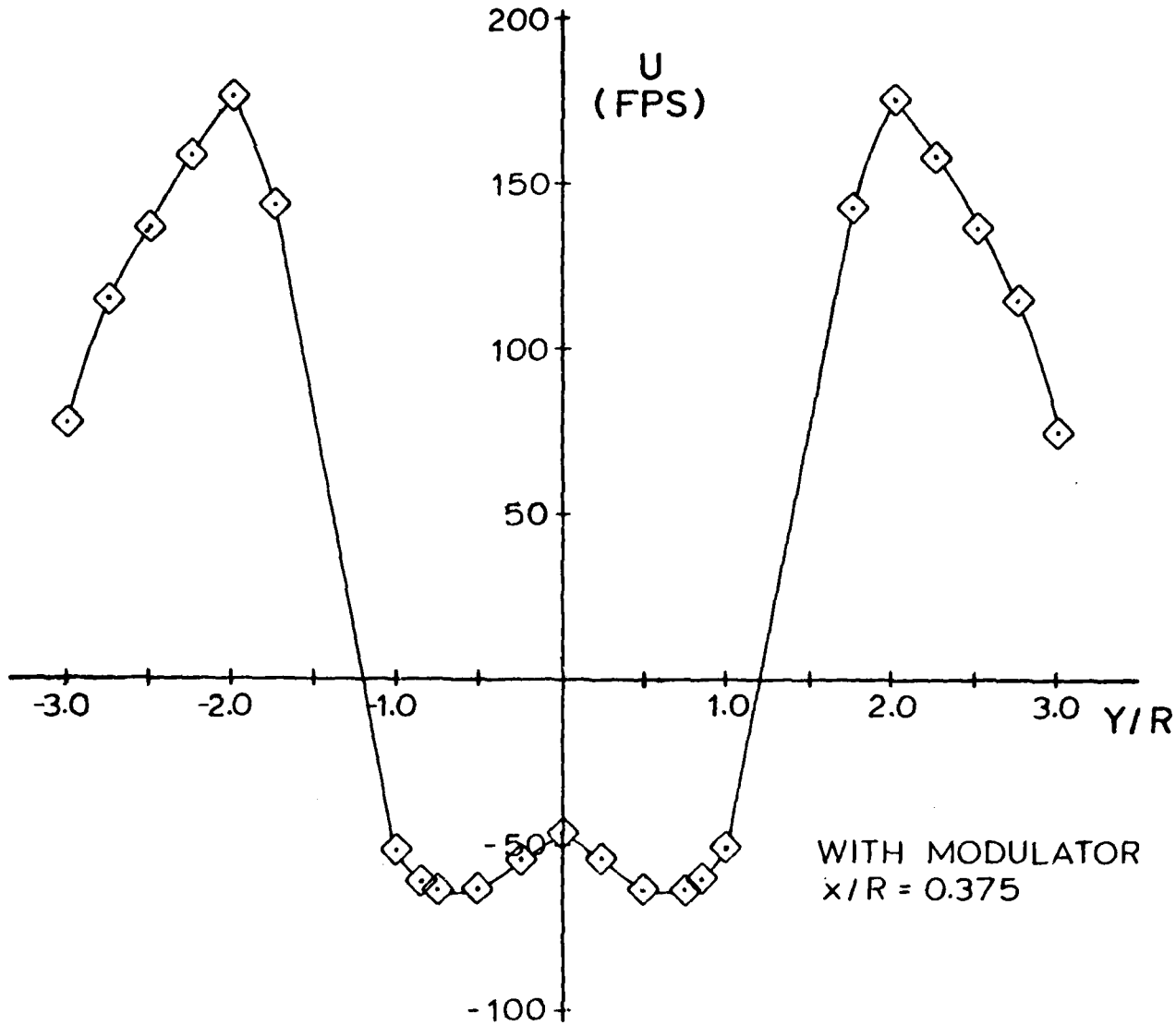

Fig 21. Mean Velocity Profile, 2.0 Inch Diameter Disk

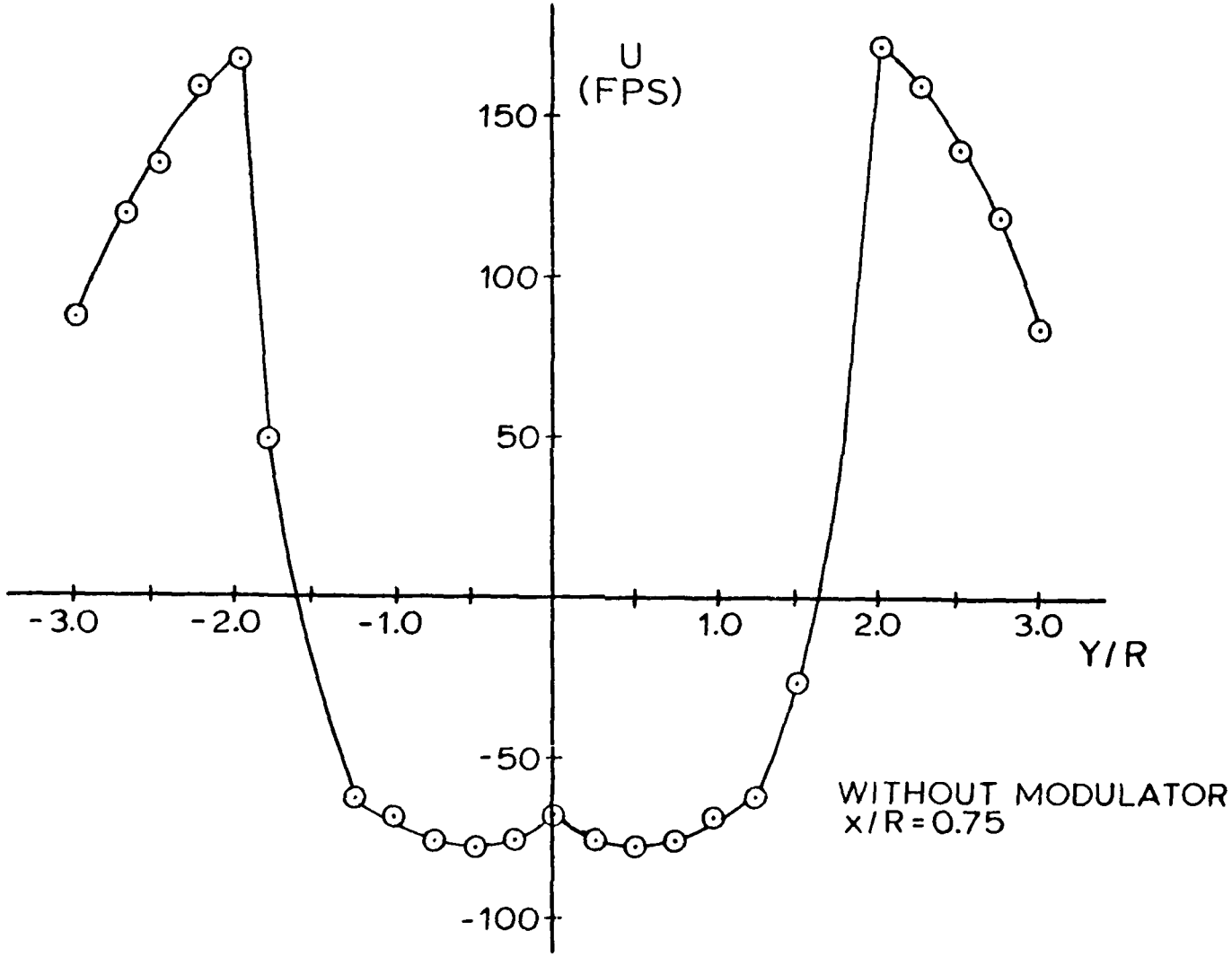

Fig 22. Mean Velocity Profile, 2.0 Inch Diameter Disk

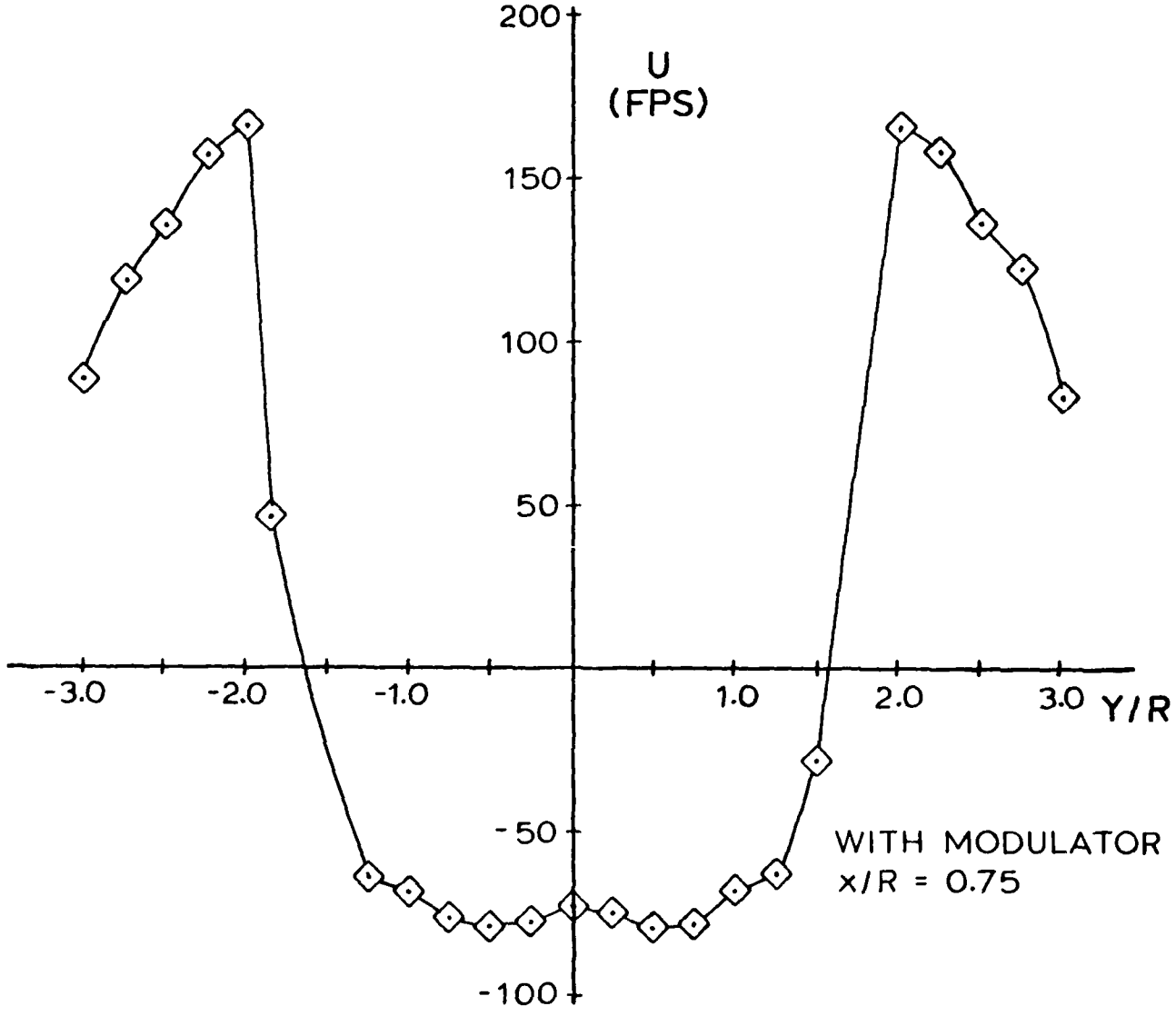

Fig 23. Mean Velocity Profile, 2.0 Inch Diameter Disk

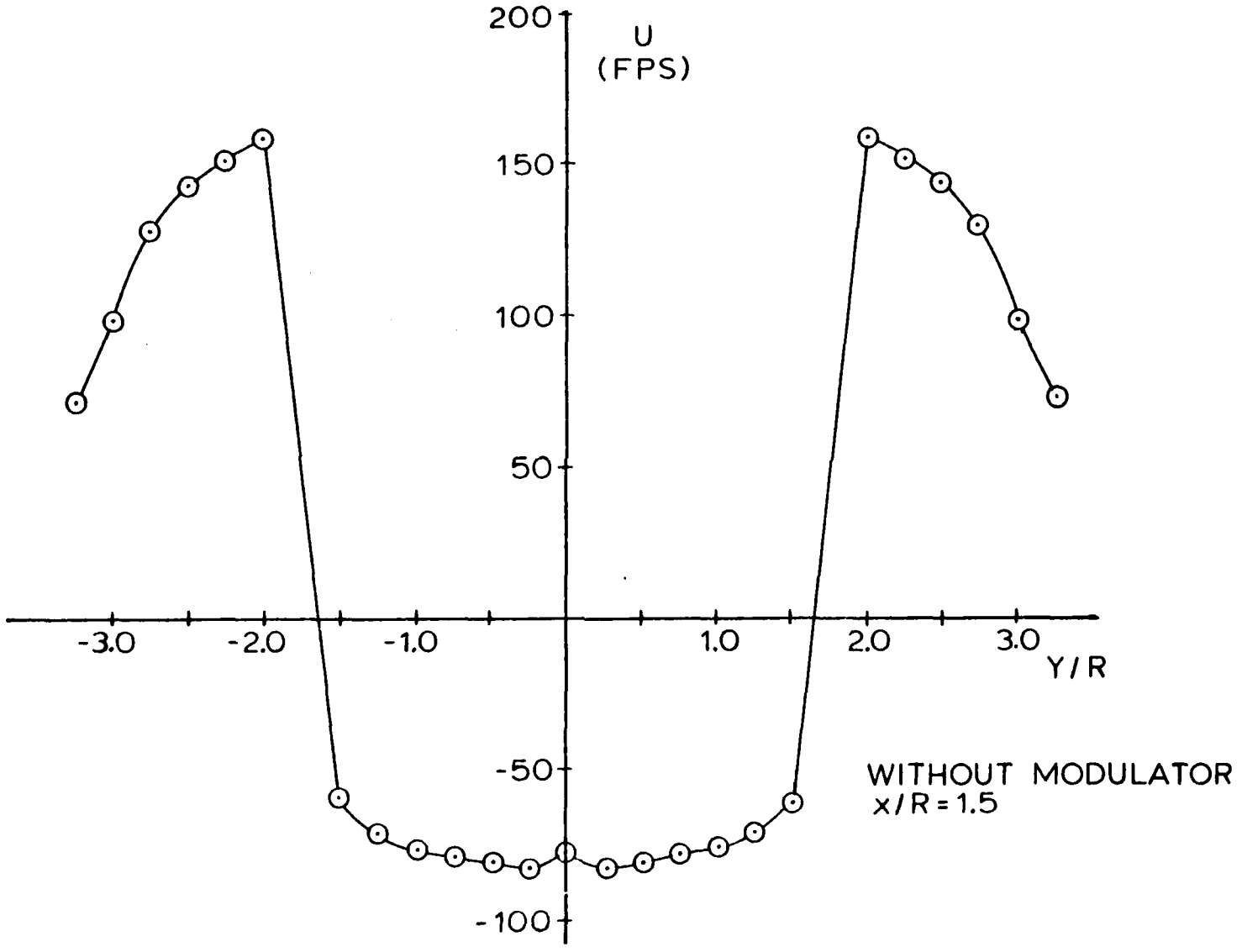

Fig 24. Mean Velocity Profile, 2.0 Inch Diameter Disk

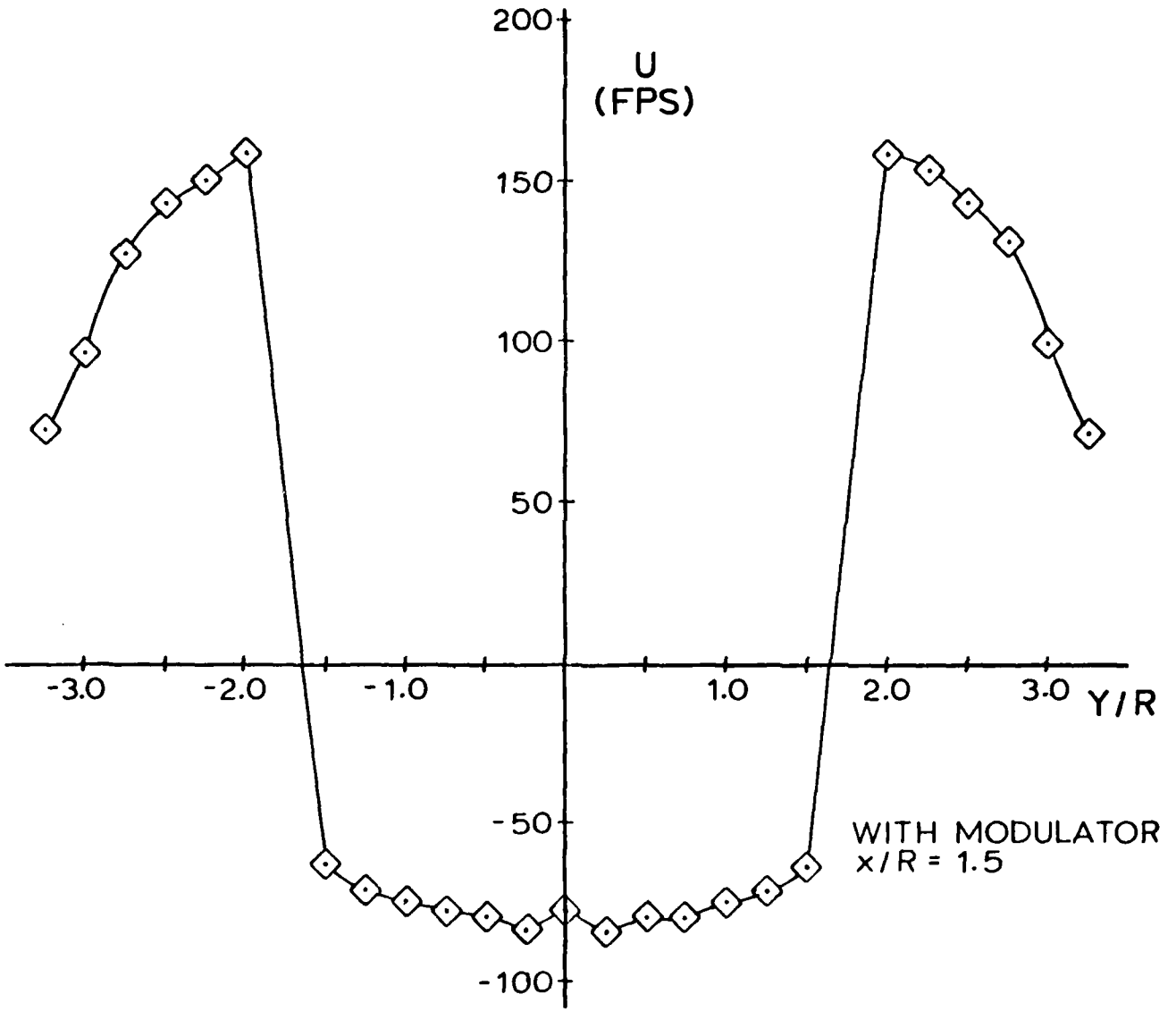

Fig 25. Mean Velocity Profile, 2.0 Inch Diameter Disk

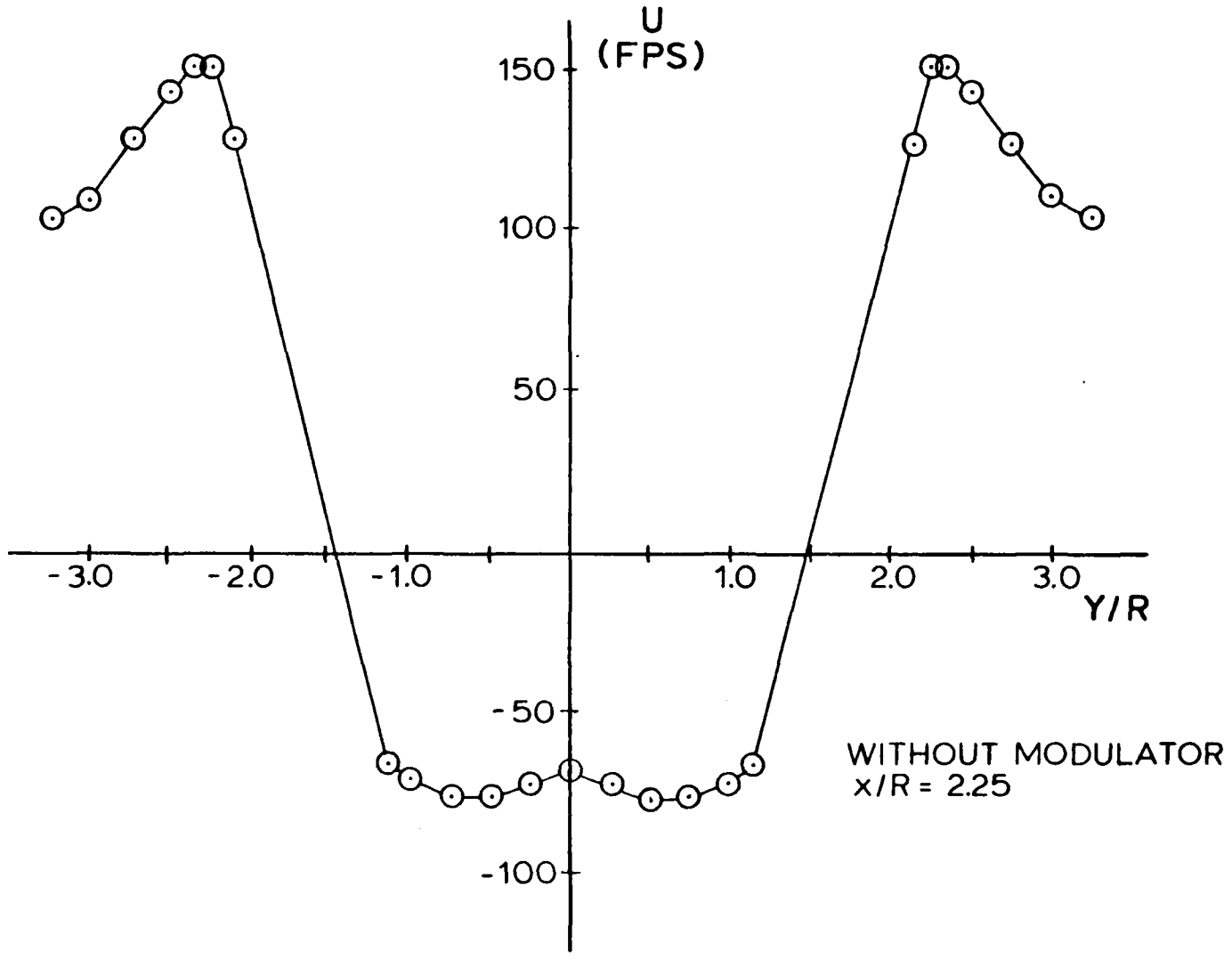

Fig 26. Mean Velocity Profile, 2.0 Inch Diameter Disk

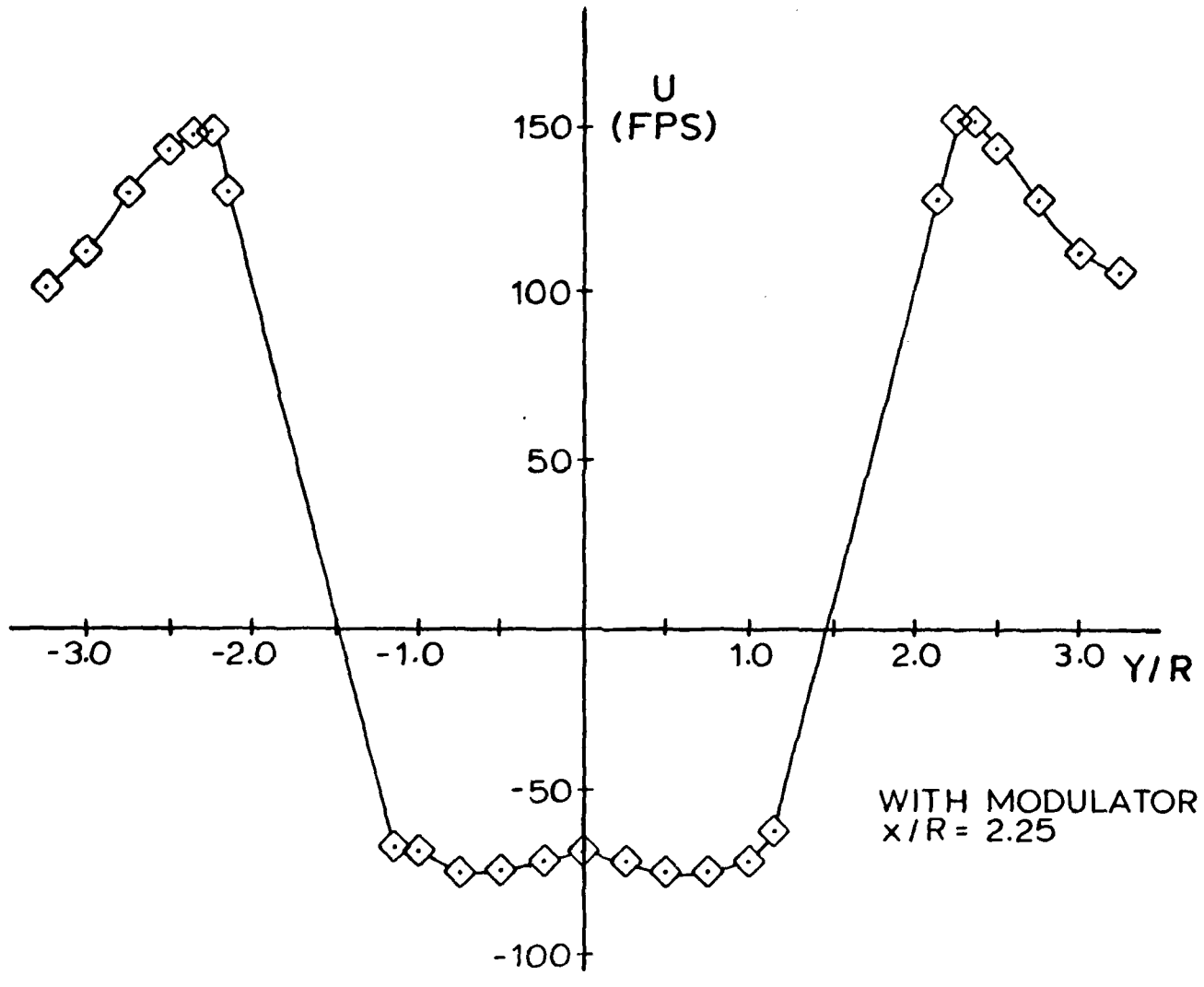

Fig 27. Mean Velocity Profile, 2.0 Inch Diameter Disk

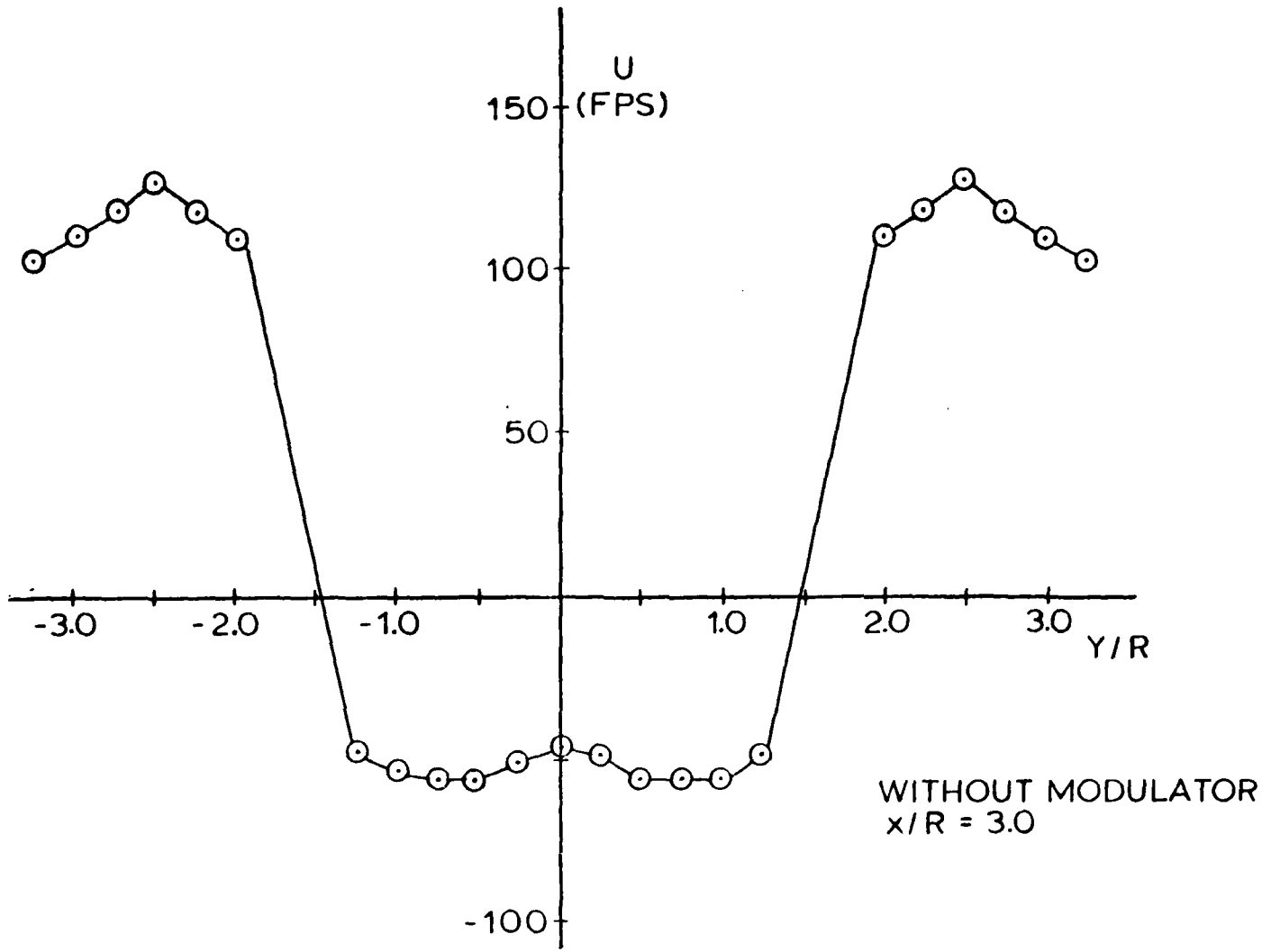

Fig 28. Mean Velocity Profile, 2.0 Inch Diameter Disk

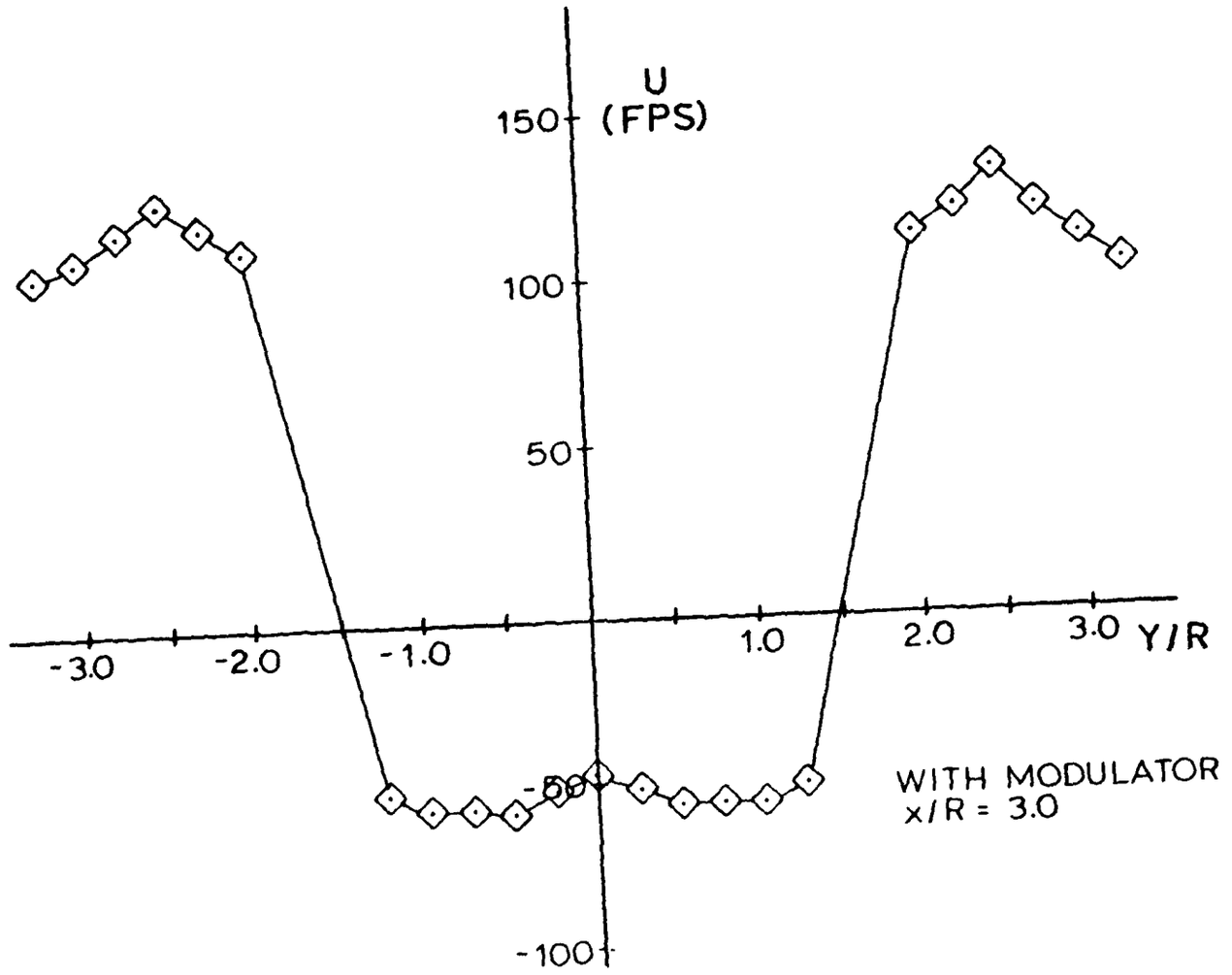

Fig 29. Mean Velocity Profile, 2.0 Inch Diameter Disk

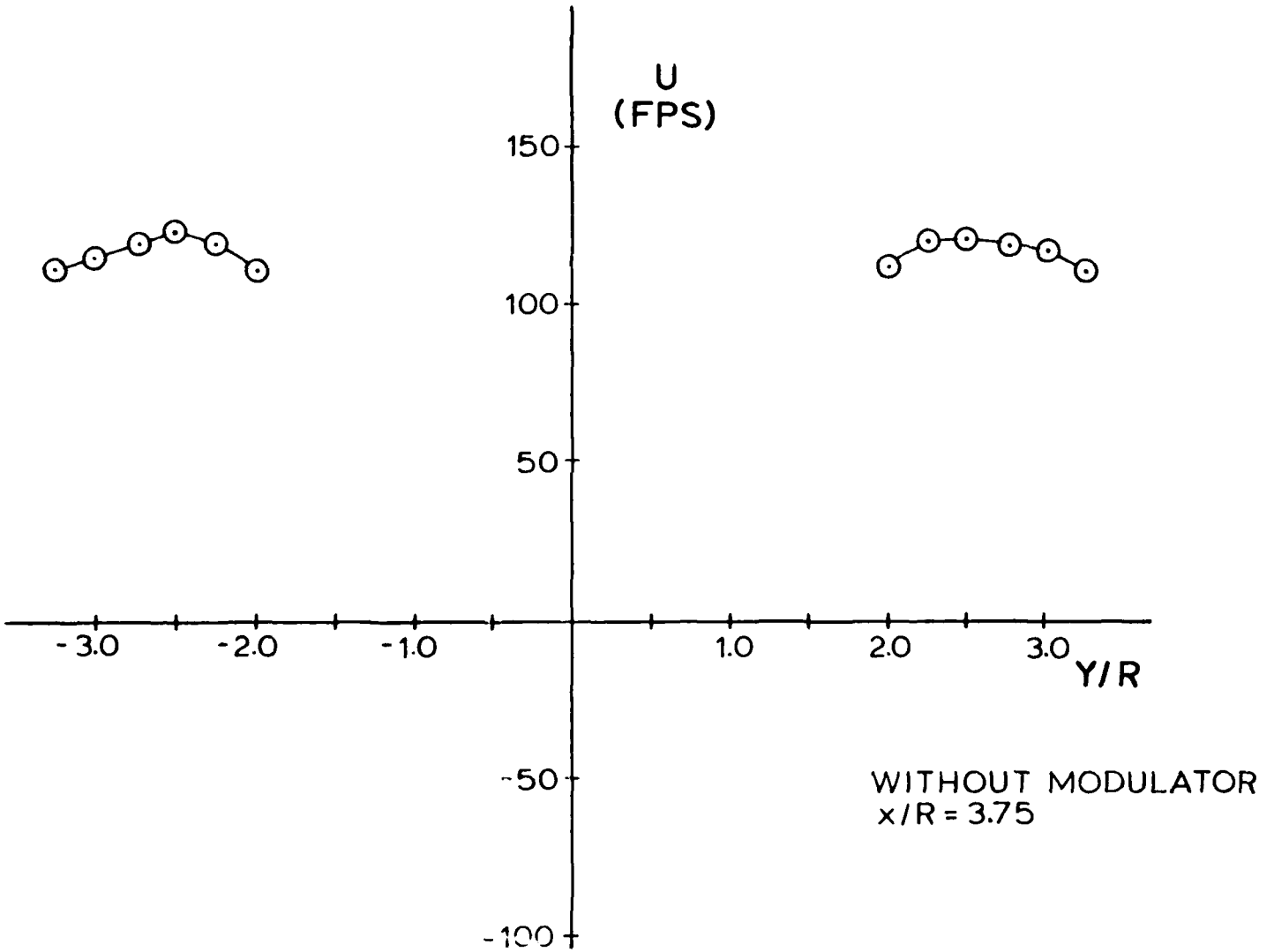

Fig 30. Mean Velocity Profile, 2.0 Inch Diameter Disk

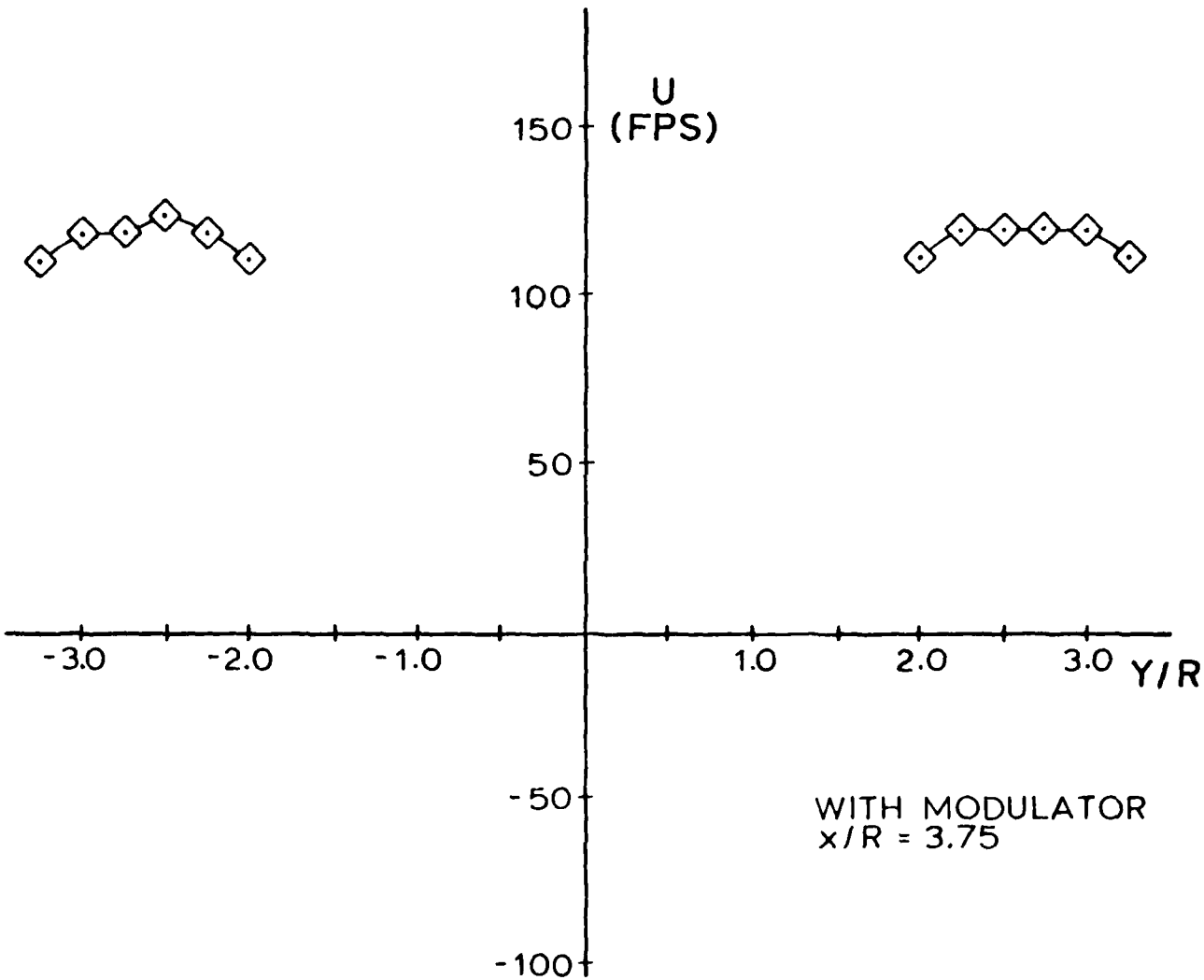

Fig 31. Mean Velocity Profile, 2.0 Inch Diameter Disk

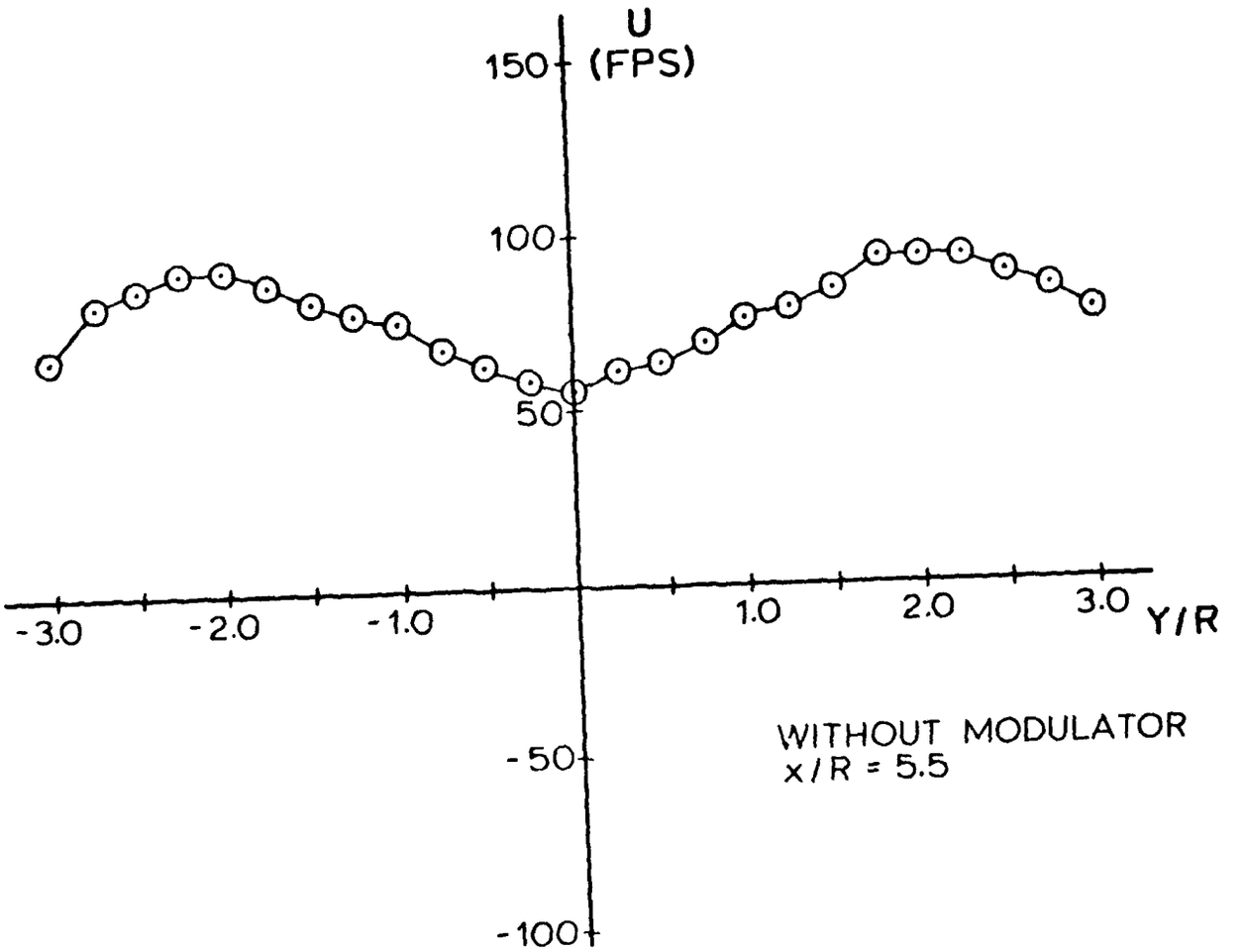

Fig 32. Mean Velocity Profile, 2.0 Inch Diameter Disk

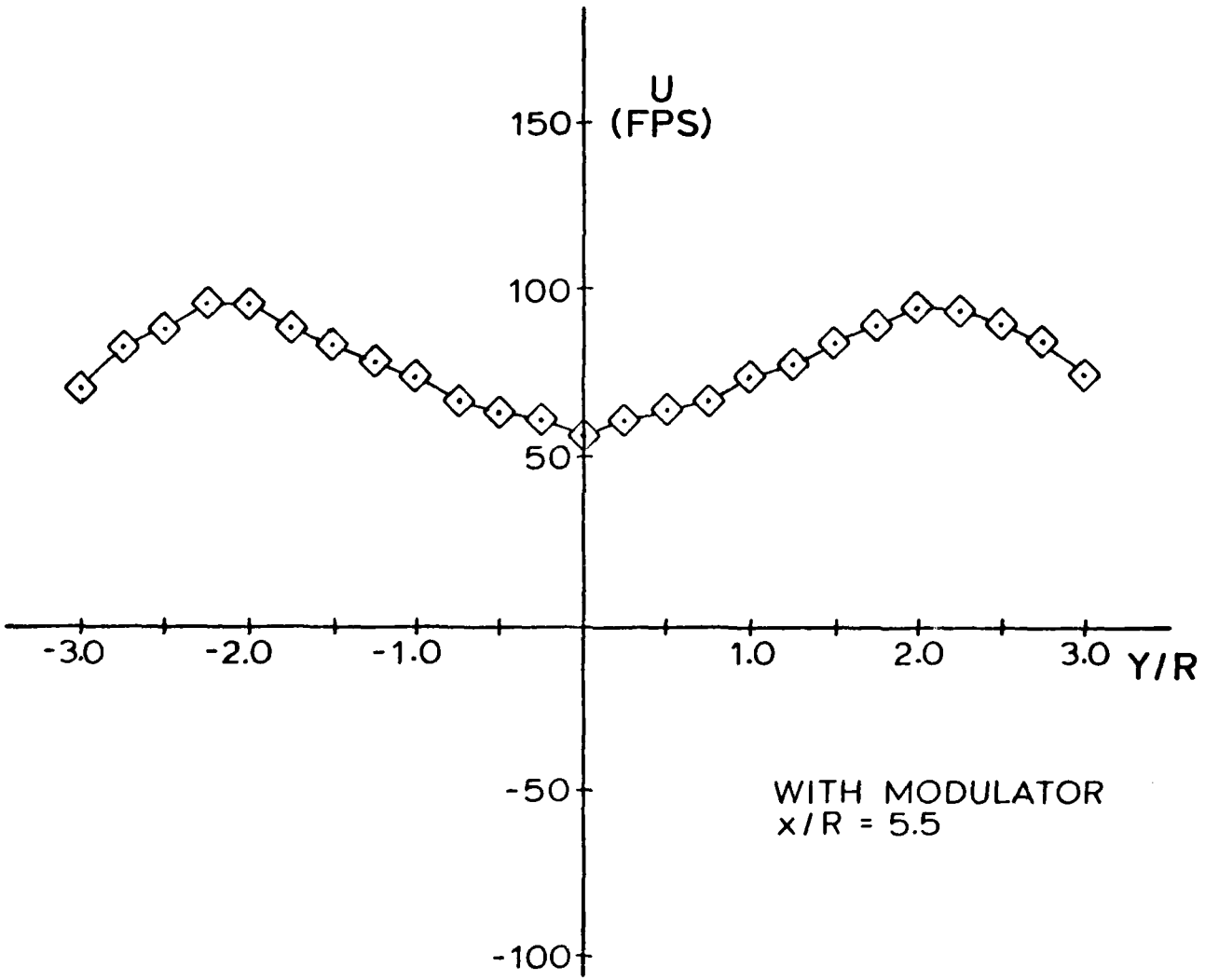

Fig 33. Mean Velocity Profile, 2.0 Inch Diameter Disk

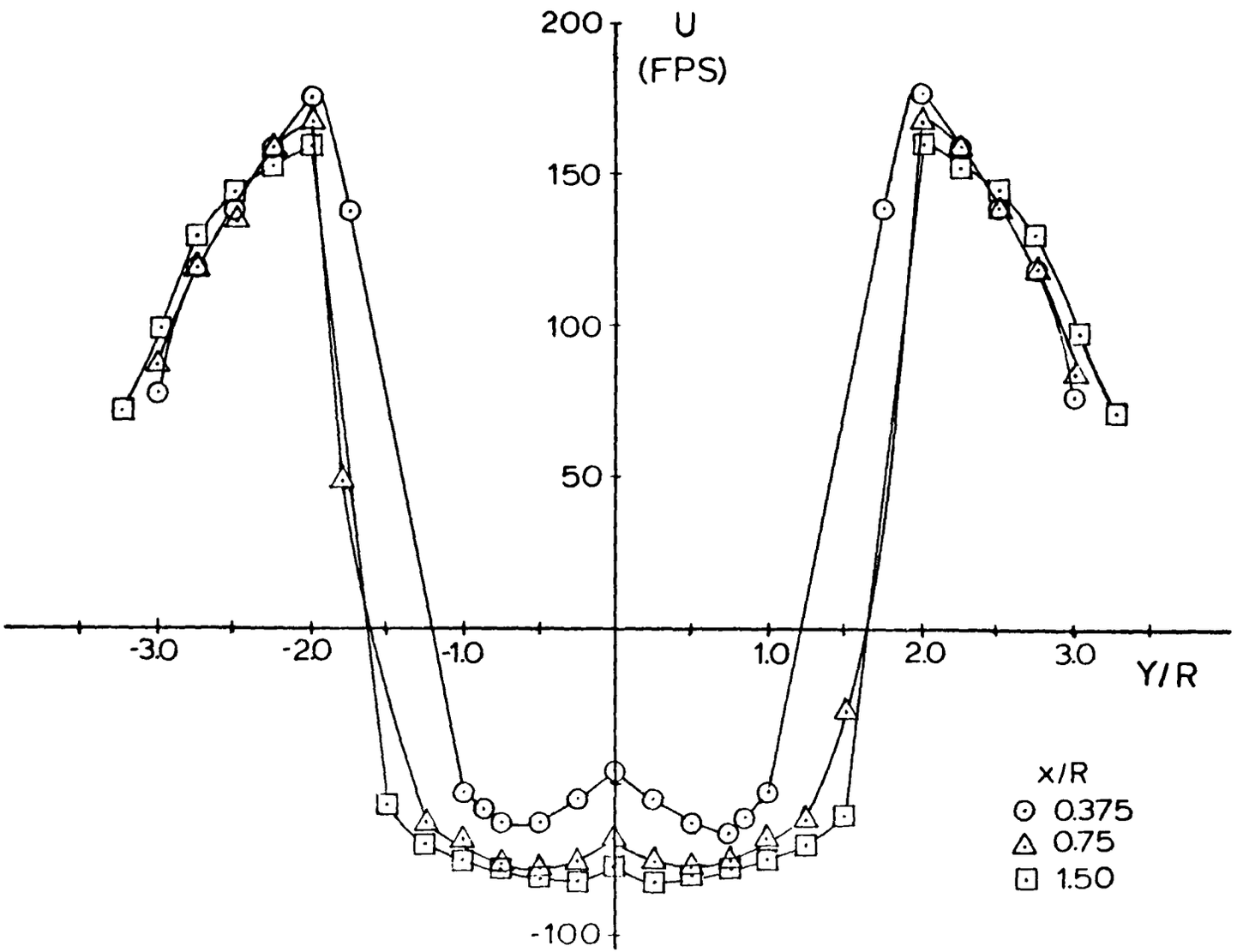

Fig 34. Mean Velocity Profile Summary, 2.0 Inch Diameter Disk

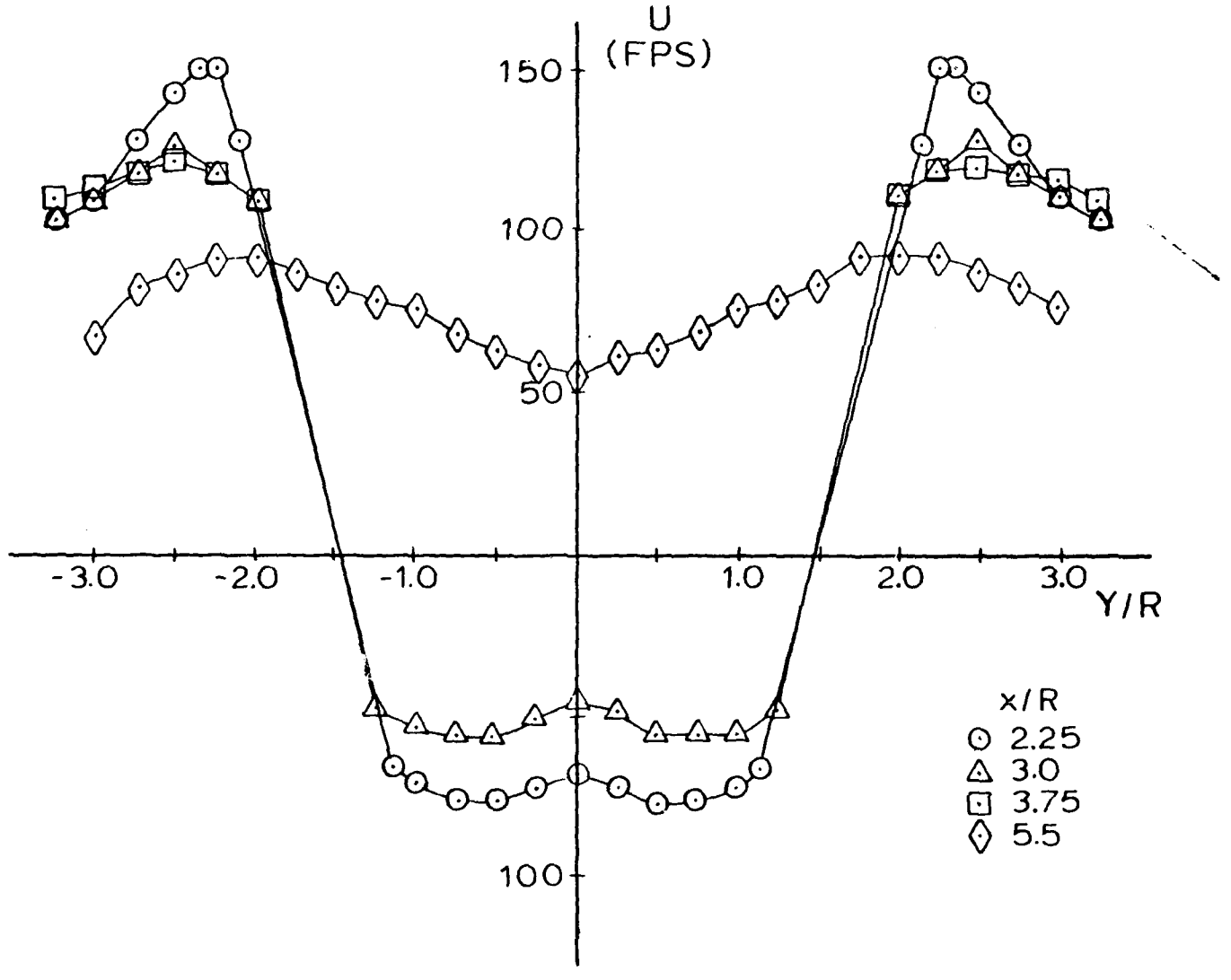

Fig 35. Mean Velocity Profile Summary, 2.0 Inch Diameter Disk

are expected. Reference 8 also indicates that a certain amount of unexplained distortion is experienced in the velocity data when the phase modulator is used.

Throughout the study, a phase modulator frequency shift of between 200 KHZ and 500 KHZ was sufficient in determining flow direction. To verify the directional results, a thin wire with a tuft on the end was placed at various points in the flow. The observations, even though they were relatively crude, concurred with the results obtained with the laser velocimeter system. The tuft also demonstrated an oscillation between the positive and negative flow directions in regions where the turbulence intensities were too high to allow suitable autocorrelation functions.

From Figs 34 and 35, the recirculation zone reaches a maximum width of between 1.5 and 2.0 disk diameters. The recirculation zone length appears to be on the order of 3.75 disk radii or slightly less than 2 disk diameters. The tuft experiment also tended to confirm this, and indicated that this rearward stagnation point actually occurs over a region rather than at a specific point. These dimensions agree very well with those obtained in the schlieren study and presented in Refs 5 and 24.

Figures 34 and 35 show the changes in the flow velocities in the wake region of the disk as a function of both radial position and downstream location. The maximum

positive velocity in the wake region occurred at an $x/R = 0.375$ and $Y/R = 2.0$. The slope of the velocity curves in the outer flow regions in the Y and -Y directions decreased as the flow moved downstream of the disk. In the recirculation zone, the velocities in the negative direction reached a maximum at $x/R = 1.5$. At each downstream location, a dip in the negative velocity profile was encountered at the centerline position ($Y = 0$). At $x/R = 3.75$ turbulence intensities were such that data could not be obtained between $Y/R = -2$ and $Y/R = 2$. This region is most likely indicative of the rearward stagnation point forming a boundary for the recirculation zone. The velocity profile at $x/R = 5.5$ consists entirely of downstream flow and is characteristic of the wake flow behind a bluff body, even though it is too close to the disk for a wake similarity profile to be developed. Reference 7 indicates that such a similarity profile is not obtained until the flow is approximately 100 body diameters downstream from the object.

Figures 36 through 42 are the turbulence intensity profiles obtained in the near wake region behind the 2.0 inch diameter disk. The values presented must be viewed as approximations since the data reduction equation is only considered accurate up to turbulence intensity values of 20% (Ref 18). The agreement between the values obtained from the with and without phase modulation autocorrelation

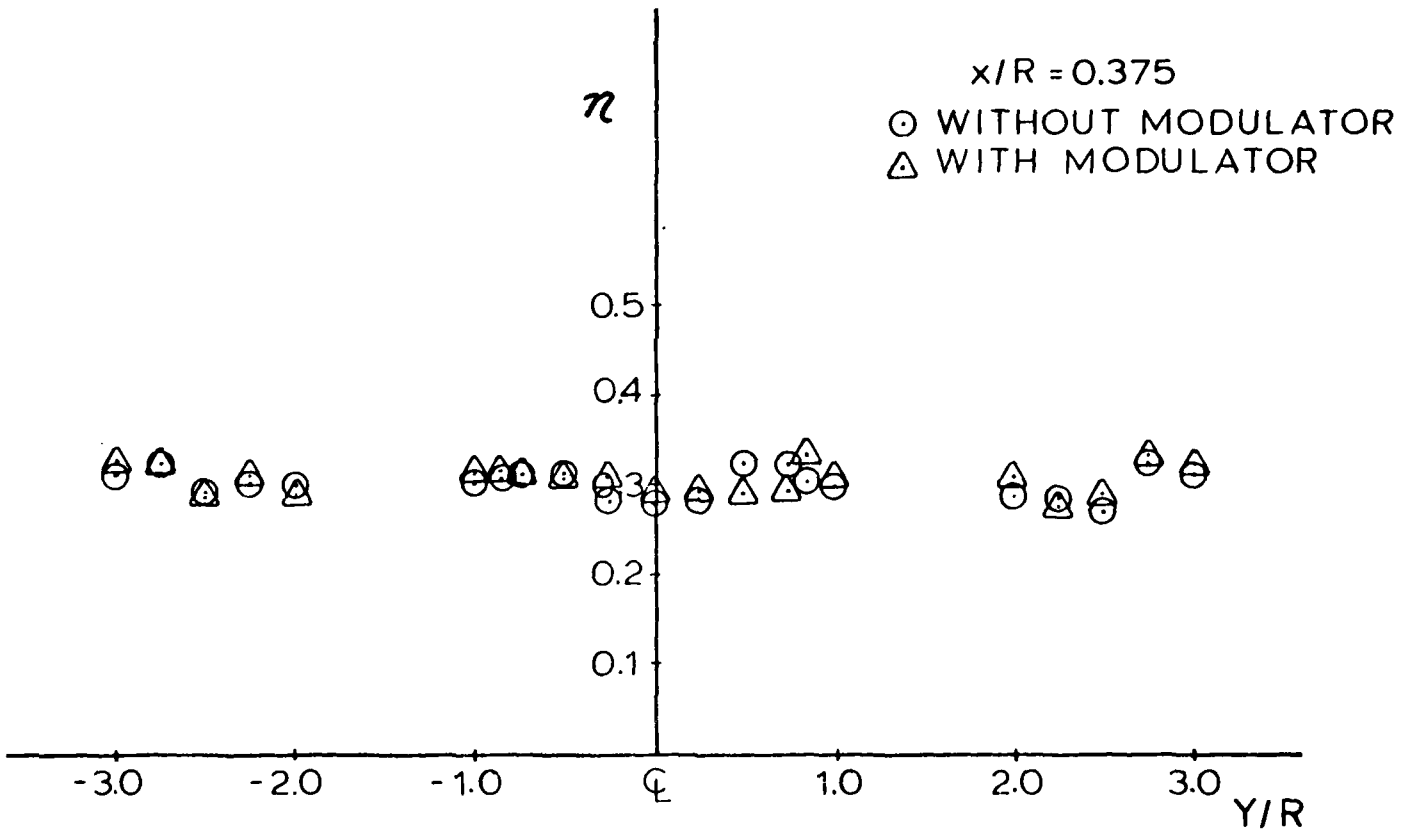

Fig 36. Turbulence Intensity Profiles, 2.0 Inch Diameter Disk

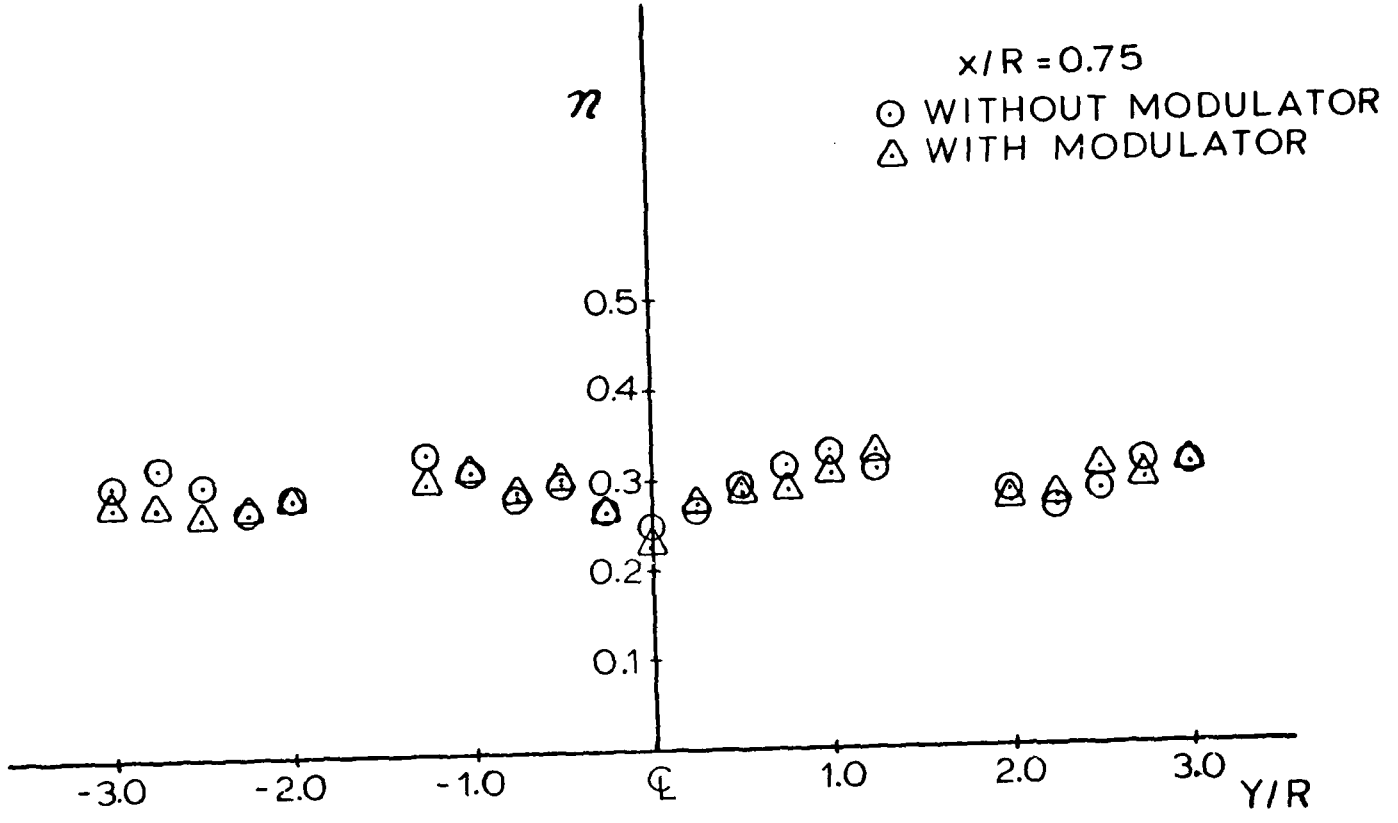

Fig 37. Turbulence Intensity Profiles, 2.0 Inch Diameter Disk

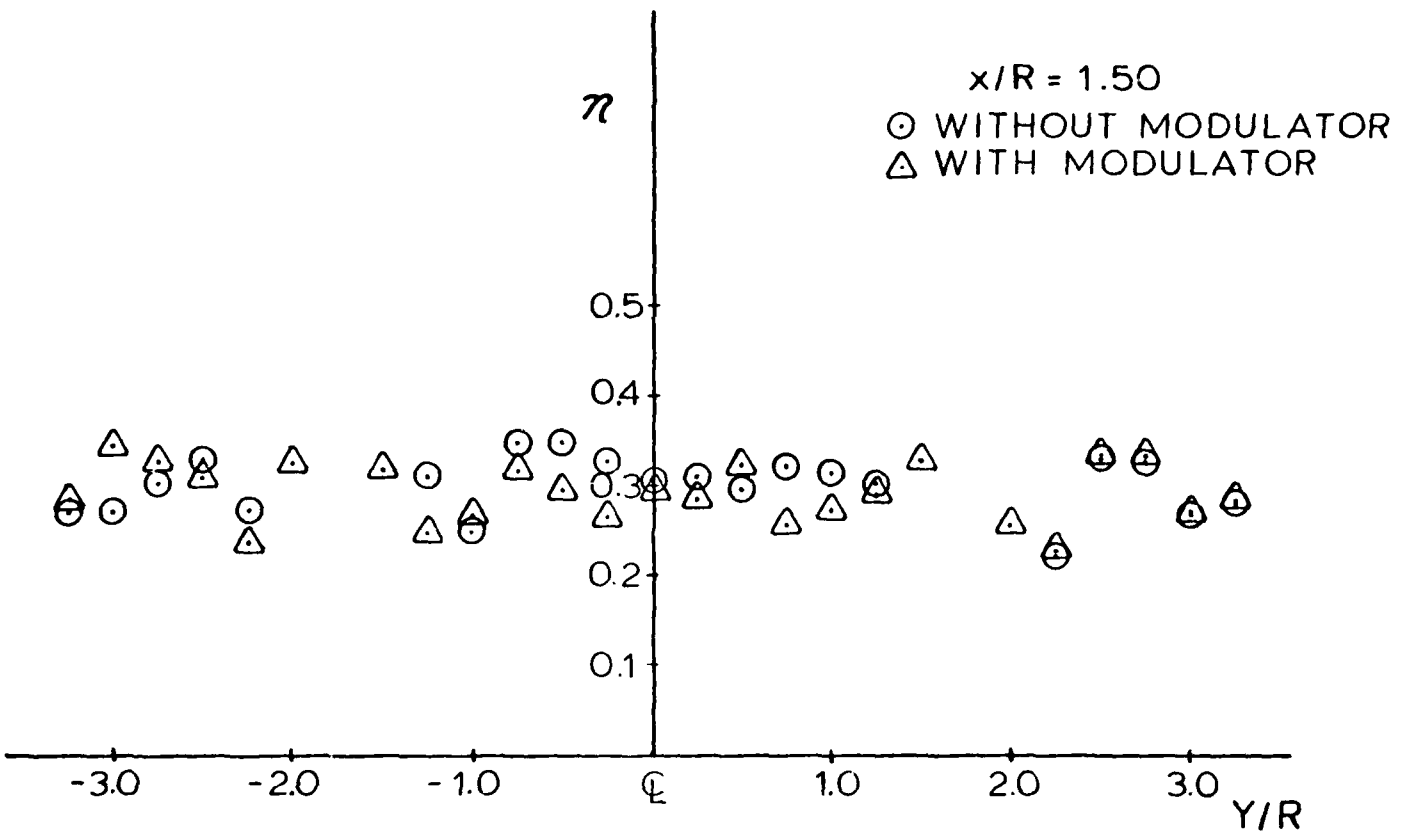

Fig 38. Turbulence Intensity Profiles, 2.0 Inch Diameter Disk

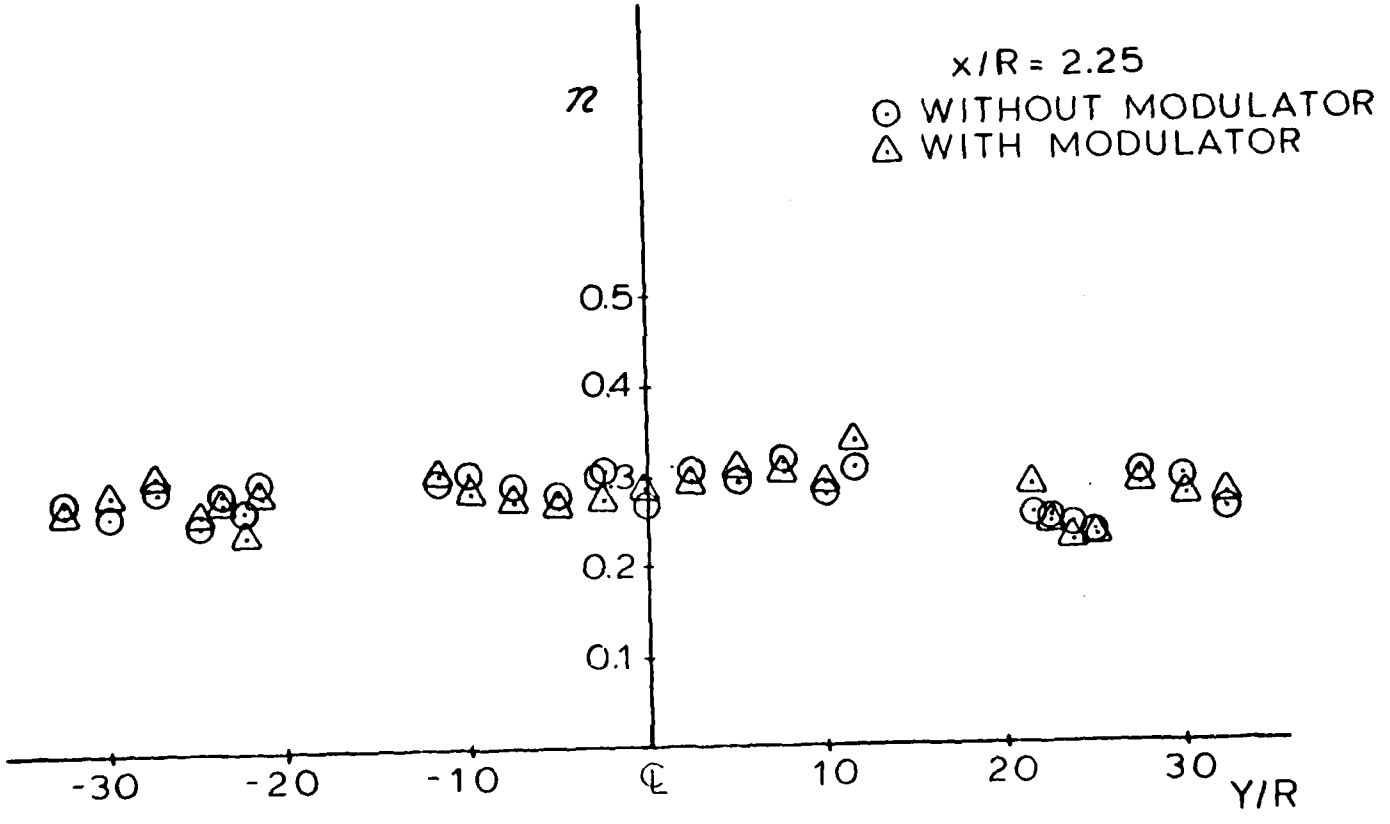

Fig 39. Turbulence Intensity Profiles, 2.0 Inch Diameter Disk

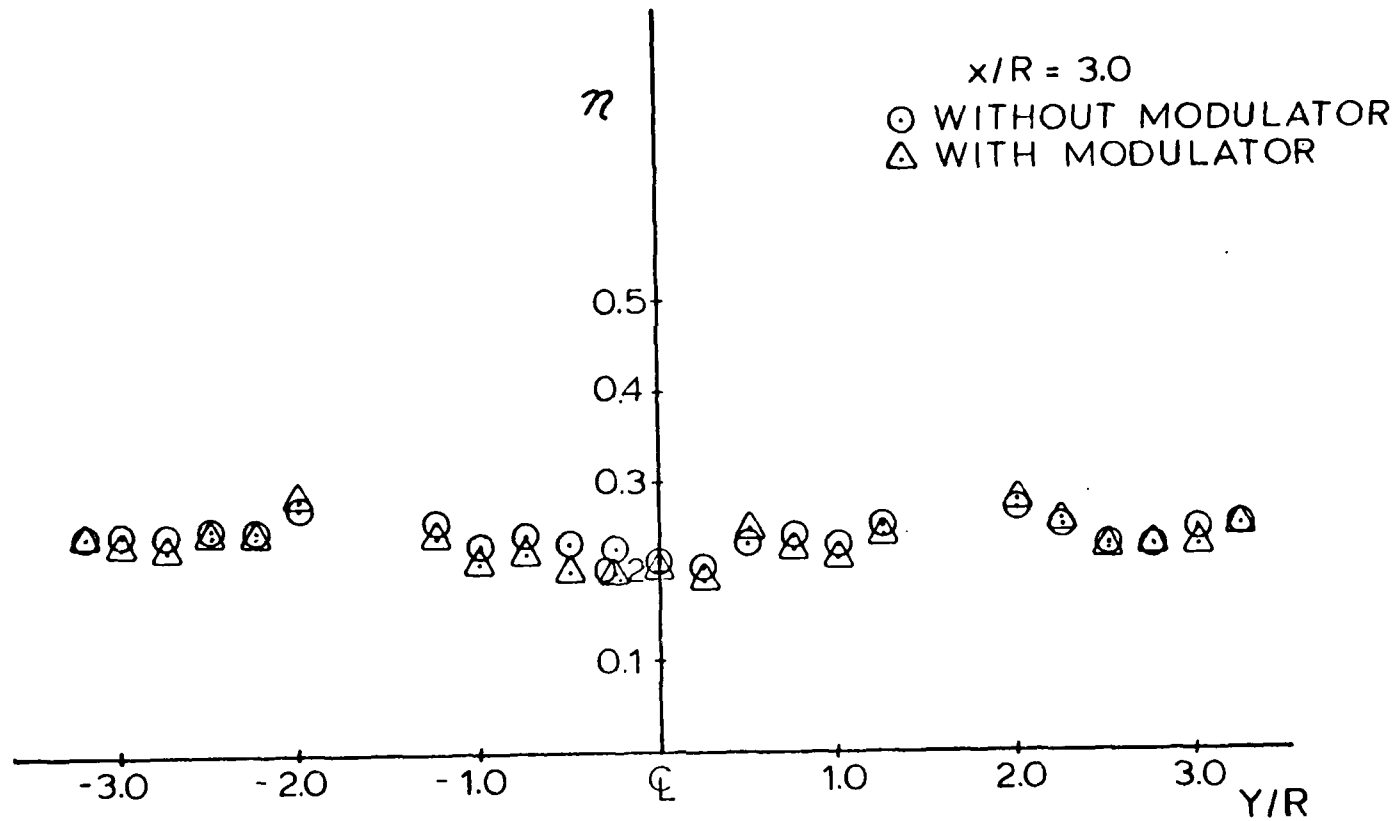

Fig 40. Turbulence Intensity Profiles, 2.0 Inch Diameter Disk

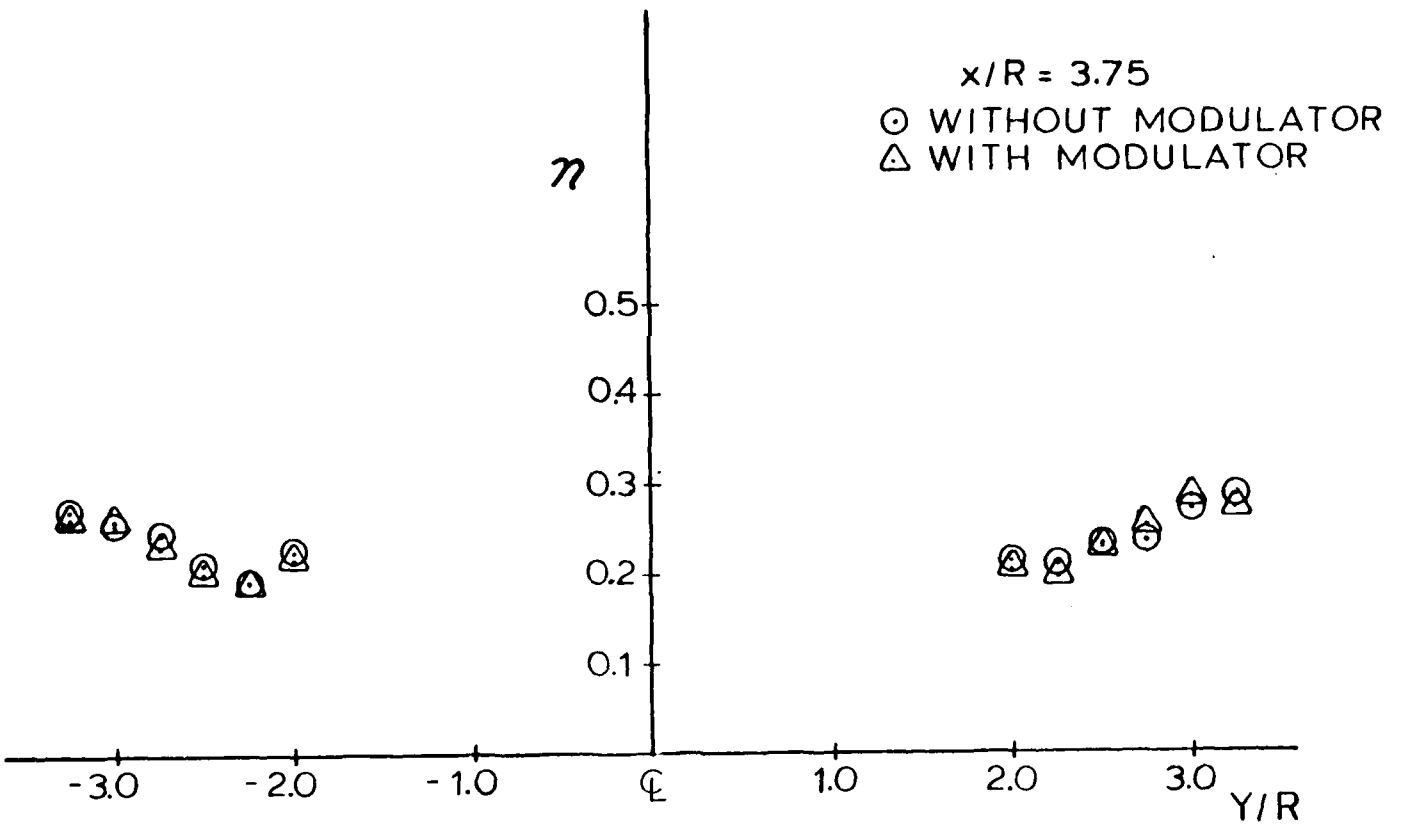

Fig 41. Turbulence Intensity Profiles, 2.0 Inch Diameter Disk

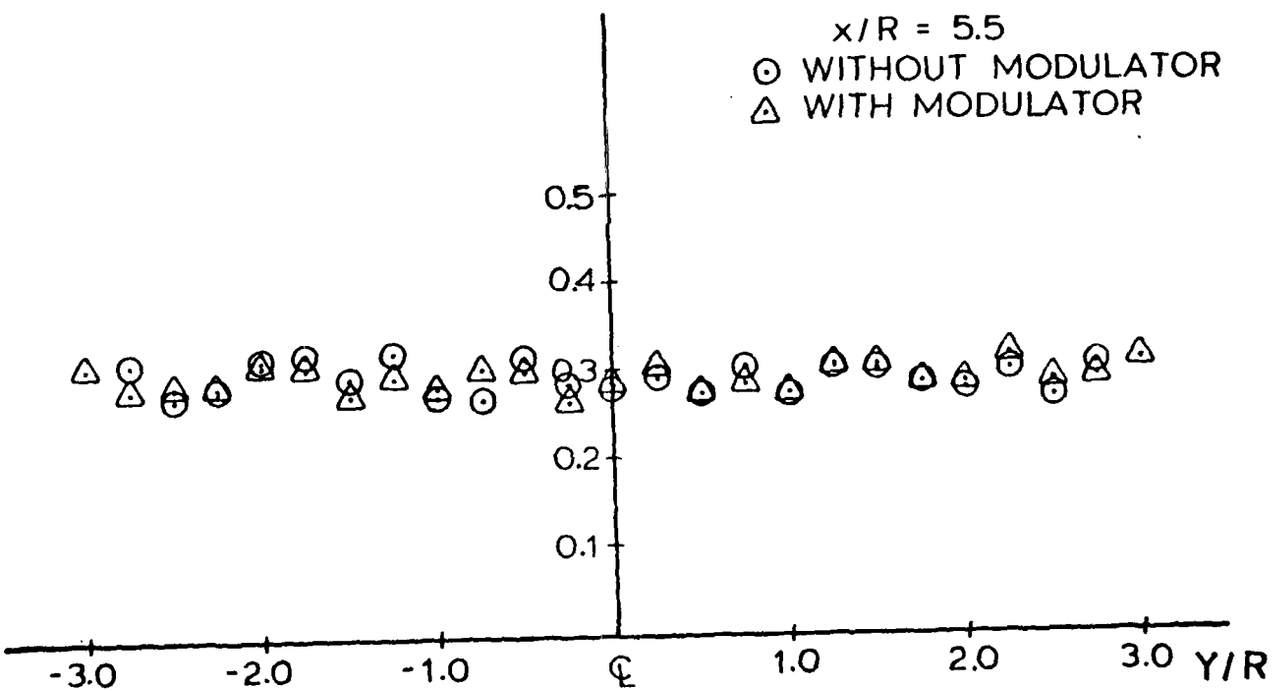

Fig 42. Turbulence Intensity Profiles, 2.0 Inch Diameter Disk

functions was generally good. Figures 43 and 44 present a summary of the turbulence intensity profiles obtained from the without modulation graphs. From these curves the turbulence intensities appear to remain relatively constant across the width of the flow. The variations in turbulence intensities as a function of downstream location also fail to produce any obvious trends of increasing or decreasing values. $x/R = 3.0$ does appear to have consistently lower levels in the recirculation zone; however, due to the approximate nature of these values, a conclusion cannot be made.

1.5 inch diameter disk. This section presents data obtained in the near wake of the 1.5 inch diameter circular disk. These tests were accomplished at the same flow conditions as the 2.0 inch diameter disk with a downstream location of $X/D = 12.0$, and an exit Mach number of 0.35. Table I presents the downstream locations at which traverses were made. These dimensions were chosen such that the nondimensional values of x/R would be the same for both disks. An x/R of 0.375 was not accomplished for the 1.5 inch diameter disk because of interference created by the proximity of the laser beam passage to the circular disk. Data obtained in this area was erratic with an autocorrelation function resulting even in the absence of flow and phase modulation.

Figures 45 through 56 present the mean velocity curves at the respective downstream locations. As in the case with the 2.0 inch diameter disk, agreement between the

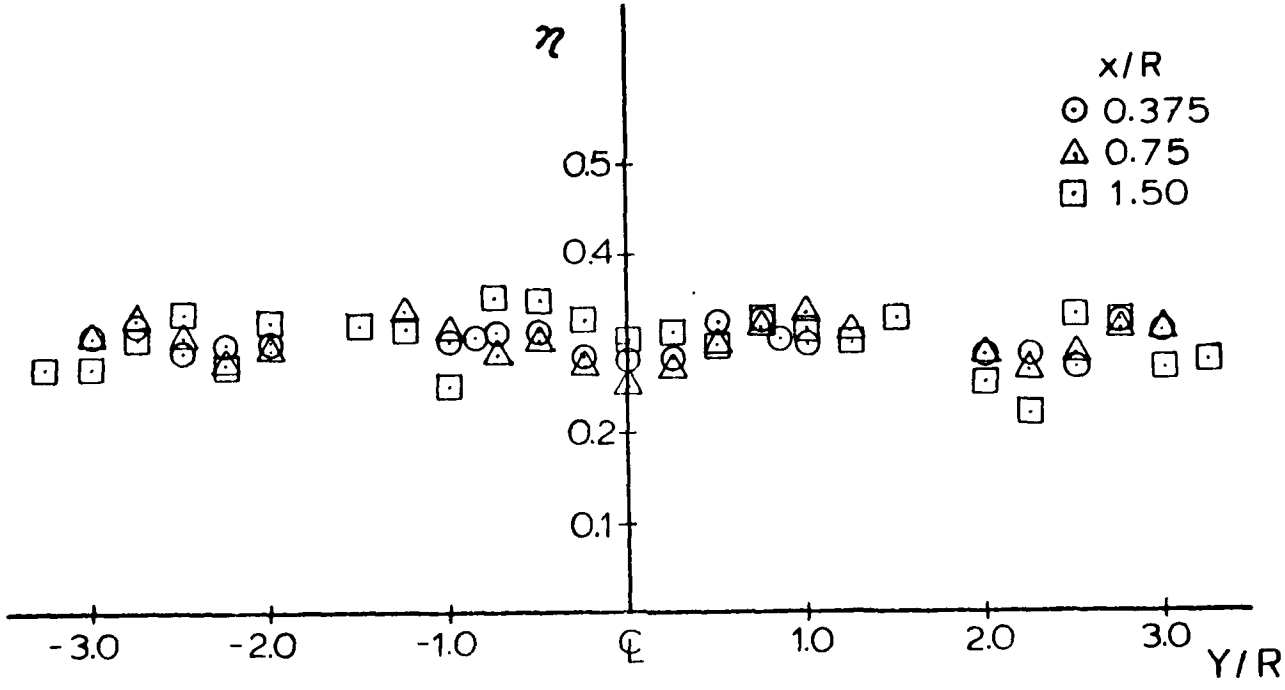

Fig 43. Turbulence Intensity Profile Summary, 2.0 Inch Diameter Disk

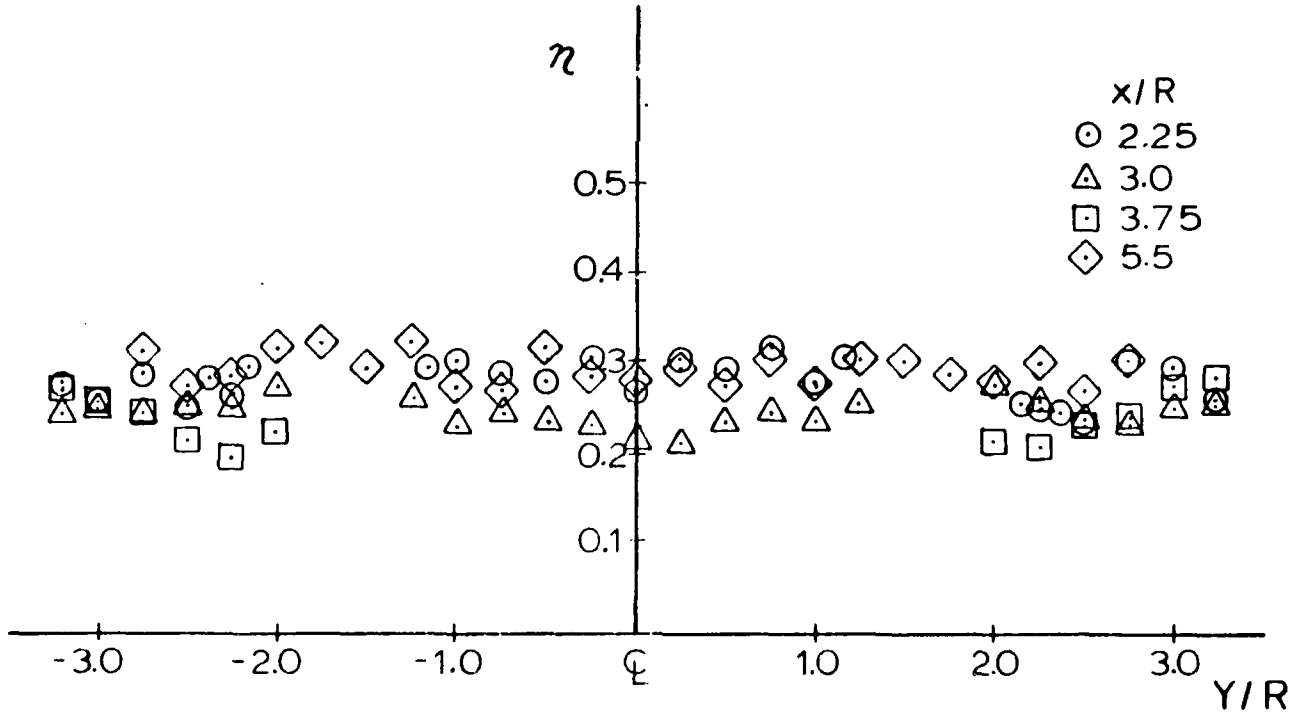

Fig 44. Turbulence Intensity Profile Summary, 2.0 Inch Diameter Disk

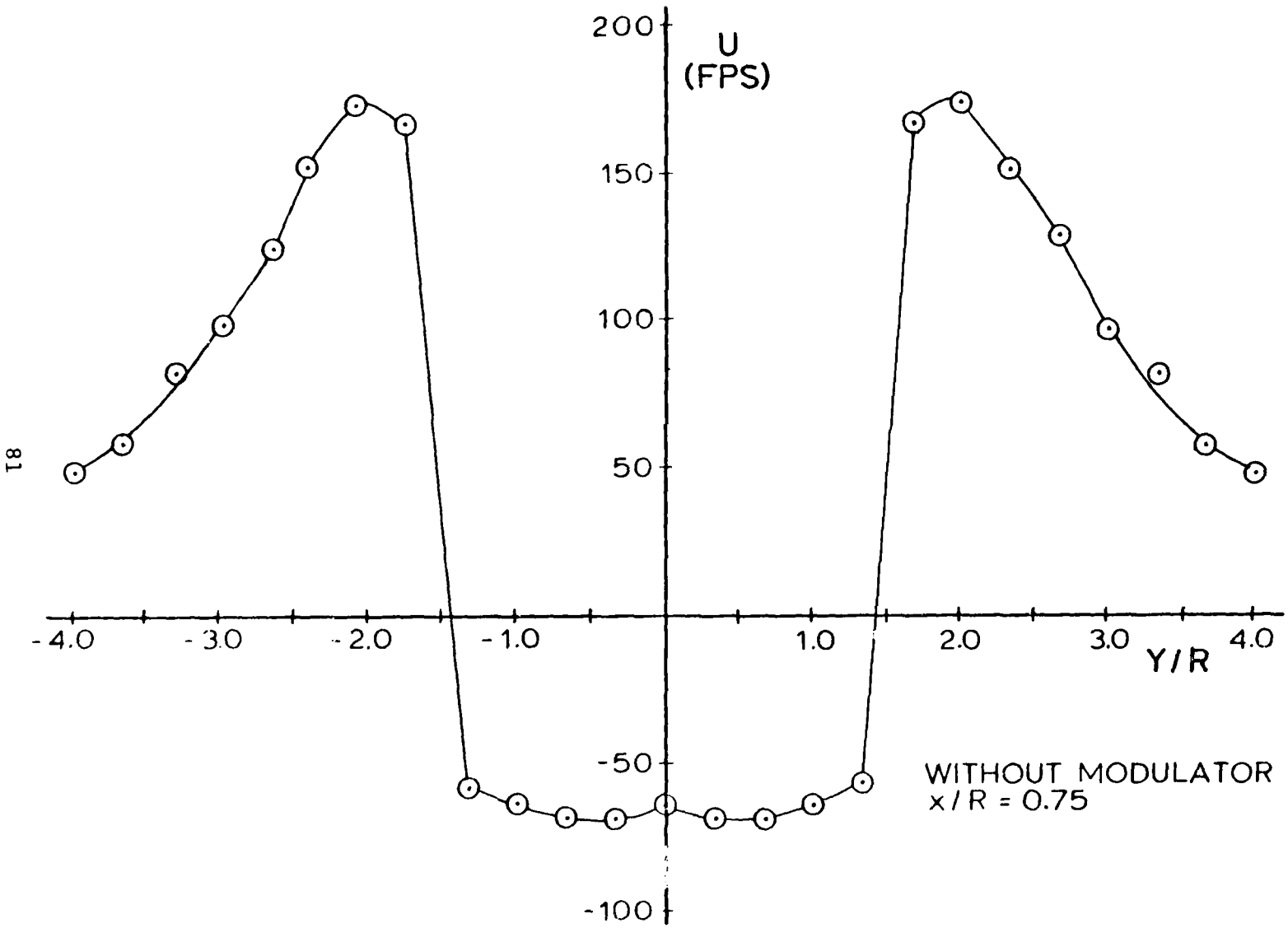

Fig 45. Mean Velocity Profile, 1.5 Inch Diameter Disk

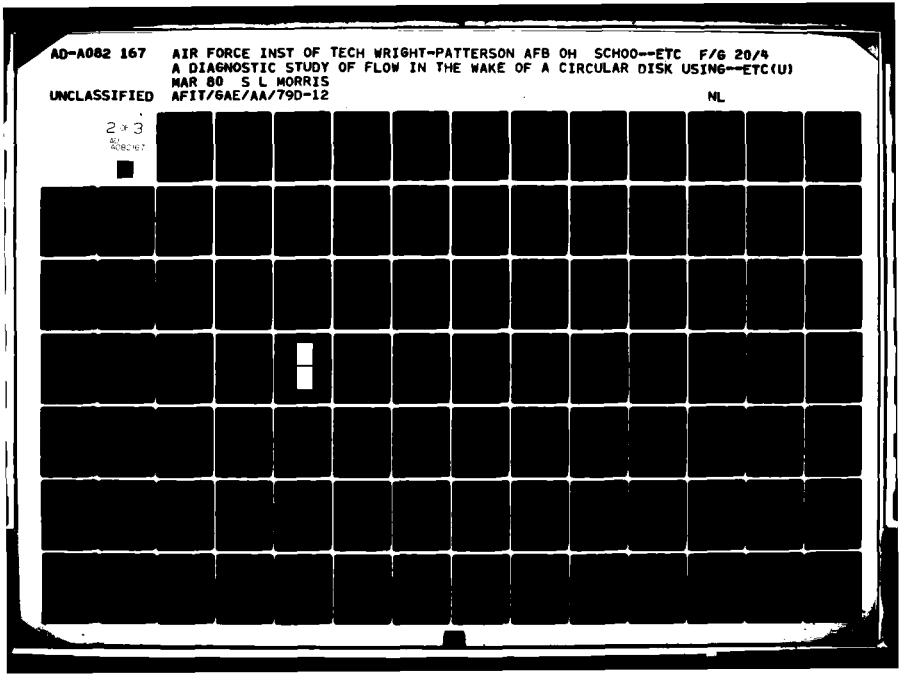
AD-A082 167
AIR FORCE INST OF TECH WRIGHT-PATTERSON AFB OH SCHOO--ETC F/G 20/4
A DIAGNOSTIC STUDY OF FLOW IN THE WAKE OF A CIRCULAR DISK USING--ETC(U)
MAR 80 S L MORRIS
UNCLASSIFIED AFIT/GAE/AA/79D-12
NL
2 * 3
AD
A082167

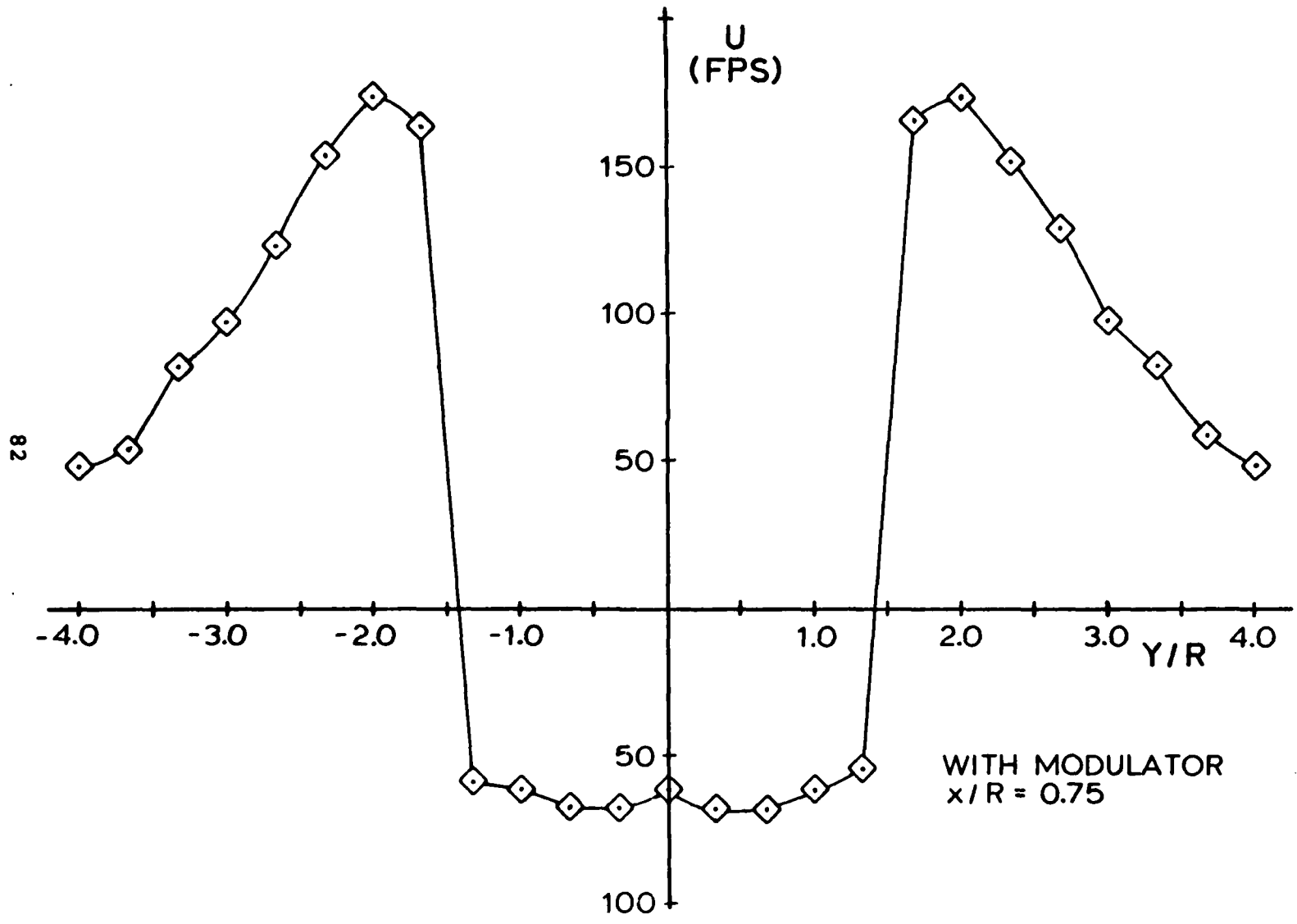

Fig 46. Mean Velocity Profile, 1.5 Inch Diameter Disk

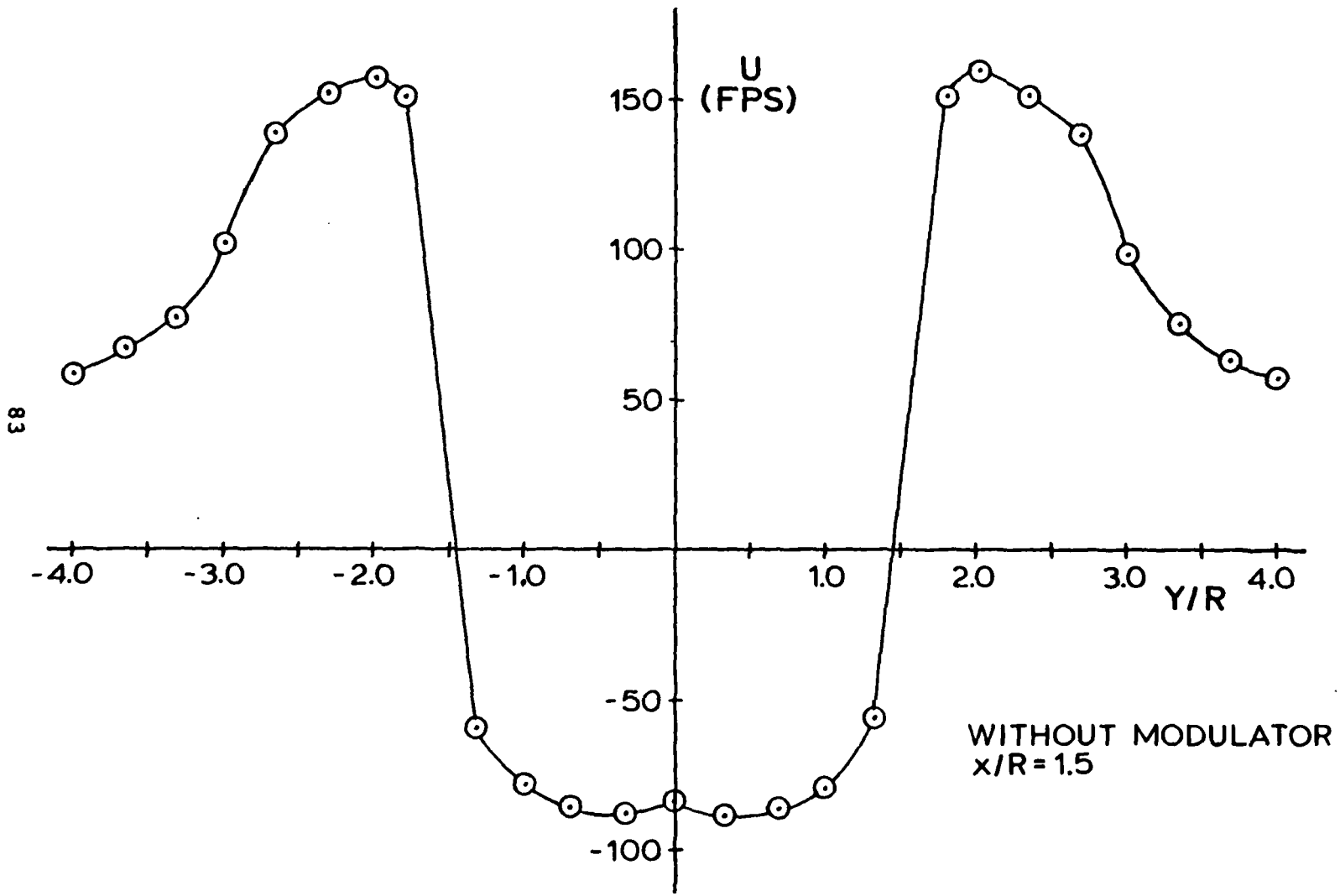

Fig 47. Mean Velocity Profile, 1.5 Inch Diameter Disk

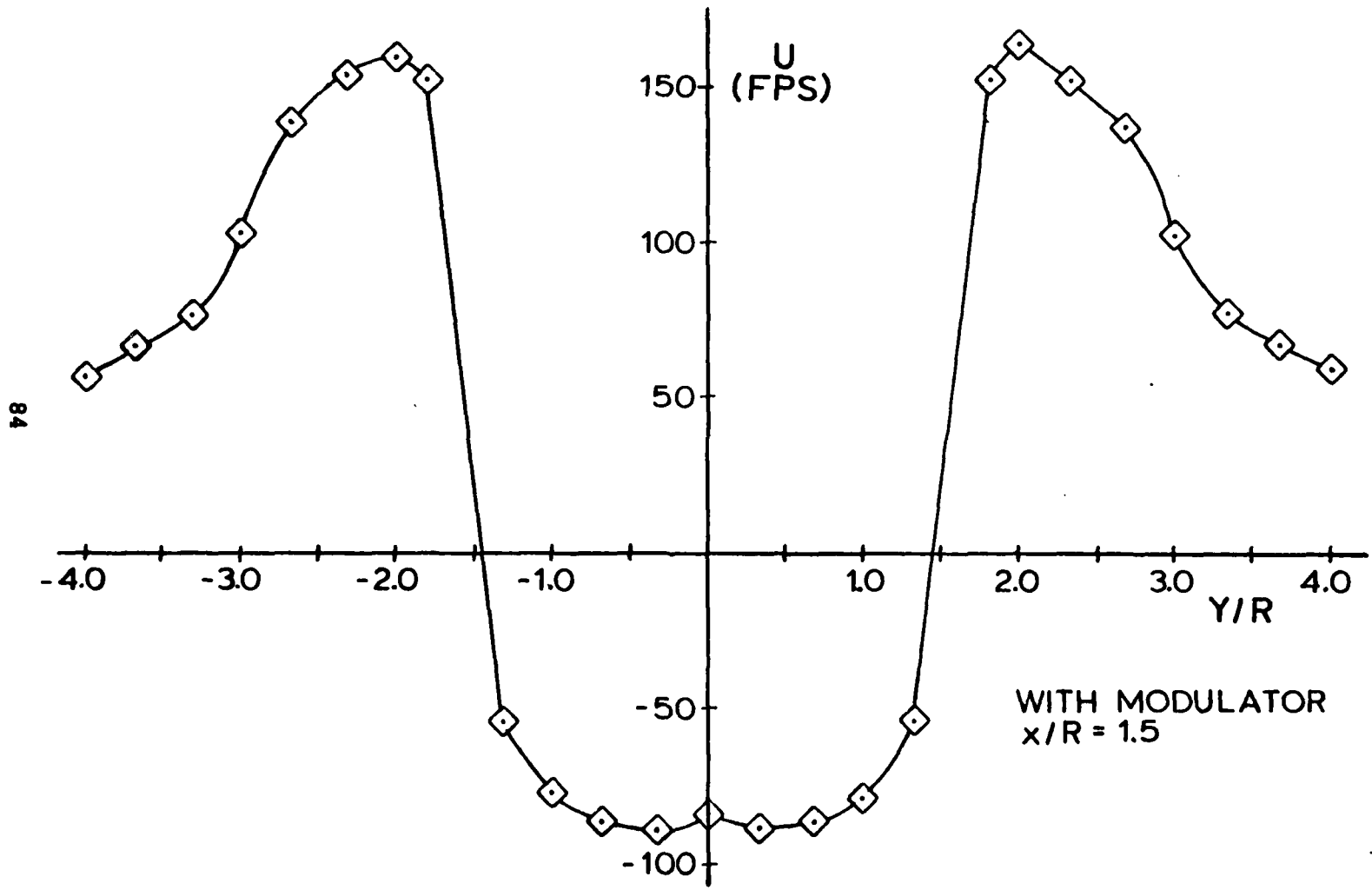

Fig 48. Mean Velocity Profile, 1.5 Inch Diameter Disk

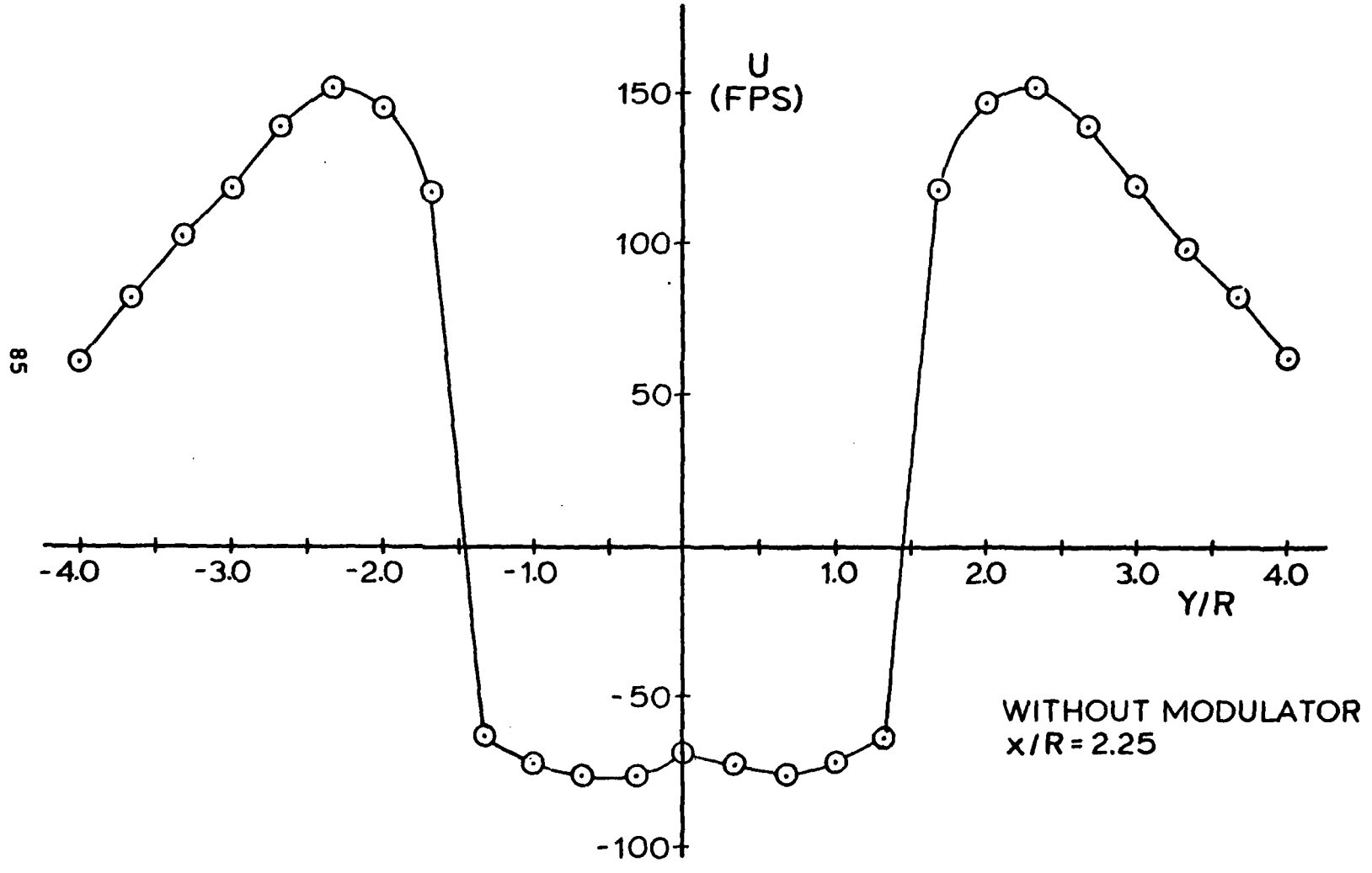

Fig 49. Mean Velocity Profile, 1.5 Inch Diameter Disk

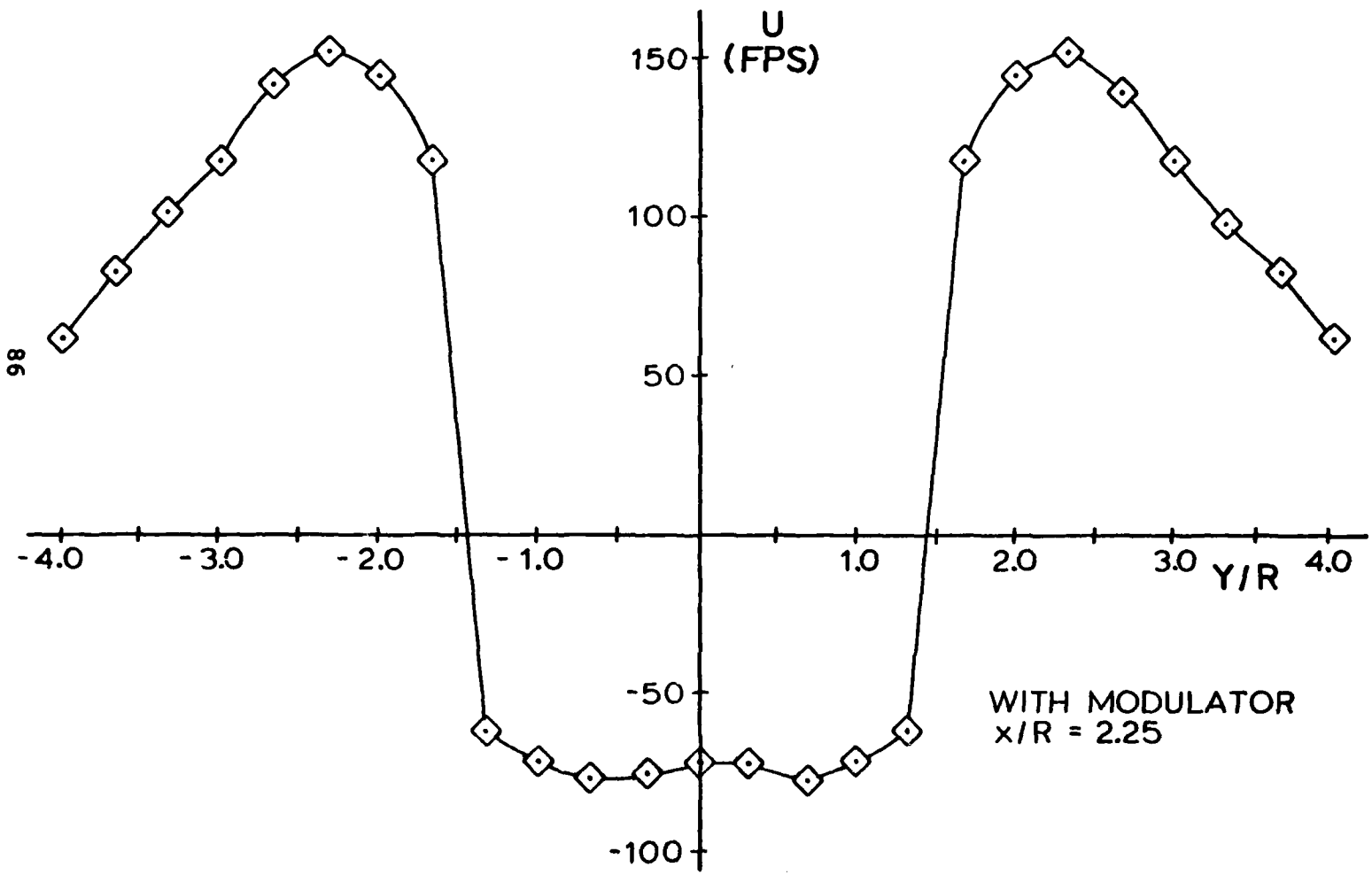

Fig 50. Mean Velocity Profile, 1.5 Inch Diameter Disk

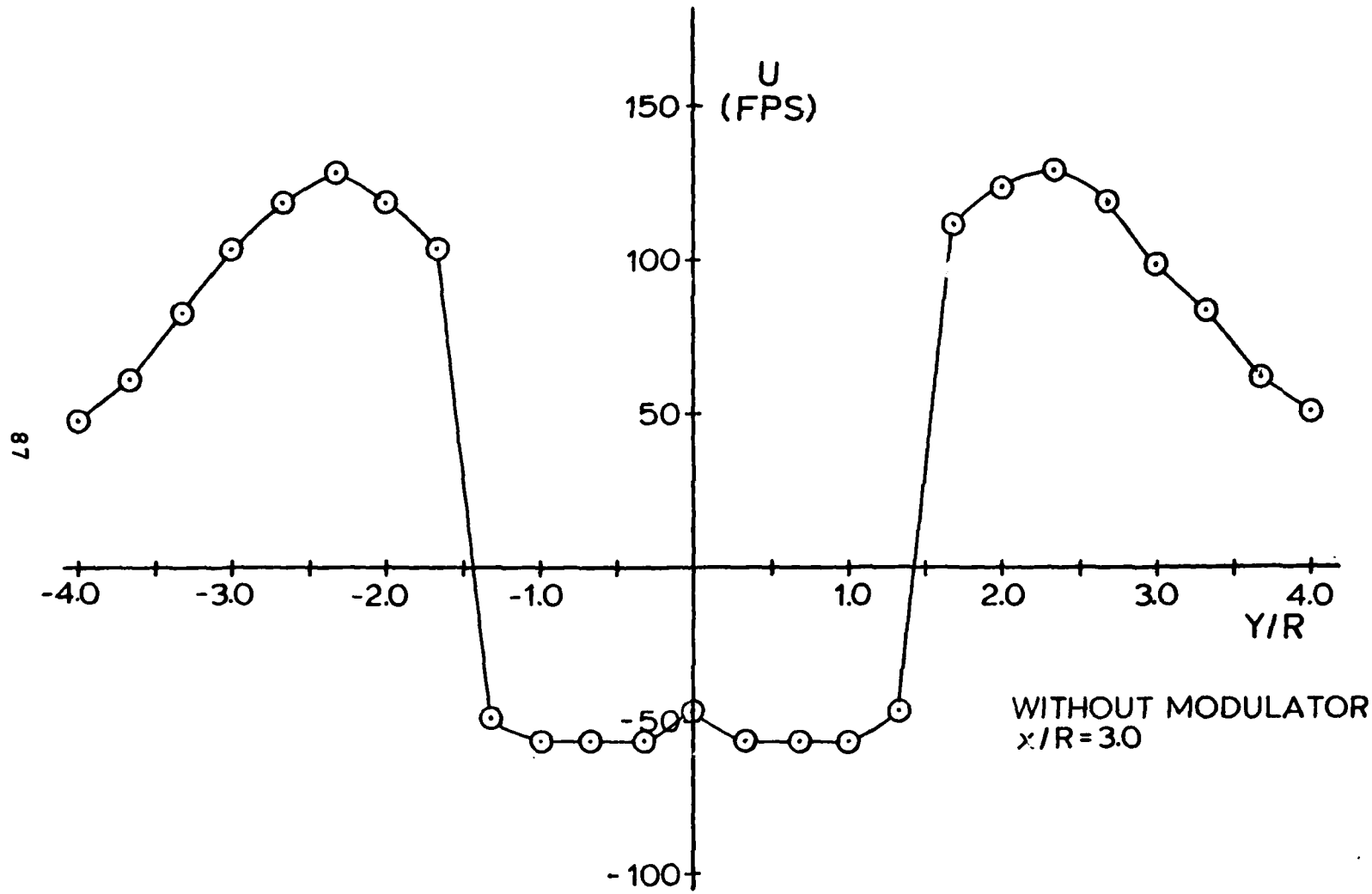

Fig 51. Mean Velocity Profile, 1.5 Inch Diameter Disk

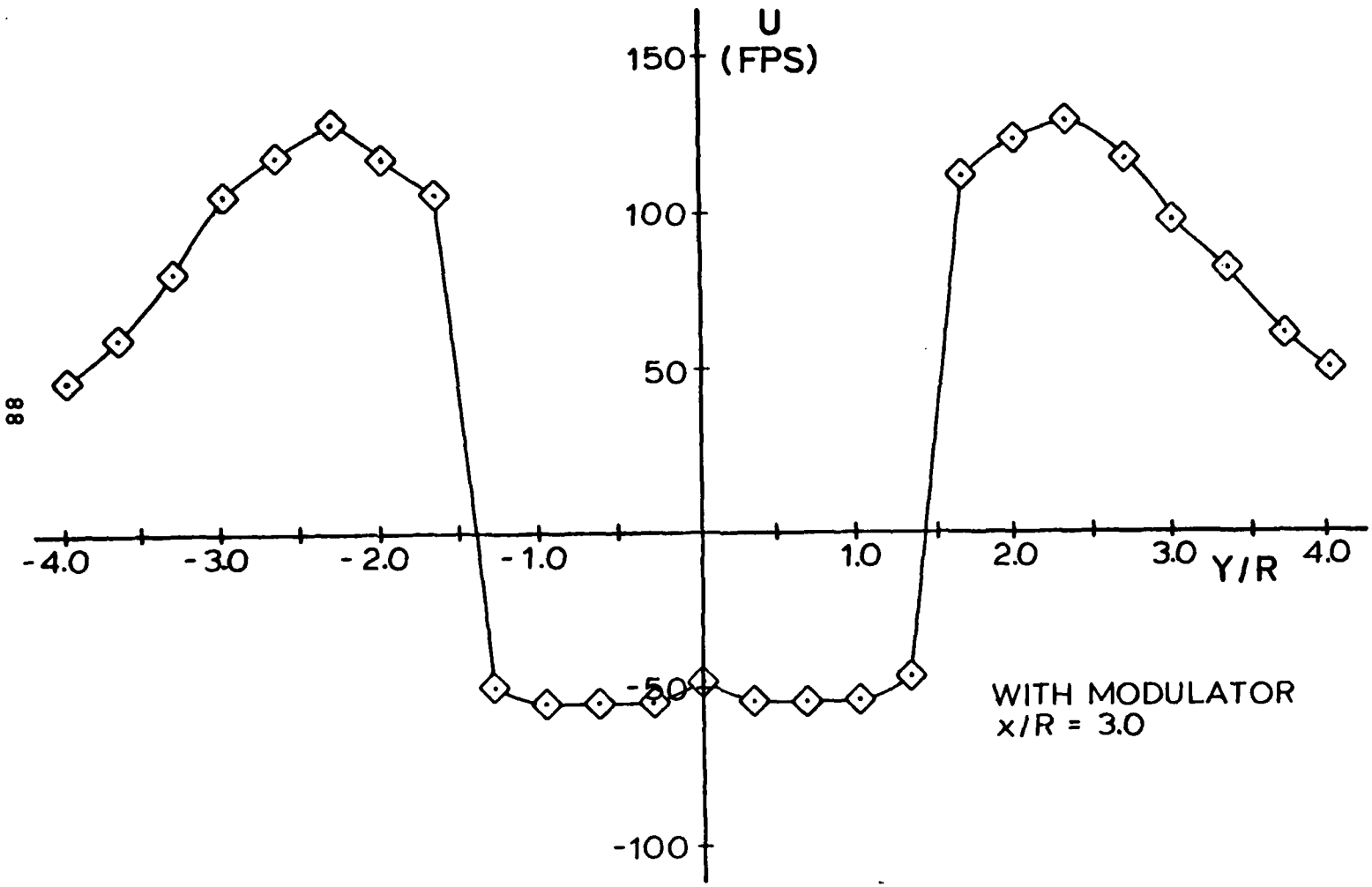

Fig 52. Mean Velocity Profile, 1.5 Inch Diameter Disk

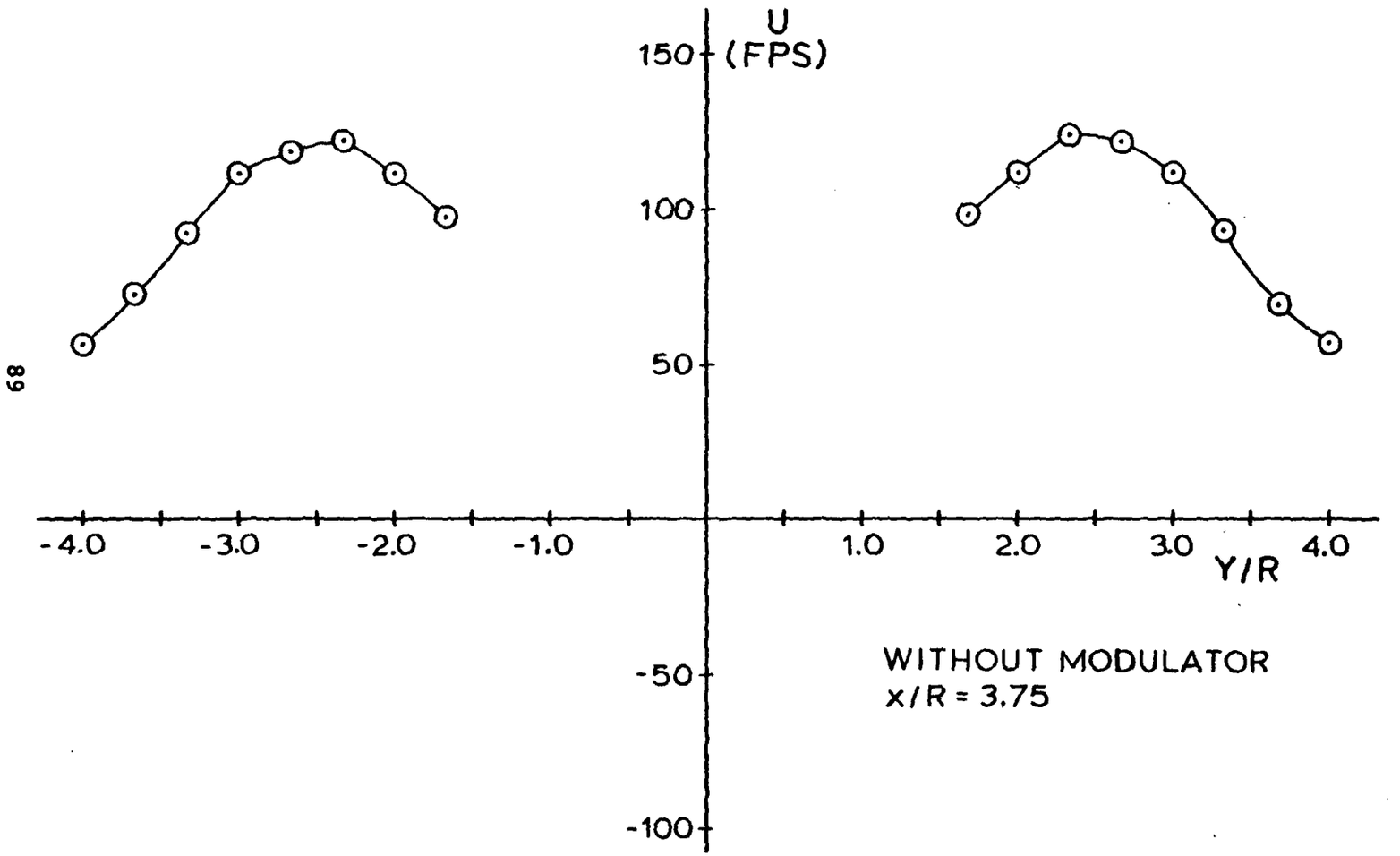

Fig 53. Mean Velocity Profile, 1.5 Inch Diameter Disk

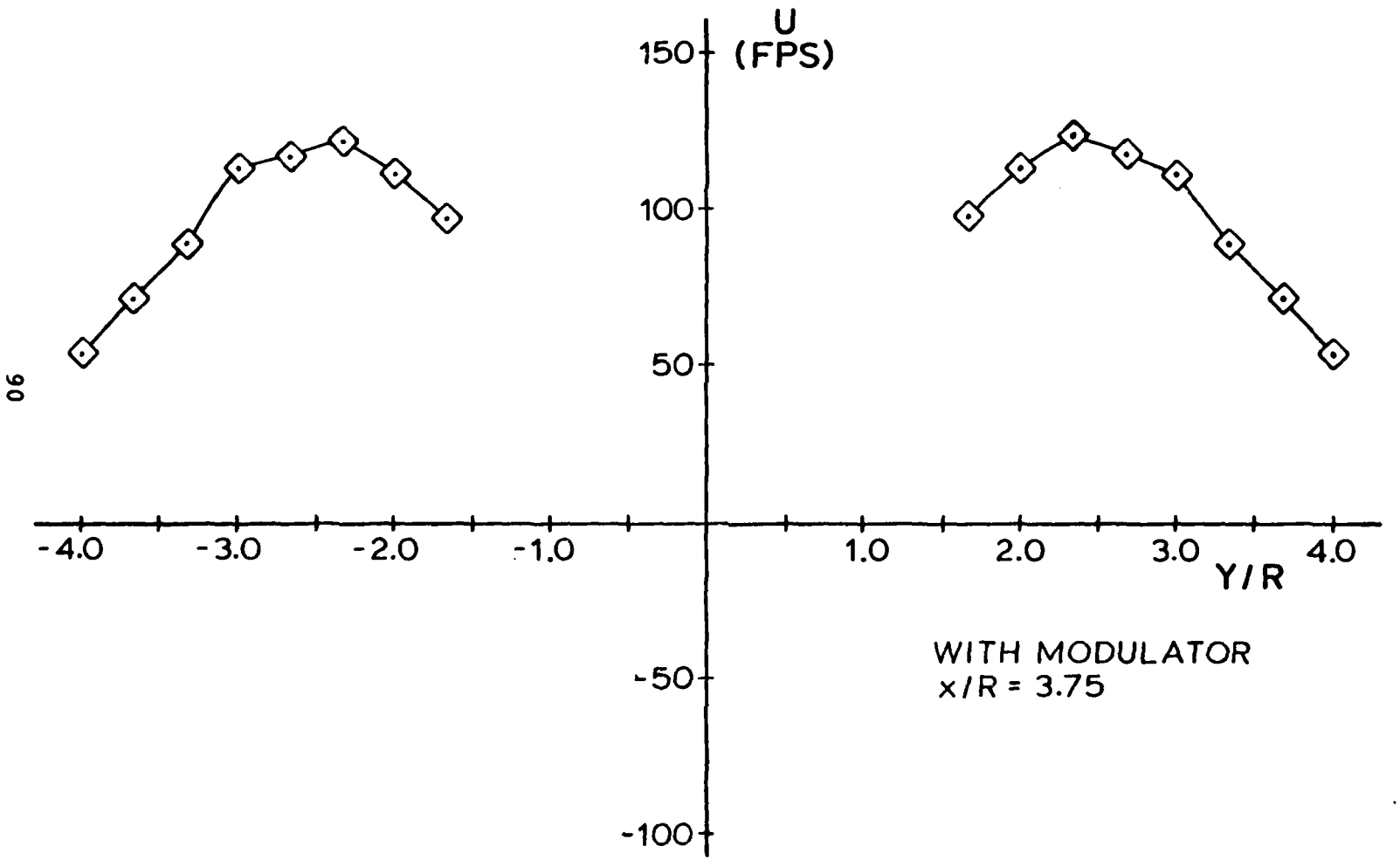

Fig 54. Mean Velocity Profile, 1.5 Inch Diameter Disk

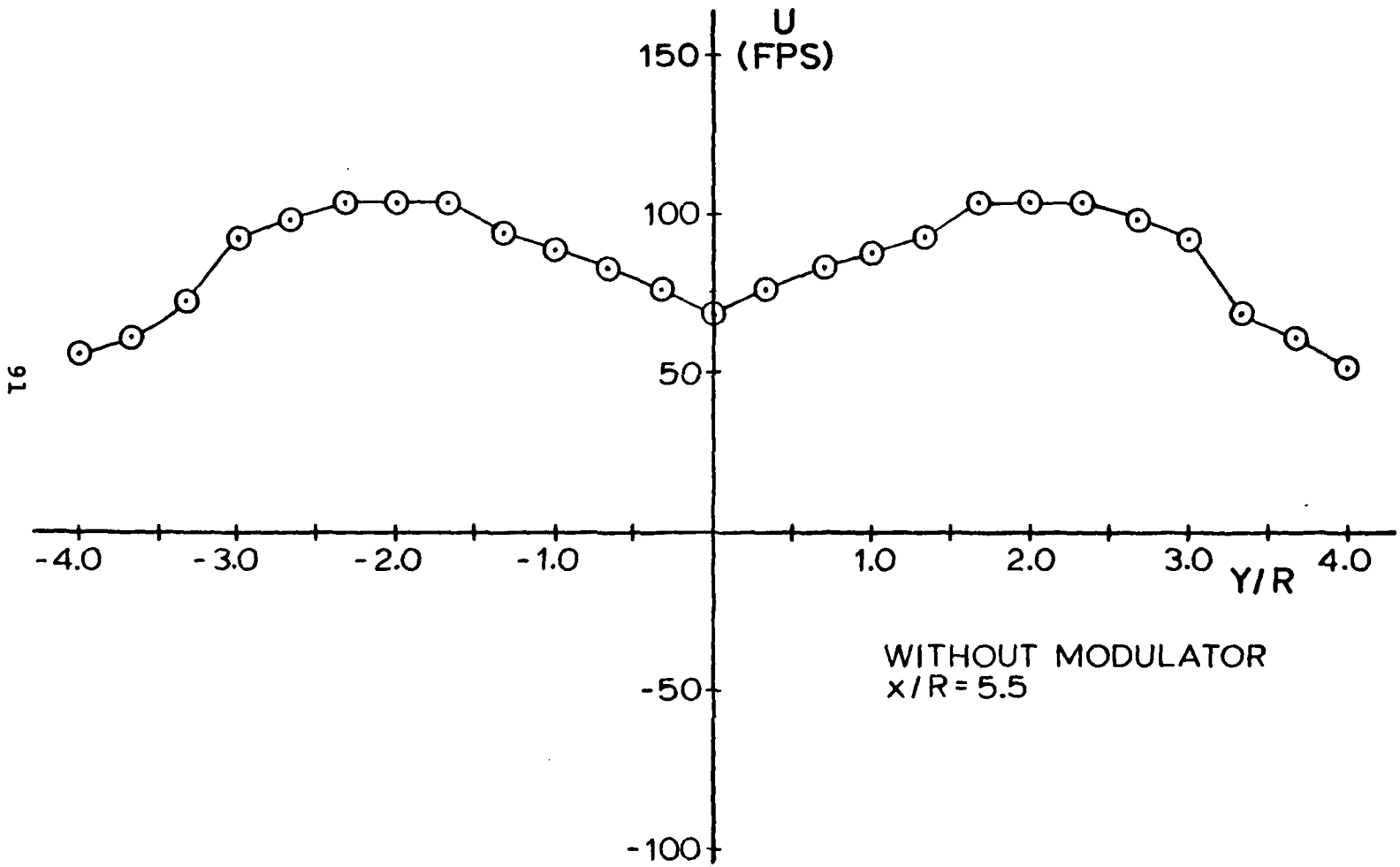

Fig 55. Mean Velocity Profile, 1.5 Inch Diameter Disk

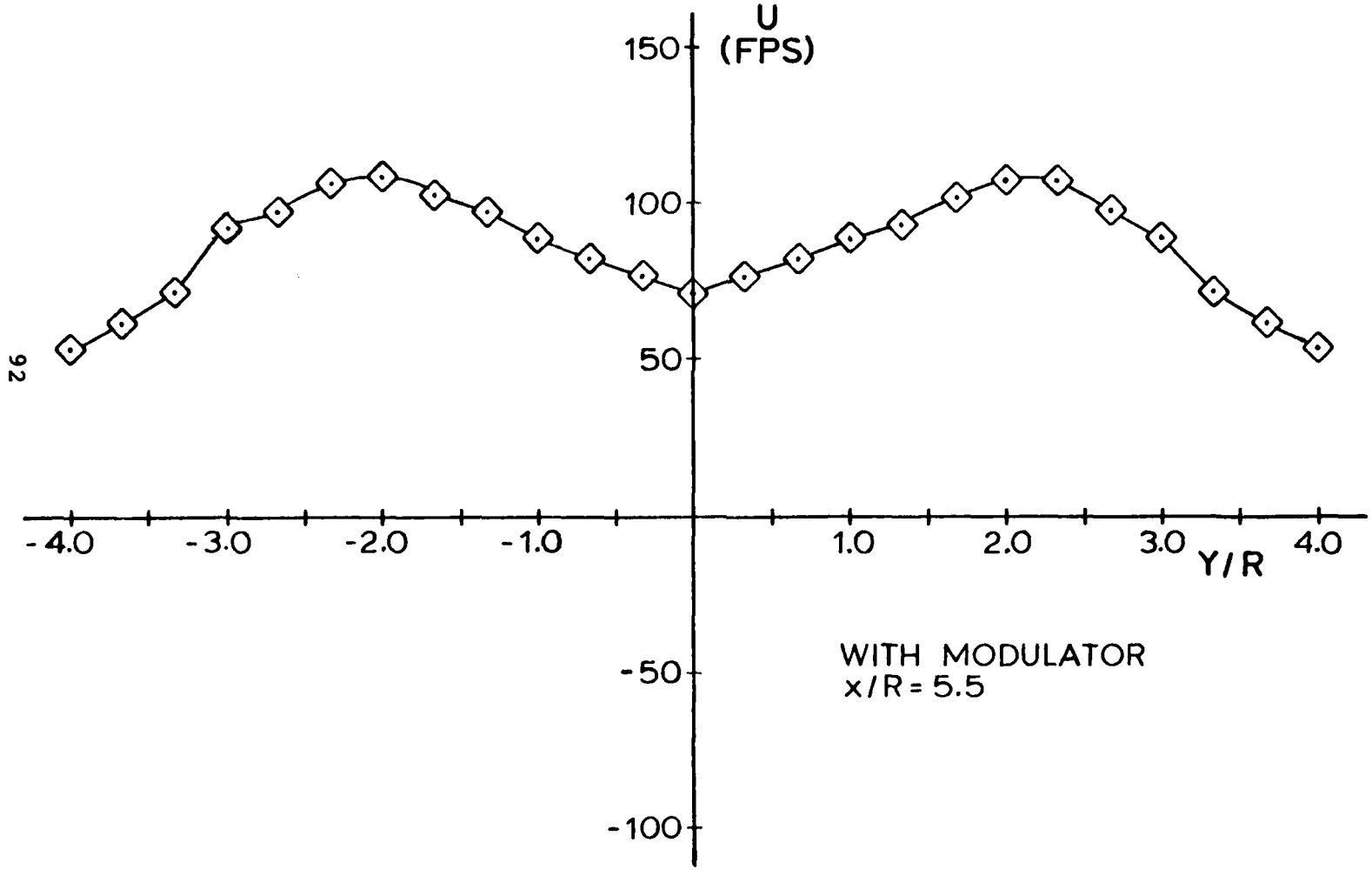

Fig 56. Mean Velocity Profile, 1.5 Inch Diameter Disk

curves obtained from the with and without phase modulation autocorrelation functions was very good. Figure 57 provides a summary of the mean velocity profiles acquired with the laser velocimeter system (taken from the without phase modulation autocorrelation functions).

From Fig 57, the width of the recirculation zone reached a maximum value of approximately 1.4 disk diameters. This differs slightly from the width of the zone found with the 2.0 inch diameter disk. The region over which data was unobtainable due to high turbulence intensities was greater for the 2.0 inch disk than for the 1.5 inch disk, making the recirculation zone boundary less of an approximation for the later case. The recirculation length was determined to be approximately 3.75 disk radii. This is in total agreement with the results obtained with the 2.0 inch diameter disk and is further supported by the schlieren study and the findings in Refs 5 and 24.

Figure 57 compares the velocity profiles obtained at each stream-wise location. The trends which were exhibited with the 2.0 inch diameter study are also exemplified by the 1.5 inch diameter disk. The maximum velocity of each profile decreased as the flow moved downstream of the disk. The slope of the curves in the outer flow regions also decreased as x/R increased. A maximum negative velocity was obtained in the recirculation zone at $x/R = 1.5$. A dip in each negative velocity profile also occurred along the centerline in the near wake of the disk. The velocity profile at $x/R = 5.5$ consisted of only downstream flow

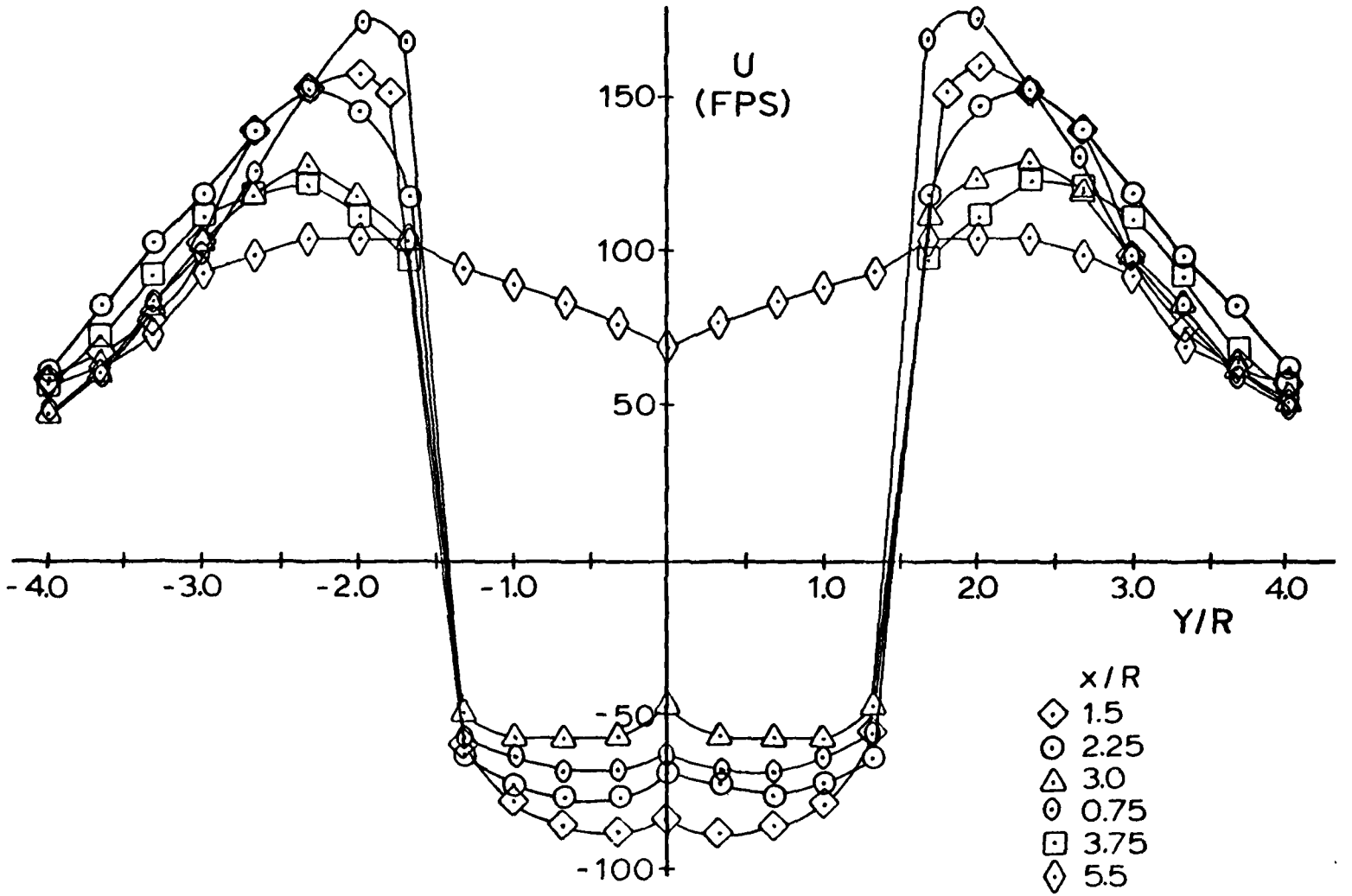

Fig 57. Mean Velocity Profile Summary, 1.5 Inch Diameter Disk

presenting an appearance characteristic of wake flow behind a bluff body.

Figures 58 to 63 provide a comparison of the mean velocity profiles obtained for the two disks at similar nondimensionalized downstream locations. There is a definite similarity observed in the maximum value of the downstream velocity occurring on each profile at the same x/R, with the exception of $x/R = 5.5$. For $x/R = 5.5$, the trends in the curves are similar; however, the velocities are higher for the 1.5 inch diameter disk. This is believed to be due to the decaying nature of the flow originating from a free jet. While the nondimensionalized downstream location is the same for both disks, the physical measurement actually occurs 1.375 inches further downstream of the free jet in the case of the 2.0 inch diameter disk. The velocity profiles of the recirculation zone show a good agreement for both disks at the same x/R, with the maximum values occurring at $x/R = 1.5$.

Variations occurring in the mean velocity profiles of the two disks when compared at the same x/R, could be due in part to the relationship between the disk size and fixed geometry of the free jet. This would not create a problem in a uniform flow; however, in the jet flow, it results in the larger disk encountering a larger portion of the free jet profile. Therefore, the velocities occurring at the edges of the larger disk are not the same as the

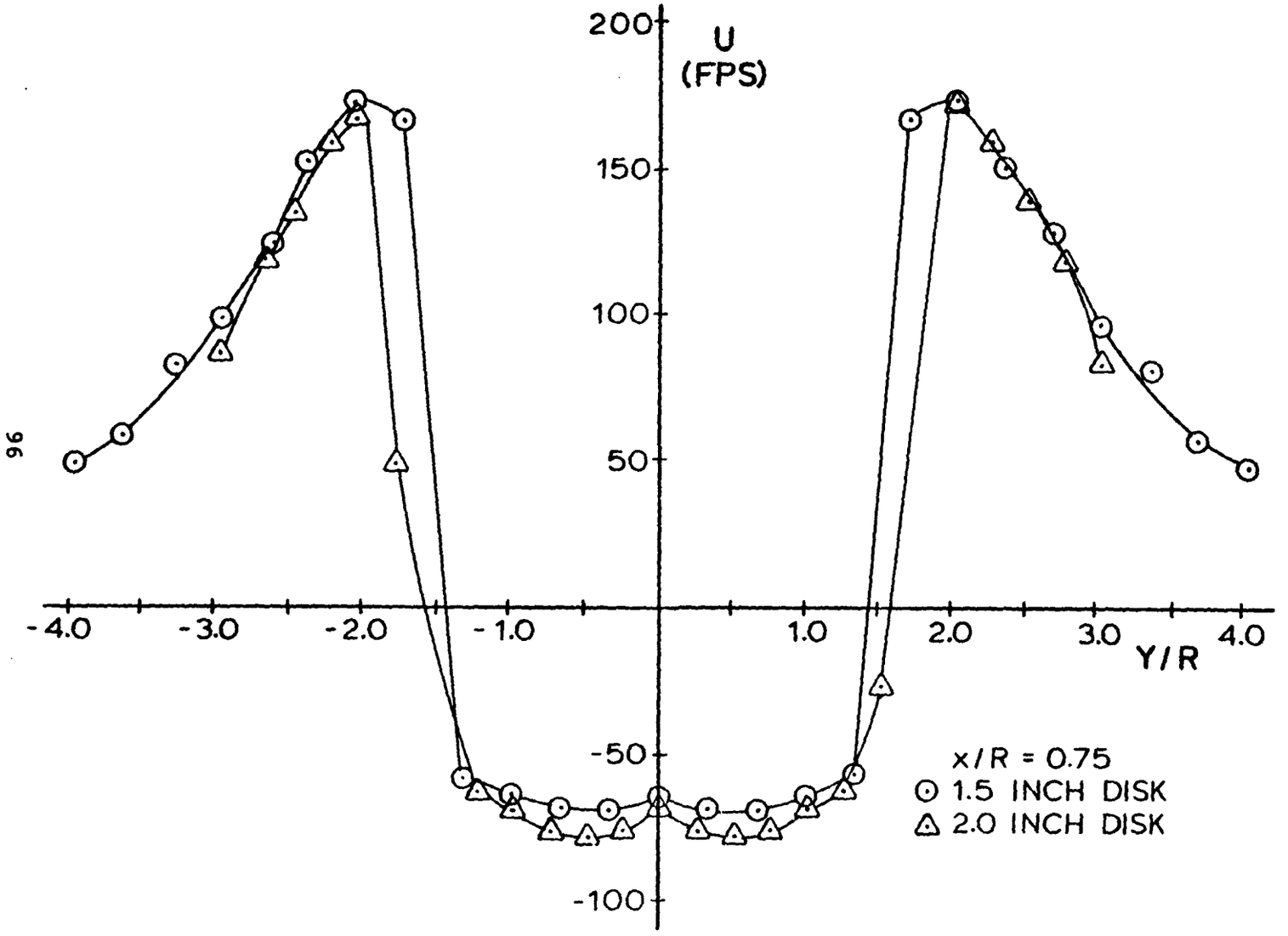

Fig 58. Mean Velocity Profile Comparisons

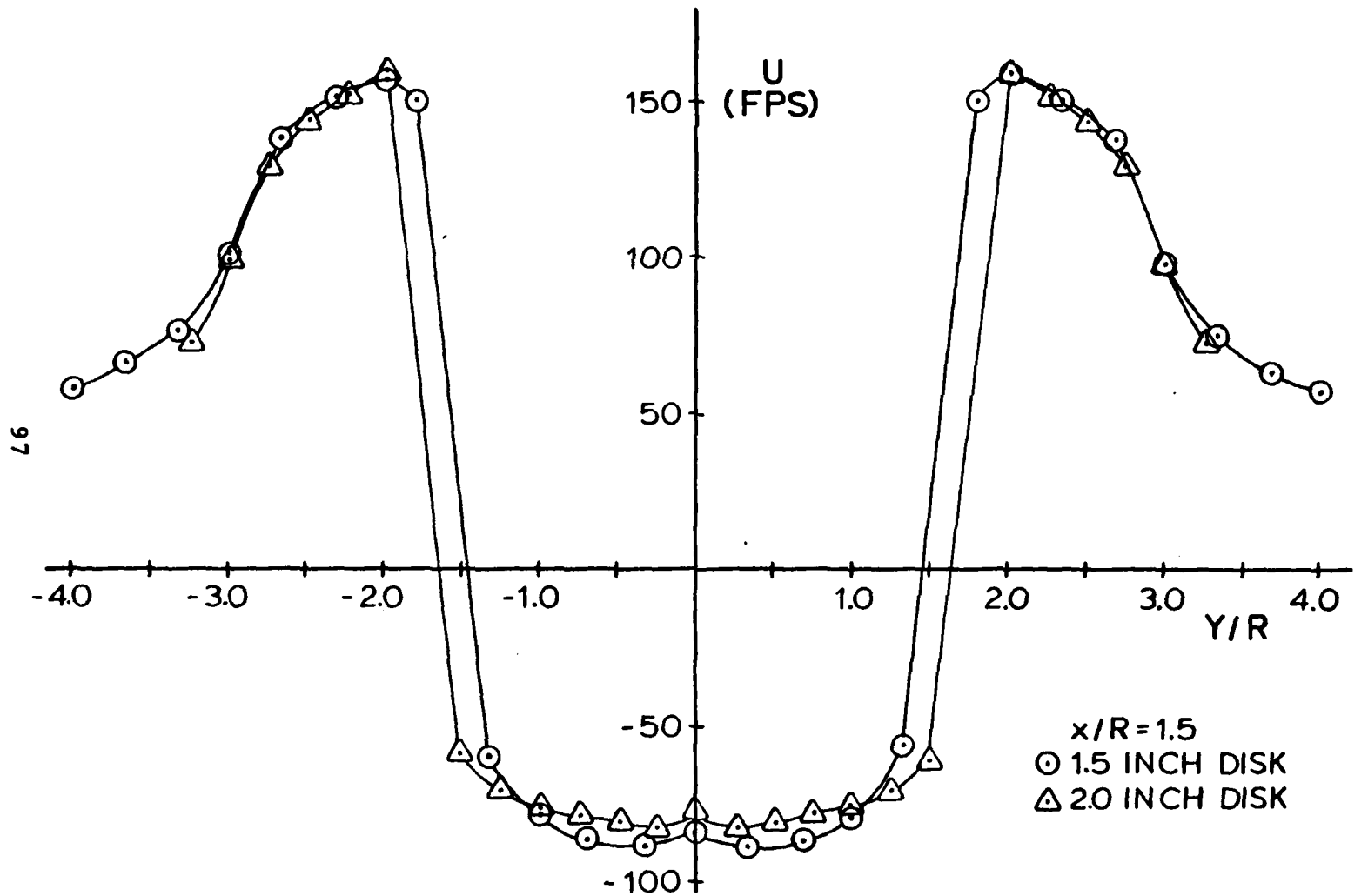

Fig 59. Mean Velocity Profile Comparisons

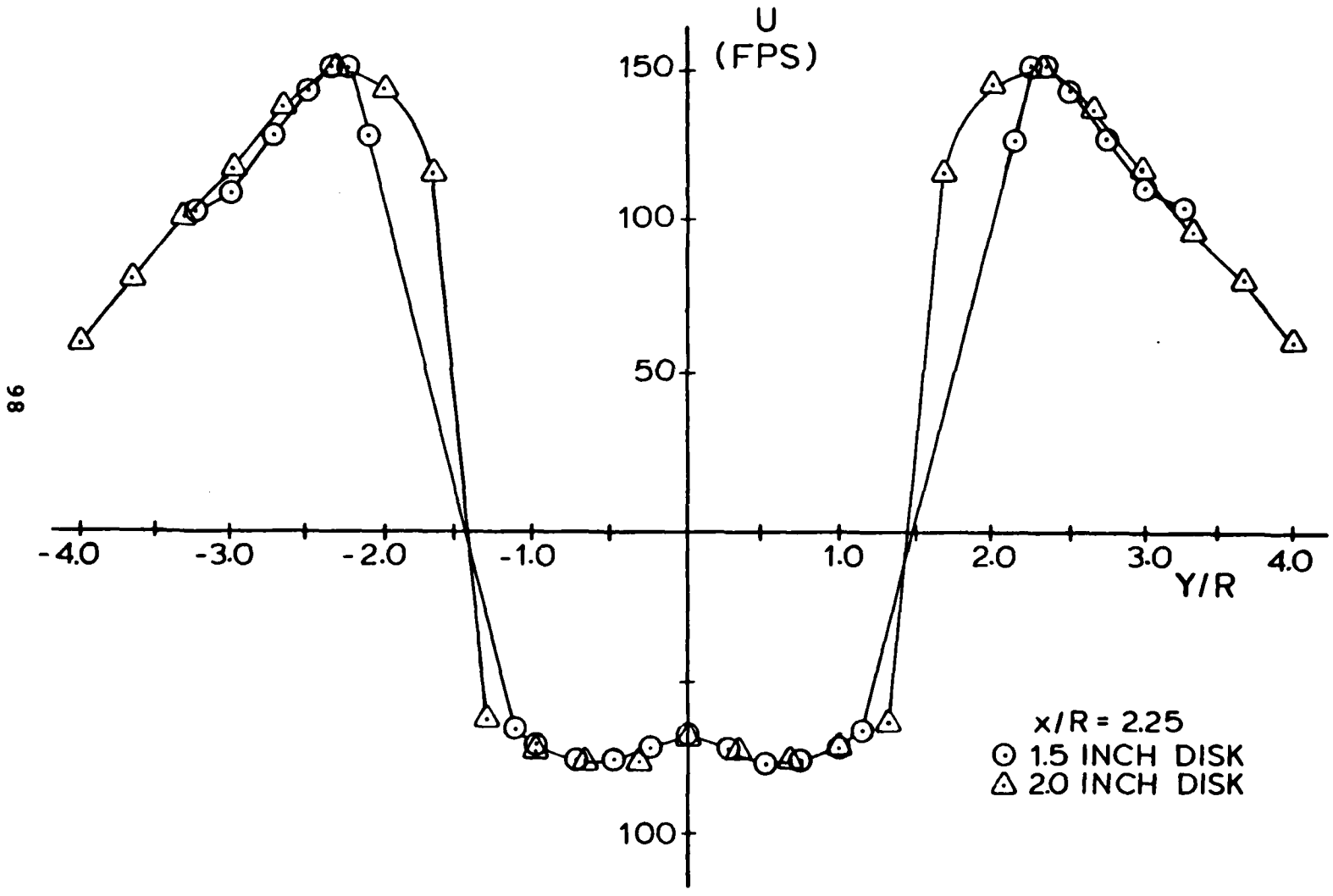

Fig 60. Mean Velocity Profile Comparisons

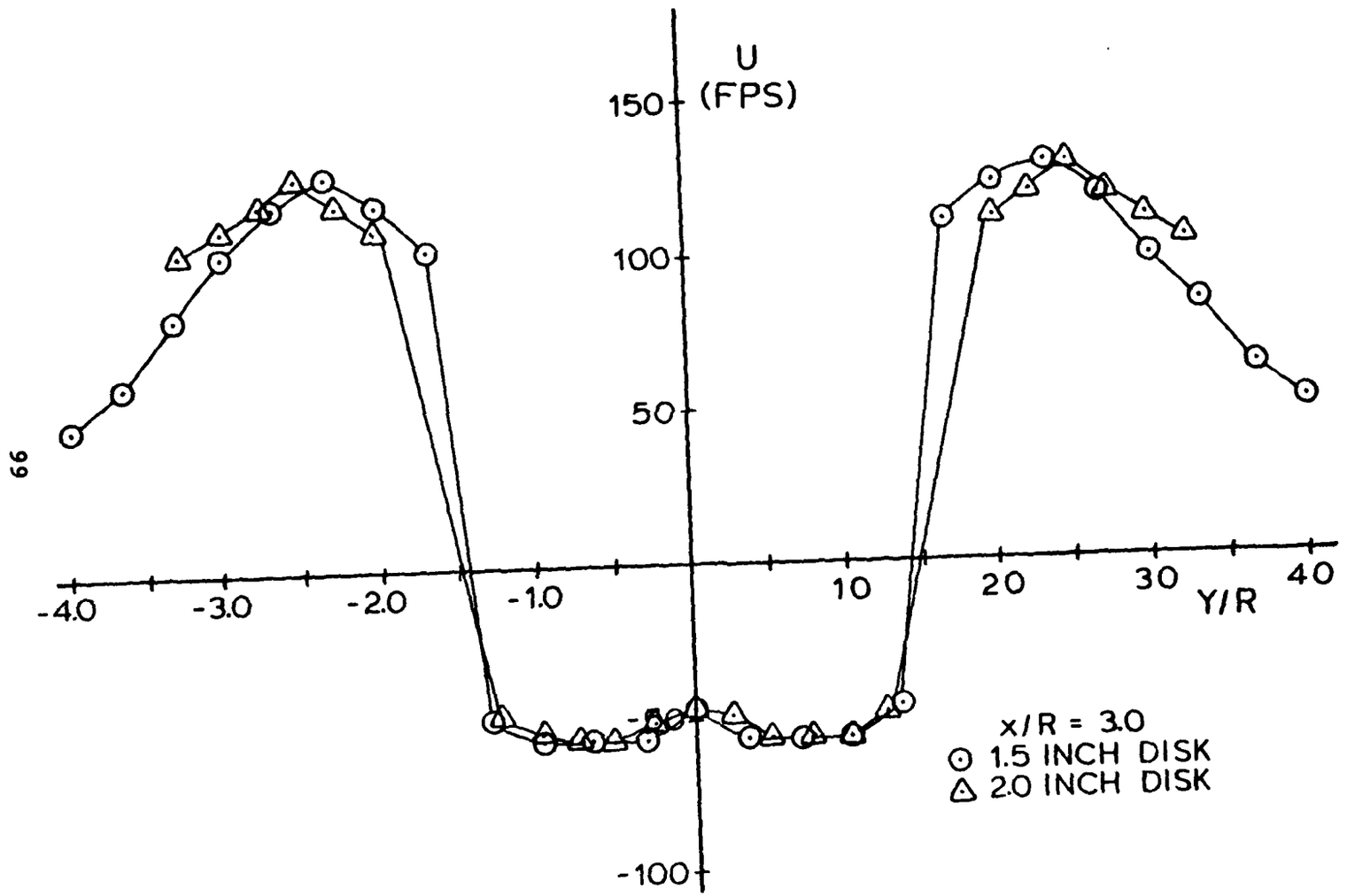

Fig 61. Mean Velocity Profile Comparisons

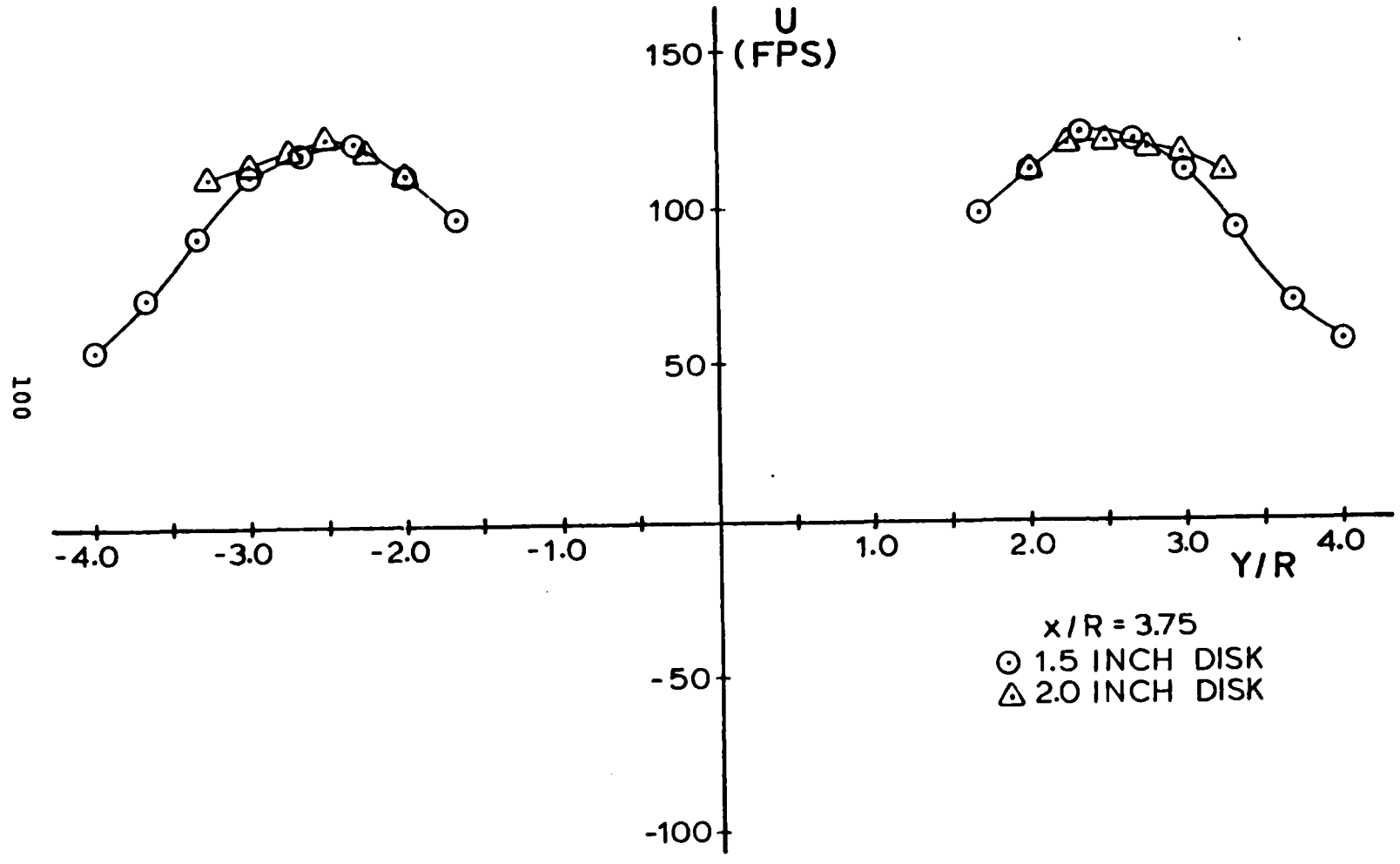

Fig 62. Mean Velocity Profile Comparisons

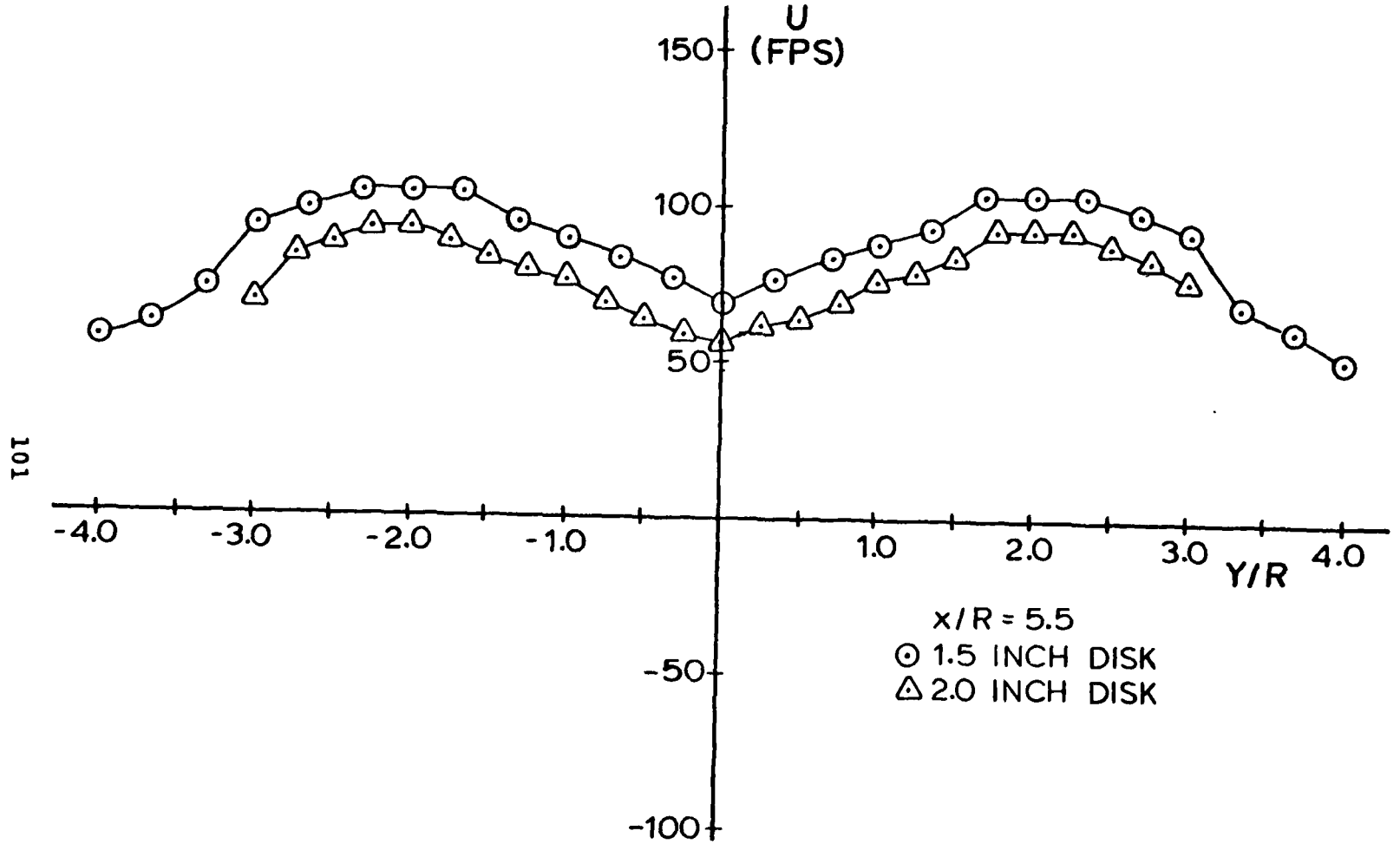

Fig 63. Mean Velocity Profile Comparisons

velocities encountered at the edges of the smaller one. To create an identical test condition for both disks, the jet size should be varied such that the ratio of the disk to jet diameters would be the same in each case. This would also require that the distances from the exit plane be different for the two disks such that their X/D values were the same.

The turbulence intensities for the 1.5 inch diameter disk are presented in Figs 64 through 69. The profiles tend to demonstrate a relatively constant level across the width of the flow with the most common turbulence intensities occurring in the "neighborhood of" 25% to 30%. For the x/R = 3.0 profile the turbulence intensities appear to be slightly less than at the other locations, but due to the inexactness of these values, a definite statement cannot be made. The turbulence levels observed in the wake of the 1.5 inch disk are comparable to those seen with the 2.0 inch diameter disk.

The laser velocimeter data and the respective values of velocities and turbulence intensities from which the preceding graphs were compiled are presented in Appendices C and D. In the next section, the conclusions drawn from this study will be considered.

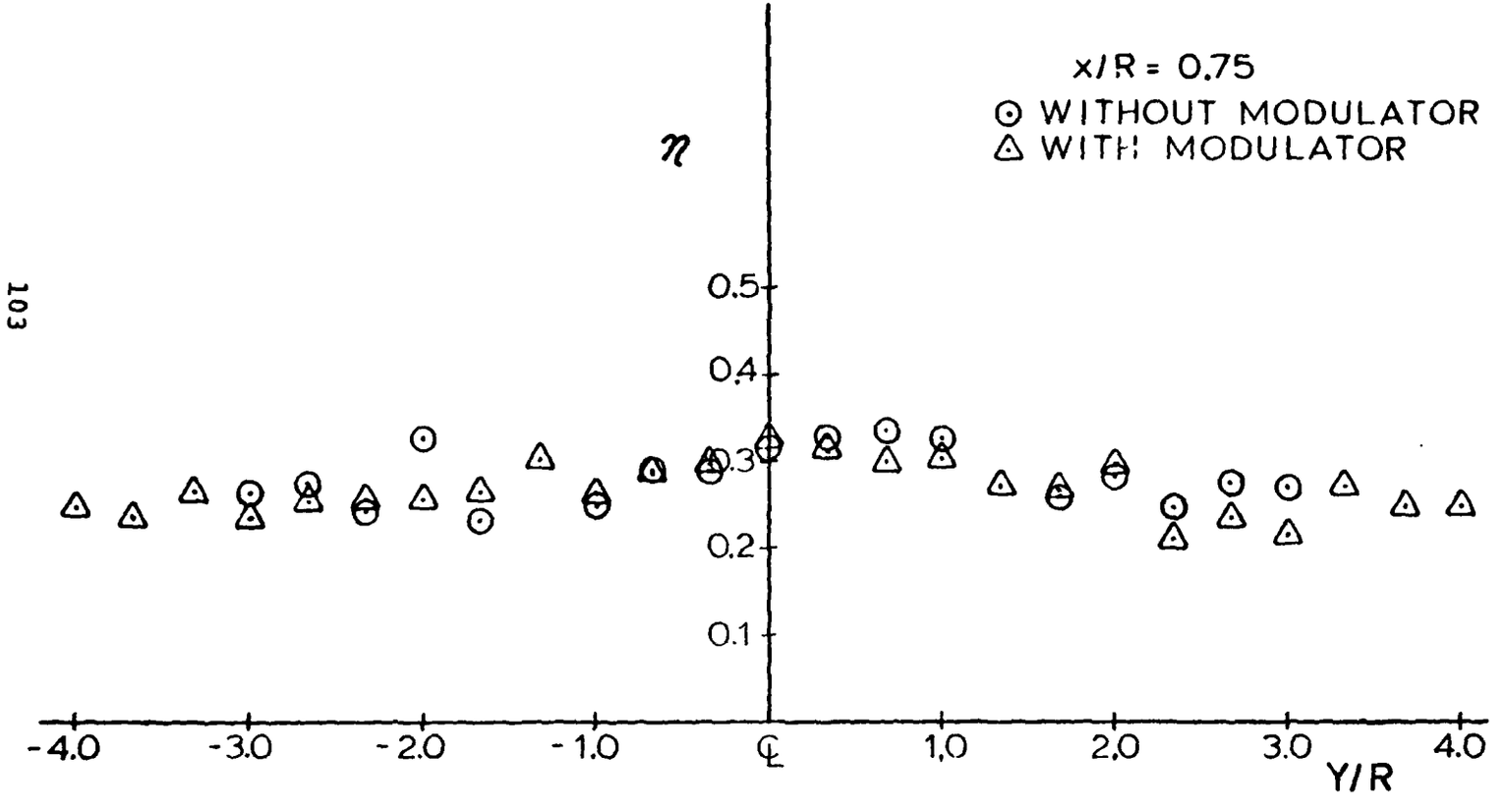

Fig 64. Turbulence Intensity Profiles, 1.5 Inch Diameter Disk

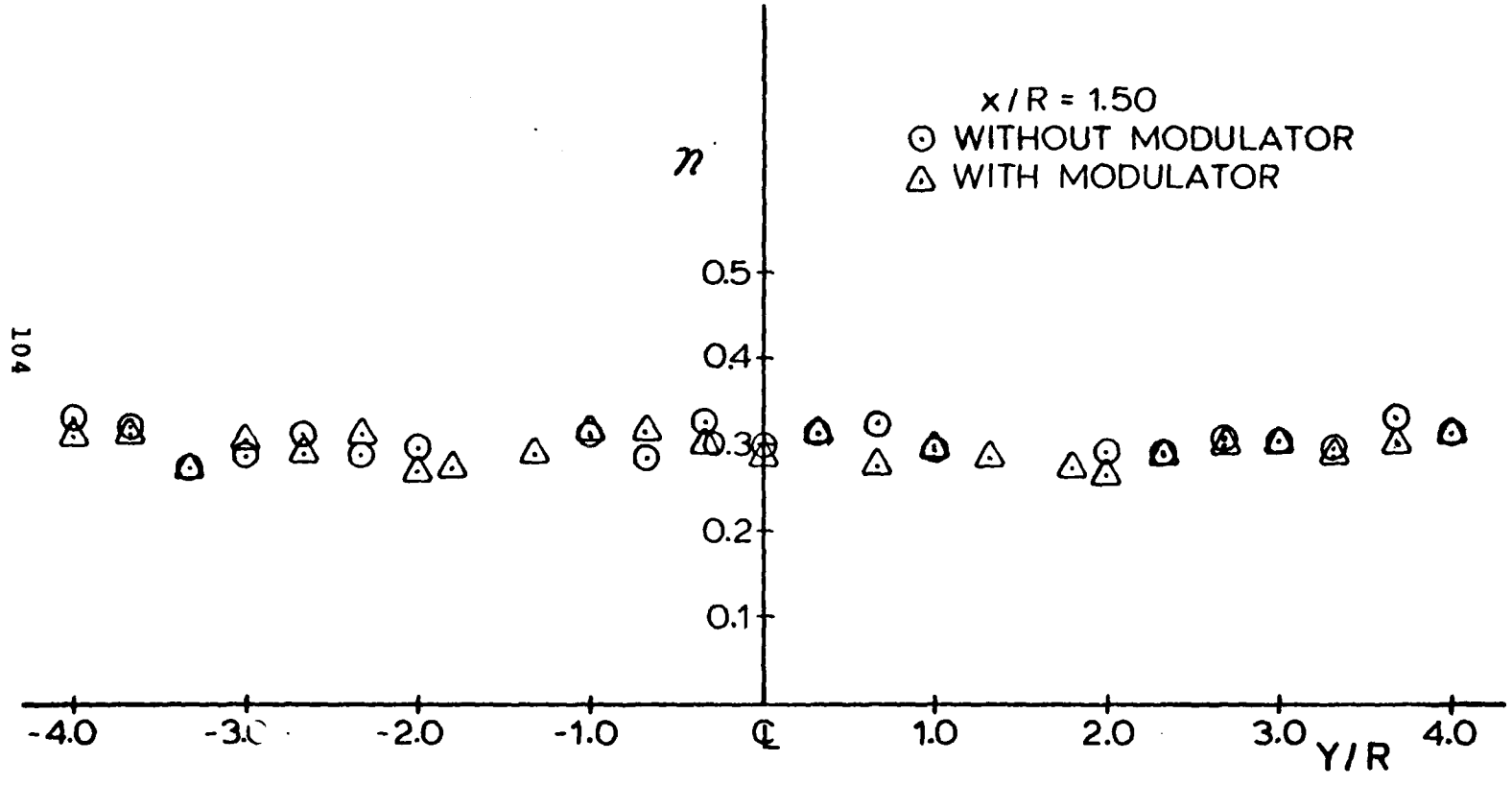

Fig 65. Turbulence Intensity Profiles, 1.5 Inch Diameter Disk

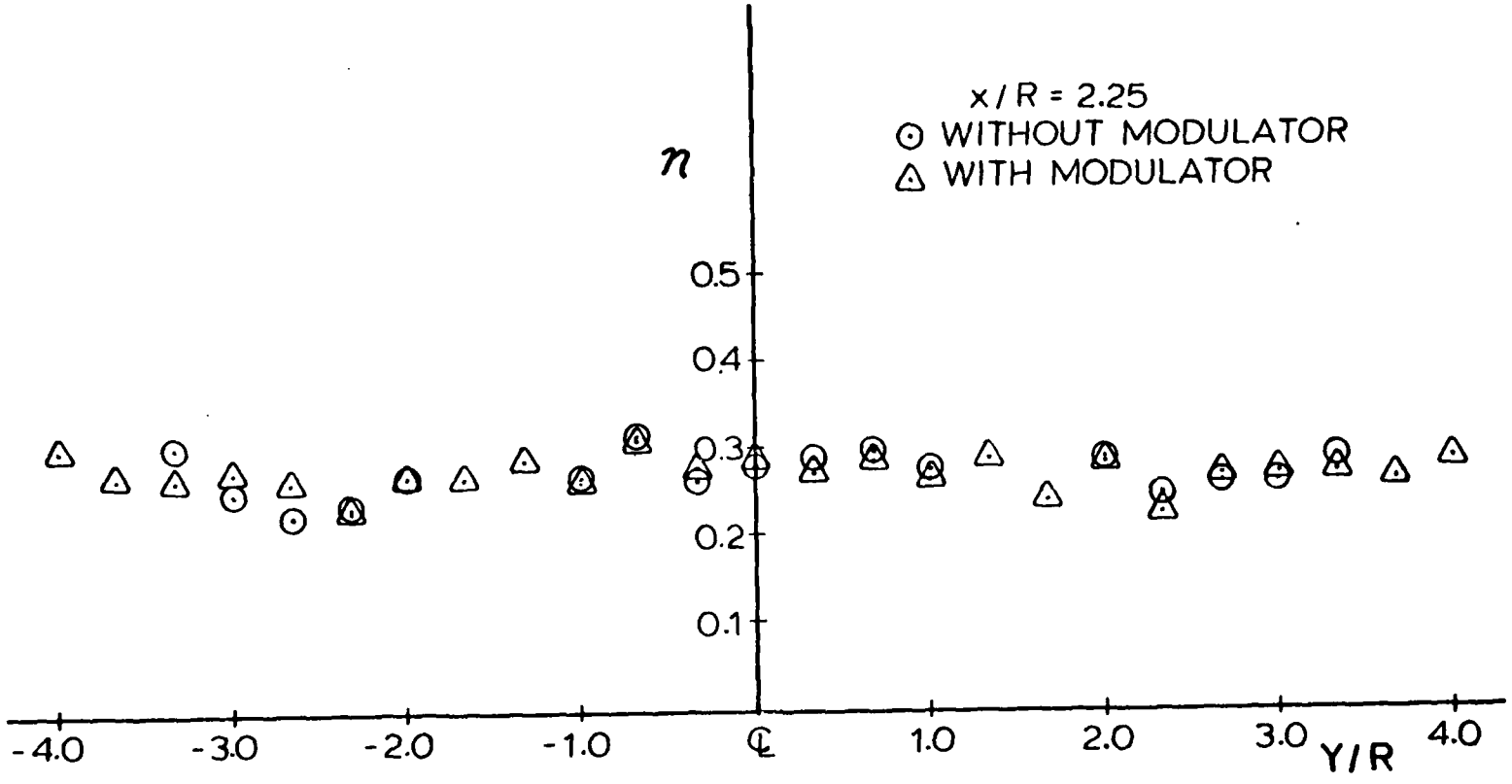

Fig 66. Turbulence Intensity Profiles, 1.5 Inch Diameter Disk

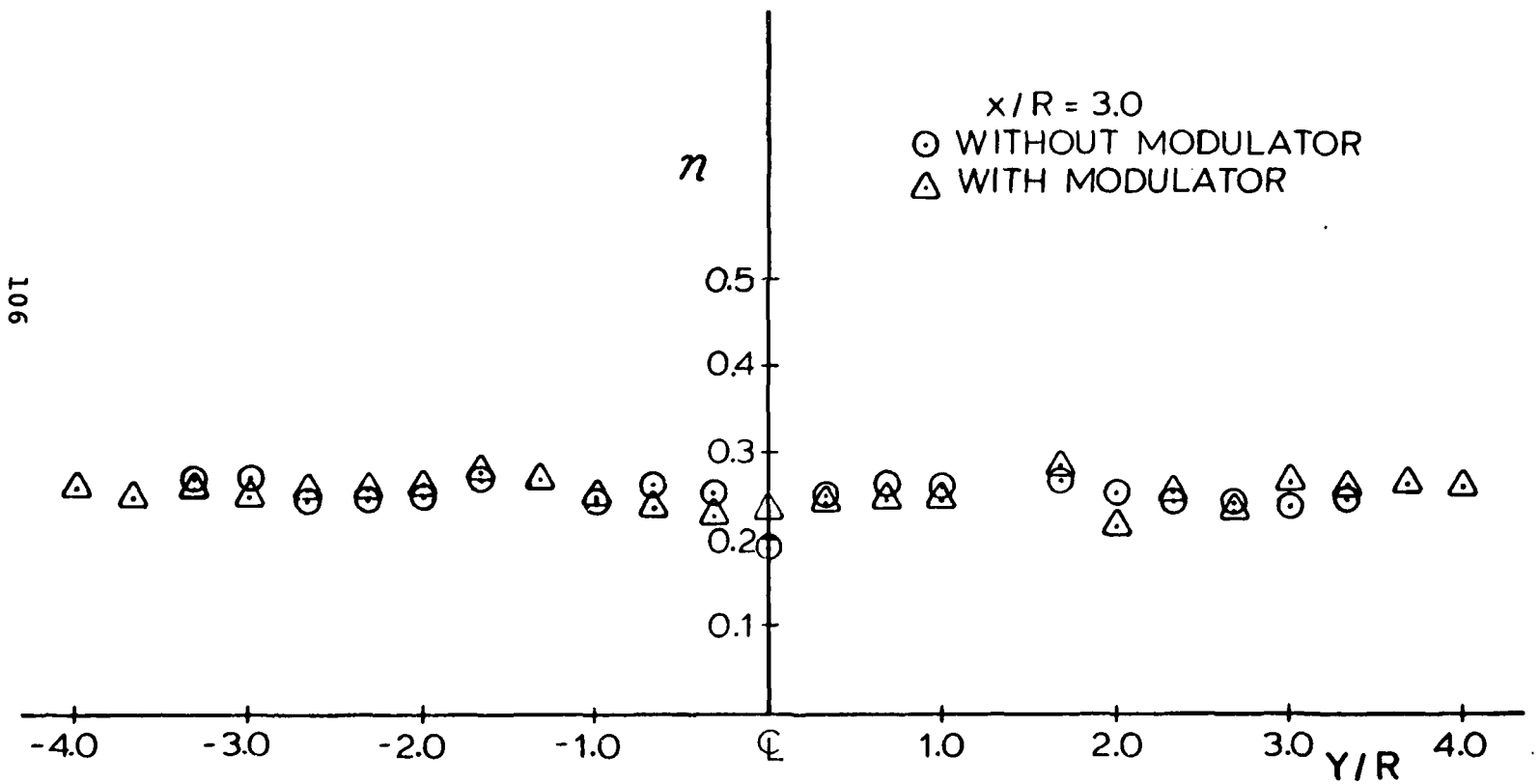

Fig 67. Turbulence Intensity Profiles, 1.5 Inch Diameter Disk

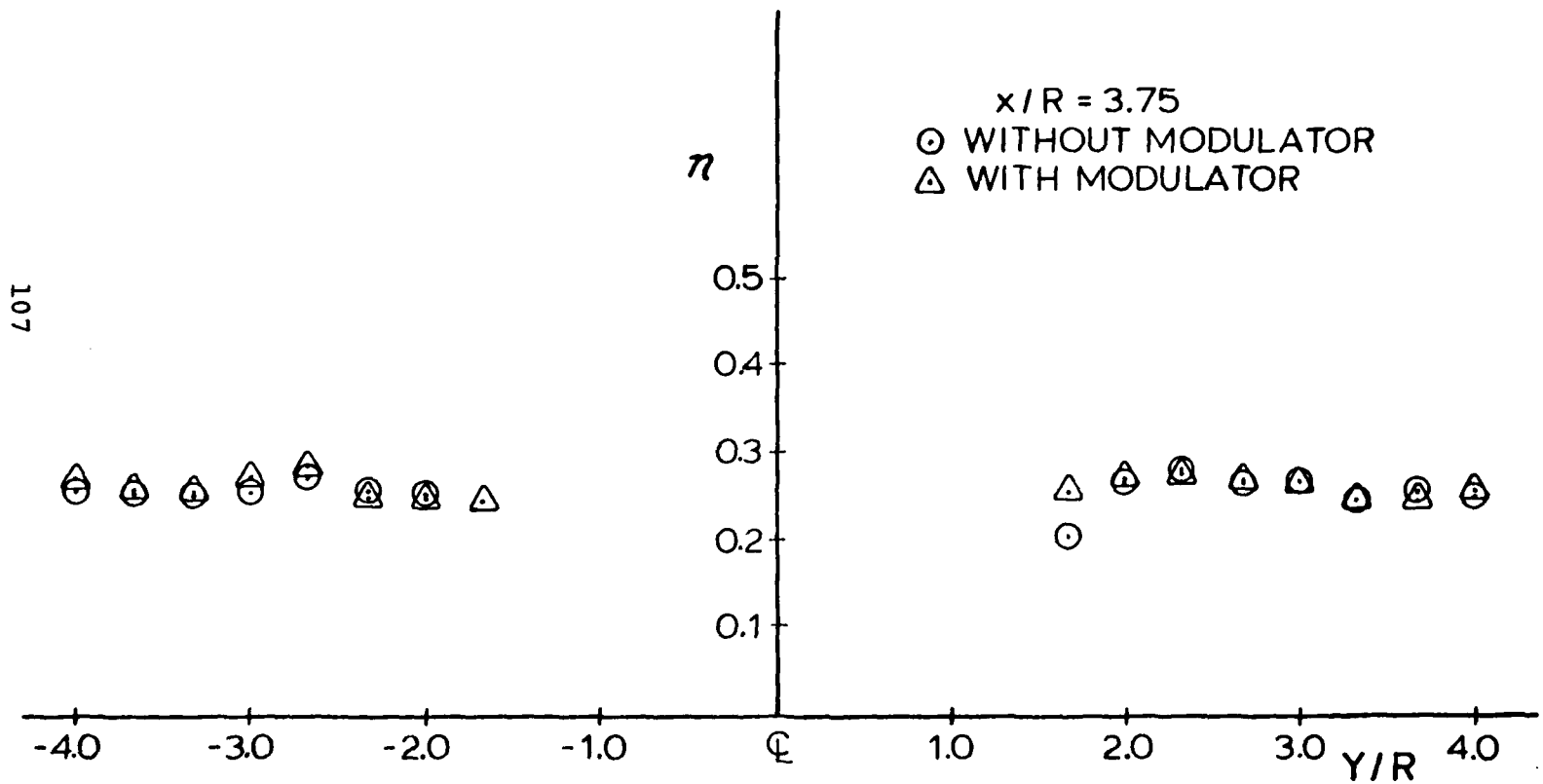

Fig 68. Turbulence Intensity Profiles, 1.5 Inch Diameter Disk

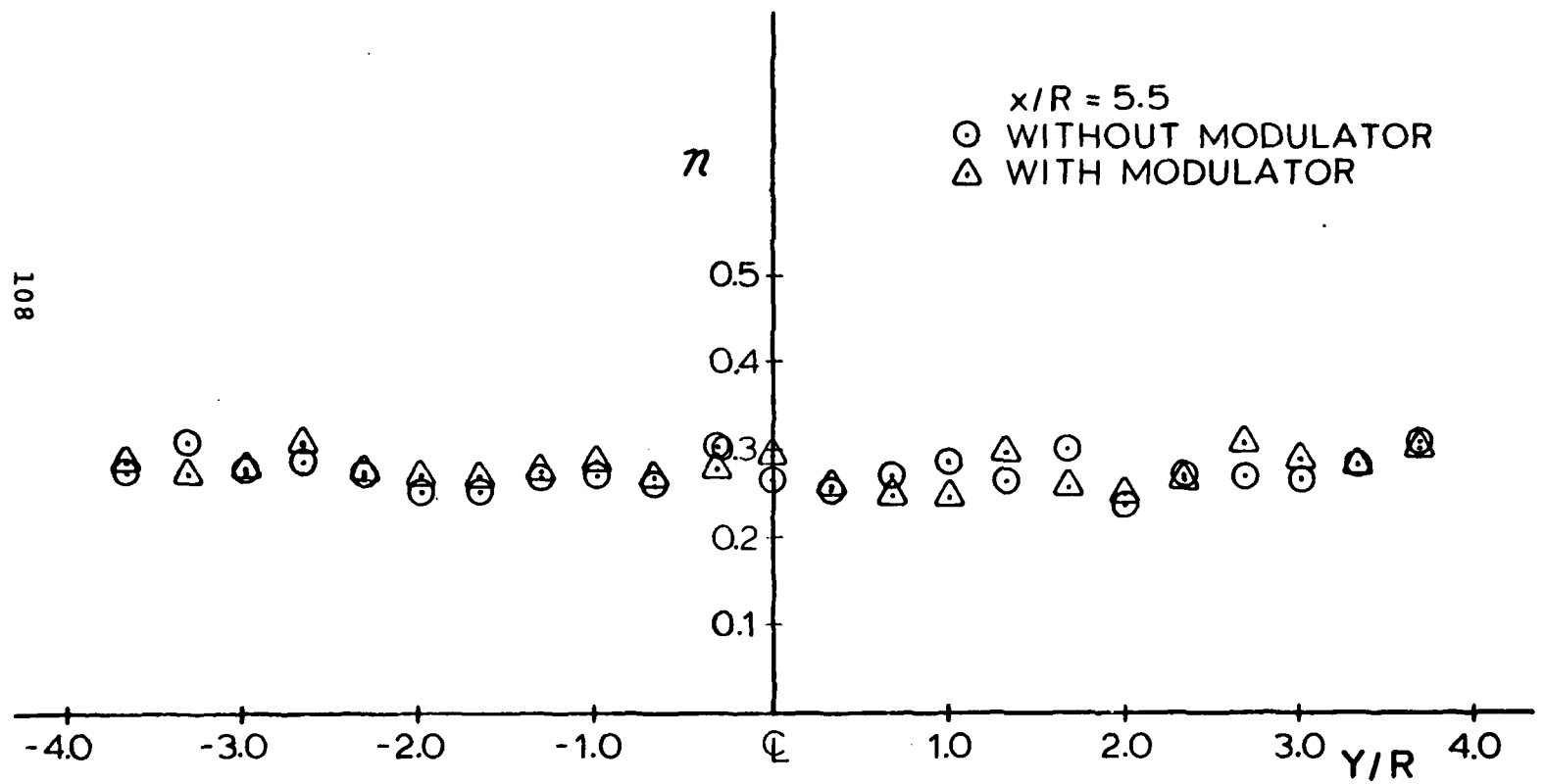

Fig 69. Turbulence Intensity Profiles, 1.5 Inch Diameter Disk

VII. Conclusions

The present investigation of flow over a circular disk achieved all of its initial objectives. A number of conclusions have been derived as a result of the study. They are as follows:

1. The schlieren system provided good photographs of the flow pattern in the near wake of a 2.0 inch diameter disk. The best view of the recirculation zone was attained with a continuous light source and a shutter speed of 1/200 second with helium injected into the zone. From the photographs, the boundary of the recirculation zone was found to be on the order of 1.5 disk diameters with a zone length of between 1.5 and 2.0 disk diameters. These results agree well with those presented in Refs 5 and 24. The spark lamp photographs provided little information on the dimensions of the recirculation; however, they illustrated an oscillatory motion of the flow about the disk centerline.

2. The capability of the laser velocimeter system, when used in conjunction with a phase modulator, to accurately determine flow direction was successfully demonstrated without the aid of seeding. Frequency shifts in the range of 200 KHZ to 520 KHZ resulted in the distinct changes in the autocorrelation function's frequency necessary in obtaining directional properties.

3. The similarity profile of the mean velocity data obtained from a free jet survey by the laser velocimeter system was in close agreement with the theoretical predictions.

This serves to support the credibility of the results obtained throughout the study with the laser velocimeter system.

4. The free jet turbulence intensities obtained with the LDV system varied between 10% and 37%. While Ref 18 indicates that the turbulence intensity equation is only accurate up to levels of 20%, the trends exhibited by the data obtained in the free jet survey resemble free jet turbulence intensity data presented in Ref 19. As such, values of turbulence intensities above 20% should be viewed as "in the neighborhood" of their respective values.

5. Mean velocity and turbulence intensity data was obtained in the near wake of both the 2.0 and a 1.5 inch diameter circular disk with the laser velocimeter system. In each case, the zone of reversed flow was clearly established with the system. The length of the recirculation zone was determined to be on the order of 3.75 disk radii in the case of each disk. The width on the recirculation zone was found to be on the order of 1.5 to 2.0 disk diameters for the 2.0 inch disk and approximately 1.4 disk diameters for the 1.5 inch disk. These results are close to those presented in Refs 5 and 24, supporting the capability of the LDV system.

6. The laser velocimeter system functioned well without the injection of particulate matter in the flow. This reasserted the "no seeding" capability of the system for the range of the experimental investigation.

7. A similarity profile to which all the mean velocity profiles in the wake of the disk would collapse was not obtained in this study. However, there was a resemblance noted between the mean velocity profiles obtained for the two disks when viewed at the same x/R . The similarity may have been even greater if the dimensions of the free jet and disk locations had been adjusted for the change in disk sizes.

8. Turbulence intensity values were found to be similar between the two disks and relatively constant across the widths of the flow. Generally, they were in the neighborhood of 30%. Trends were unable to be established since the variations in the intensities were within the range of uncertainty. The turbulence intensities found with and without the phase modulator at each point were generally in close agreement.

9. Despite the results obtained in Ref 8 indicating that the phase modulator may result in a certain amount of distortion of the velocity, close correlation was noted between the with and without phase modulation velocity profiles.

10. The recirculation zone dimensions obtained with the schlieren system and the laser velocimeter system were very close.

11. The investigation with the free jet facility, which negates the use of windows, is a worthwhile experimental test bed.

VIII. Recommendations

The following recommendations are put forth as a result of the present study:

1. A diagnostic study of flow over a circular disk should be conducted in a wind tunnel. The ratio of the test section diameter to disk diameter should be large to minimize the wall effects on the flow. The windows employed in the wind tunnel should be of a high quality optical glass to avoid unfavorable interference with the optics of the laser velocimeter system. A wind tunnel would allow the disk to be placed in a uniform flow.

2. A study of the flow through a sudden expansion combustor would be suited for the laser velocimeter system. Appendix A presents a possible combustor configuration for such a study.

3. A computer could be used in conjunction with the laser velocimeter system providing an instantaneous data reduction capability. A plotter could also be adapted to the computer system.

4. A study could be undertaken to examine the mass transport properties in the recirculation zone behind a circular disk. This could be accomplished in part with a schlieren system.

5. An indepth study of the flow structures in the wake region of the circular disk is now in order.

6. The flow over various aerodynamic shapes should be investigated with the laser velocimeter system.

7. The size and shape of the recirculation zone could be altered by mass injection or removal and the results could be obtained.

Bibliography

1. Abbis, J. B., T. W. Chubb, and E. R. Pike. "Laser Doppler Anemometry," Optics and Laser Technology: 249-261 (December 1974).

2. Abramovich, G. N. The Theory of Turbulent Jets. Cambridge, Massachusetts: The M. I. T. Press, 1963.

3. Abbott, D. E. and S. J. Kline. "Experimental Investigation of Subsonic Turbulent Flow Over Single and Double Backward Facing Steps," Transactions of the ASME: Journal of Basic Engineering: 317-325 (September 1962).

4. Advisory Group for Aerospace Research and Development. Applications of Non-Intrusive Instrumentation in Fluid Flow Research. Papers and disucssion of the Fluid Dynamics Panel Symposium held at the French-German Research Institute (ILS), Saint-Louis, Franch, May 1976. (AGARD-CP-193).

5. Birkhoff, G. and E. H. Zarantonello. Applied Mathematics and Mechanics: Jets, Wakes and Cavities, Vol 2. New York: Academic Press, Inc., 1957.

6. Bradshaw, P. An Introduction to Turbulence and Its Measurement. Oxford, England: Pergamon Press, Ltd., 1971.

7. Bradshaw, P. Topics in Applied Physics, Turbulence, Vol 12. New York: Springer-Verlag Berlin Heidelberg, 1978.

8. Catalano, G. D. "Effect of Frequency Shifting on Mean and Fluctuating Laser Velocimetry Measurements." AFFDL-TM-79-90-FXM. Wright-Patterson Air Force Base, Ohio: Air Force Flight Dynamics Laboratory, Director of Science and Technology, Air Force Systems Command, August 1979.

9. Cerullo, N. G. An Experimental Evaluation of a Laser Velocimeter by the Study of Turbulence in a Plane Free Jet at High Subsonic Velocities. MS Thesis. Wright-Patterson Air Force Base, Ohio: Air Force Institute of Technology, June 1979.

10. Curran, E. T. An Investigation of Flame Stability in A Coaxial Dump Combustor. Doctoral Dissertation. Wright-Patterson Air Force Base, Ohio: Air Force Institute of Technology, May 1979.

11. Drewry, J. E. "Fluid Dynamic Characterization of Sudden-Expansion Ramjet Compustor Flowfields," AIAA Journal, 16: 313-319 (April 1978).

12. Durrani, T. S. and C. A. Greated. Laser Systems In Flow Measurement. New York and London: Plenum Press, 1977.

13. Durst, F., A. Melling, and J. H. Whitelaw. Principles and Practice of Laser-Doppler Anemometry. London and New York: Academic Press, 1976.

14. Fluid Meters - Their Theory and Application (Fifth edition). American Society of Mechanical Engineers, 1959.

15. Foord, R., A. F. Harvey, and R. Jones. "A Solid State Electro-Optic Phase Modulator For Laser Doppler Anemometry," Journal of Physics D: Applied Physics, 7: L36-L39 (1974).

16. Ladenburg, R. W., B. Lewis, R. N. Pease, and H. S. Taylor. High Speed Aerodynamics and Jet Propulsion, Physical Measurements in Gas Dynamics and Combustion, Vol IX. Princeton, New Jersey: Princeton University Press, 1954.

17. Liepmann, H. W. and A. Roshko. Elements of Gasdynamics. New York: John Wiley and Sons, Inc., 1957.

18. Malvern Instruments, Ltd. Operating and Installation Manual. Spring Lane Trading Estate, Malvern Link, Worcestershire WR14 1AL, England.

19. Pai, S. I. Fluid Dynamics of Jets. Canada: Van Norstrand Company, Inc., 1954.

20. Pennucci, M. A. Parametric Evaluation of Total Pressure Loss and Recirculation - Zone Length in a Sudden-Expansion Combustor. MS Thesis. Wright-Patterson Air Force Base, Ohio: Air Force Institute of Technology, September 1974.

21. Rogers, H. J. V. Velocity Profiles in a Long Inlet Duct Employing a Photon Correlating Laser Velocimeter Without Seeding. MS Thesis. Wright-Patterson Air Force Base, Ohio: Air Force Institute of Technology, December 1979.

22. Schlichting, H. Boundary Layer Theory (Sixth edition). New York: McGraw-Hill Book Company, 1968.

23. Shapiro, A. H. The Dynamics and Thermodynamics of Compressible Fluid Flow, Vol 1. New York: John Wiley and Sons, Inc., 1953.

24. Winterfeld, G. "Investigations on Mass Exchange Between Recirculation Areas Behind Axially Symmetrical Flame-holders and Surrounding Flow." FTD-HC-23-844-70. German Air and Space Travel Research Report 69-07, German Experimental Station for Air and Space Travel (DVL), February 1969.

Appendix A. Flow Visualization In A Sudden Expansion Combustor

This portion of the study was originally to be the main thrust of the research but due to a facility failure time did not permit the rebuilding of the apparatus for this investigation. The partial results will be reported as an appendix to the thesis. The purpose of this study was to investigate the aerodynamic flow through a sudden expansion combustor using schlieren photography. Previously various studies have looked at this phenomenom with the use of pressure measurements, surface oil film visualization, and visualization with the injection of foreign particles into the flow. These methods explored the pressure losses in the combustor and the characteristics of the recirculation zone.

Background

The background on the sudden expansion combustor and its applications may be found in Refs 9, 10, and 20. In summary, a dump combustor is used in the integral rocket-ramjet engine to minimize the volume required of the missile. The concept involves using a solid propellant rocket motor to boost the missile up to ramjet operating conditions, where the ramjet takes over. The rocket motor case, when empty, becomes the ramjet combustor, thereby saving the volume required for a separate combustor. The combustor is fed by an inlet of a smaller diameter. Figure 70 shows the flow pattern in the combustor. There exists a recirculation zone beginning at the step face and reattaching itself at some

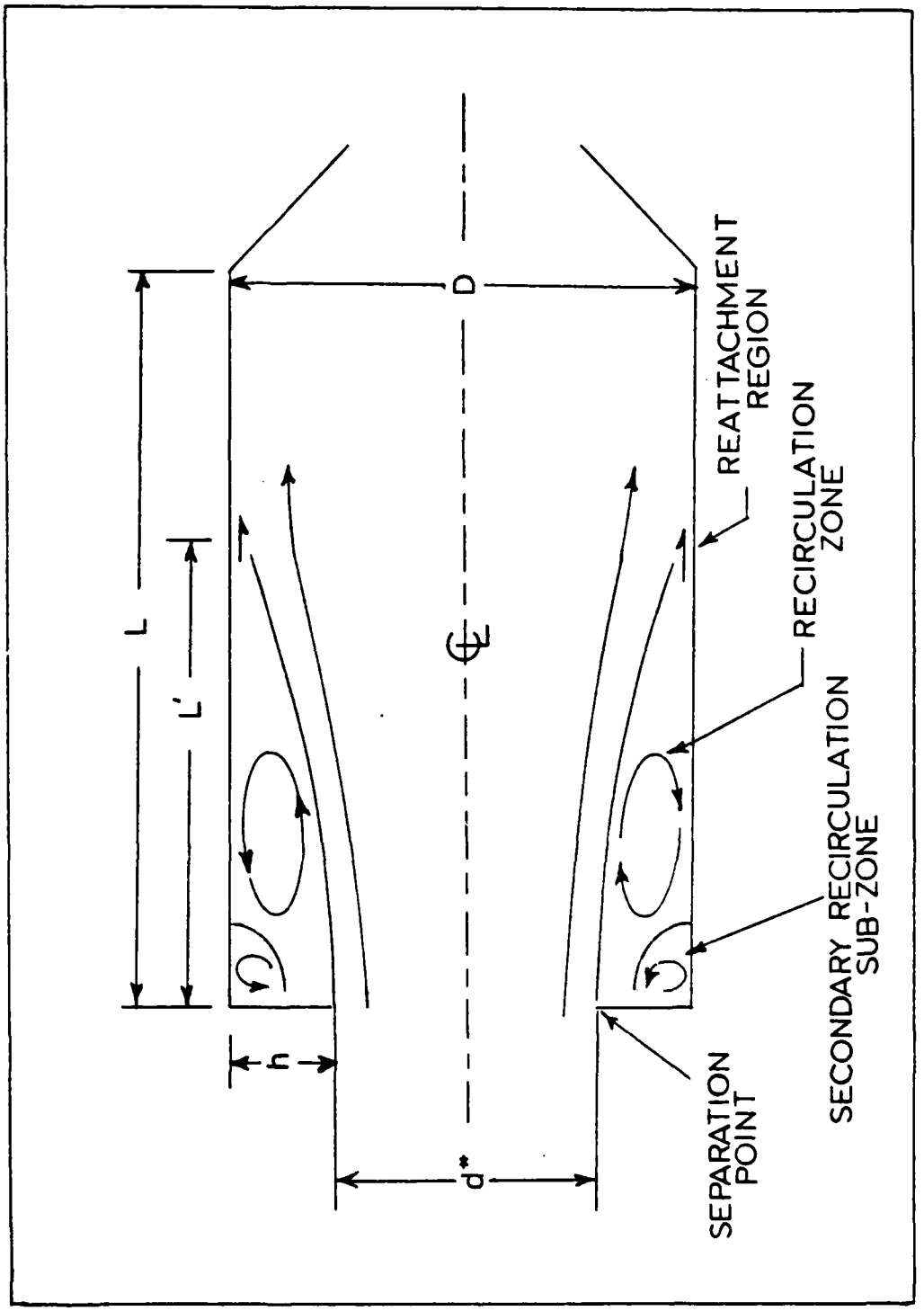

Fig 70. Combustor Flow Pattern

length downstream from the inlet. The reattachment point actually occurs over a region rather than at one specific point. The recirculation zone is an important parameter since this is the area where fuel and air are mixed to achieve a constant burning in the combustor, or flame stability. Since a flow visualization study has not been recorded in the literature for the axisymmetric configuration using the schlieren technique, this effort proposed to determine its feasibility and compare its results to others.

Apparatus and Experimentation

The model used for this study was fabricated from plexiglass tubing in two sections. The inlet, Fig 71, had an inside diameter of 1.25 inches. The combustor model, Fig 72, was of a two inch inside diameter, such that the inlet section would slide snugly into it. This allowed the combustor length to diameter ratio to be varied with the use of spacers. Pieces of inferometer quality glass was installed on opposing sides of the combustor model as shown in Fig 72. Two 3/16 inch diameter ports were placed in the combustor model such that helium could be pumped into the recirculation zone at the step face. The overall set-up of the model and apparatus is shown in Fig 73.

For this test a length to diameter ratio of 5 was chosen, with a nozzle ratio of 0.297. This configuration allowed for an inlet step of 0.375 inch or an inlet to combustor area ratio of 0.391. The choice of these parameters coincides with parameters used by Ref 20, allowing for a good comparison of results.

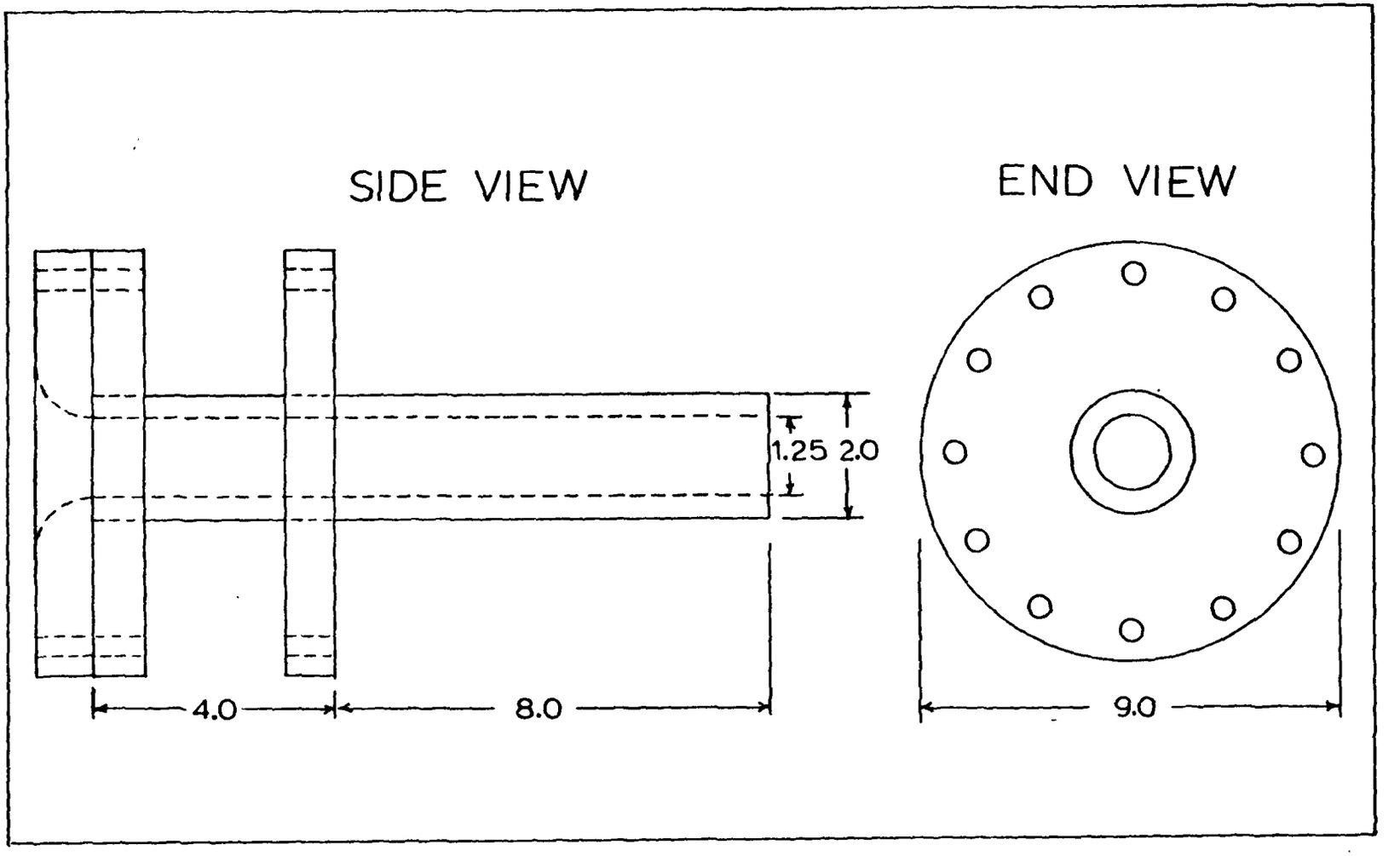

Fig 71. Combustor Inlet Section

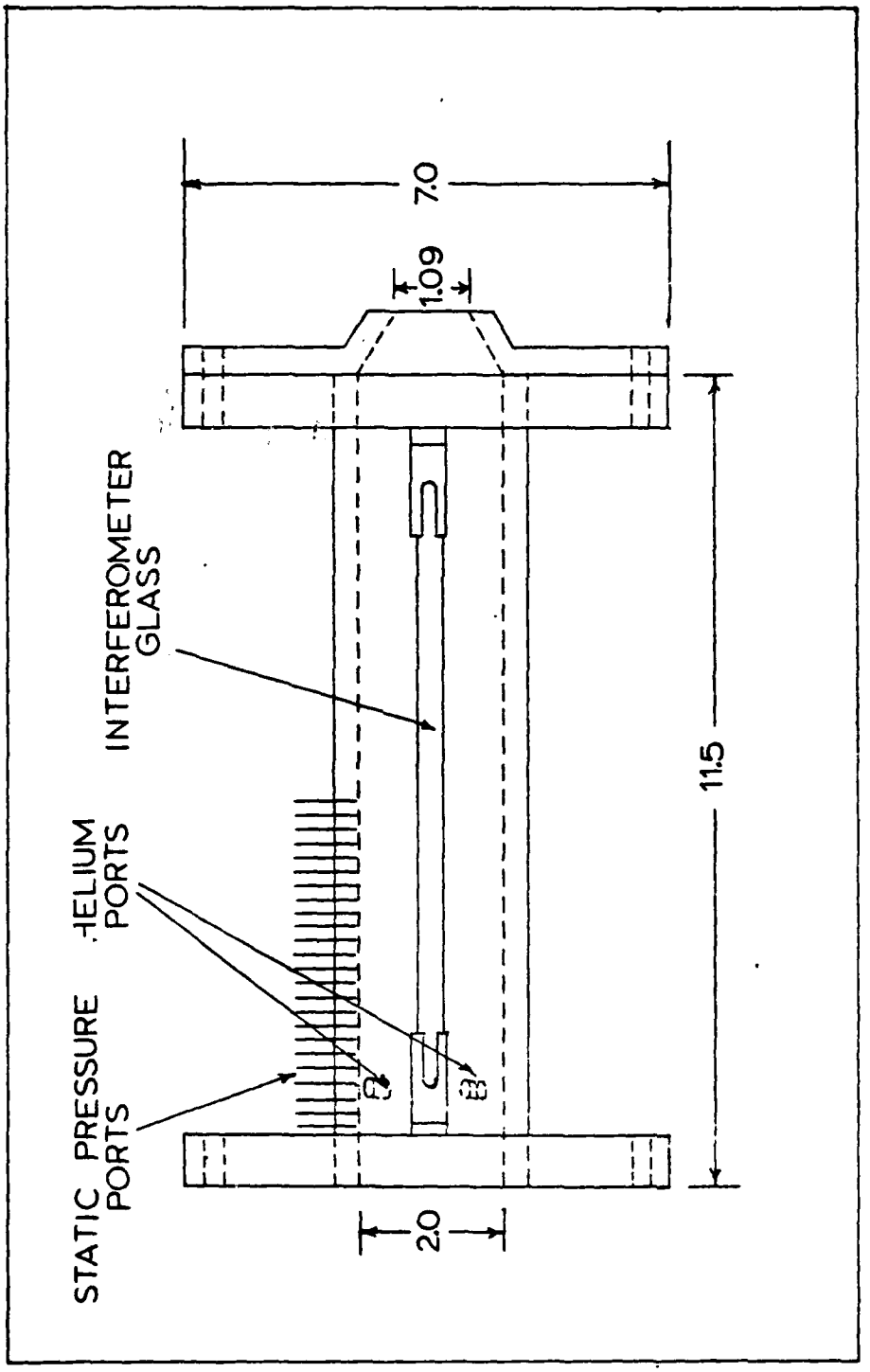

Fig 72. Combustor Model

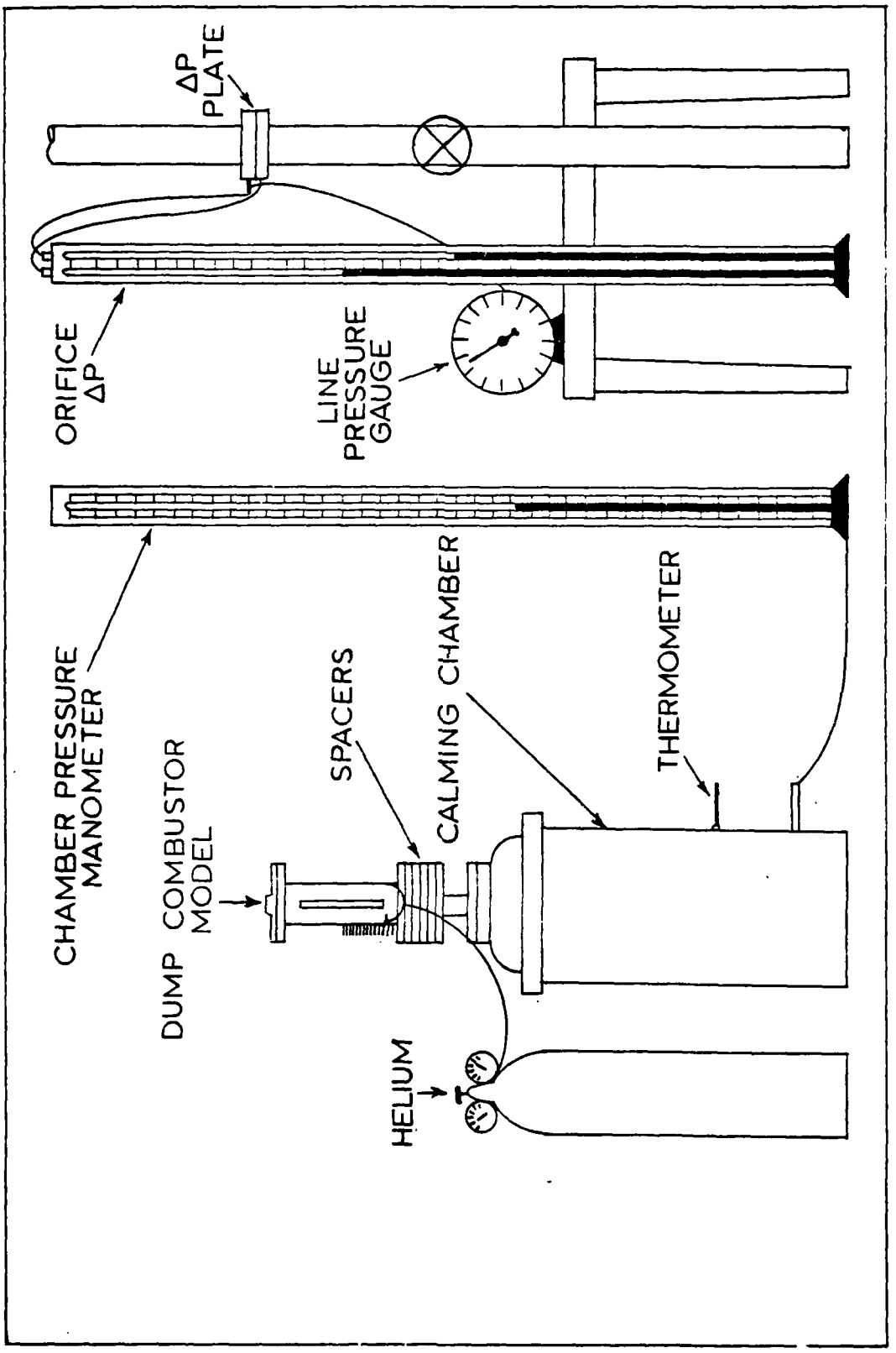

Fig 73. Dump Combustor Apparatus Set-up

The set-up of the schlieren system is shown in Fig 74. Alignment was accomplished using a continuous light source; however, a spark lamp was used during the testing. The duration of the spark lamp was on the order of a micro-second allowing for the flow to be stopped at that instant. Flow phenomenon not apparent when viewed with continuous light becomes visible when a spark lamp is used. The knife-blade was oriented such that it was in the horizontal position, allowing for the density gradient to be viewed along the direction of flow. Helium was injected into the flow under pressure to create a density gradient allowing the flow to become visible with the schlieren.

For the testing, the flow rate was adjusted such that the flow through the combustor was choked. This was considered to exist when the chamber total pressure to atmospheric pressure was 1.893 or greater. For these tests approximately 60 inches on the mercury gauge was present in the chamber, giving a ratio of 2.00. The total temperature was measured with a thermometer extending into the calming chamber. With the use of the mass flow rate equation for choked flow

$$\dot{m} = .532 \frac{P_o A^*}{\sqrt{T_o}} \qquad (9)$$

the mass flow rate was approximated. While this is a rough method it does give a close value for comparison purposes.

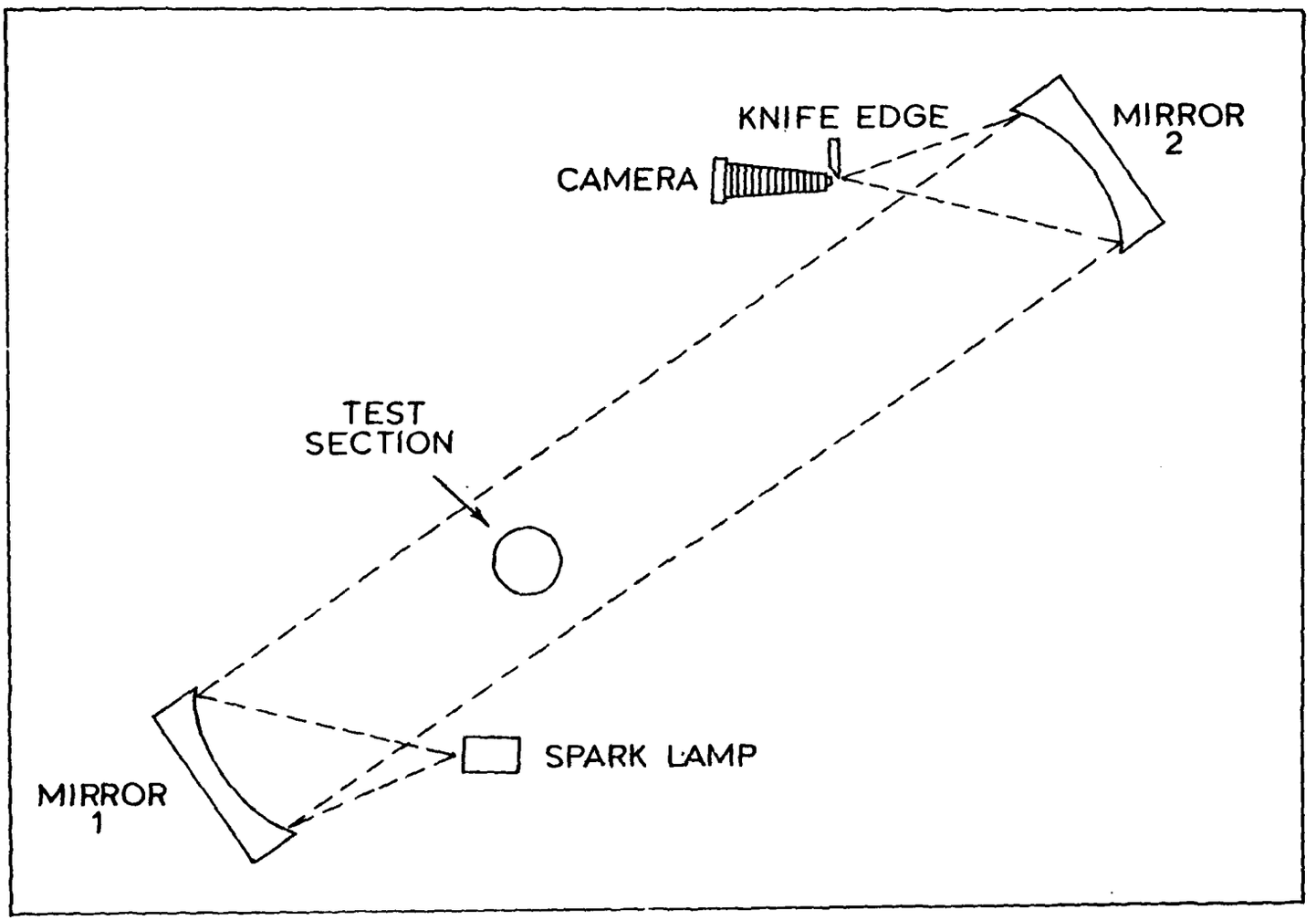

Fig 74. Schlieren System Set-up

The mass flow can more accurately be determined with the square edge orifice method. With the mass flow rate computed, Reynolds Number is found with the relation

$$Re = \frac{4\dot{m}}{\mu \pi D} \qquad (10)$$

where the value of viscosity used was 12.32×10^{-6} lbm/ft sec.

Once the desired flow rate was stabilized, helium was injected into the flow with the use of a gauge to set the pressure. The amount of helium fed into the combustor was adjusted until the flow became easily visualized in the photographs.

Results

The results of the flow visualization is seen in Fig 75. The photograph shows a very definite change in the flow pattern approximately a third of the way up the test section. This point of change corresponds to approximately three inches downstream from the inlet. This occurred at a mass flow rate of approximately .63 lbm/sec and a Reynolds Number of 6.2×10^5. The three inch point corresponds with the recirculation zone length determined in Ref 1 for similar flow conditions and geometries. When plotted against results published in Ref 10, the comparison is seen in Fig 76. The change in flow pattern was noticeable in every photograph taken at similar conditions and occurred in the same vicinity. The change in flow pattern indicates the reattachment point.

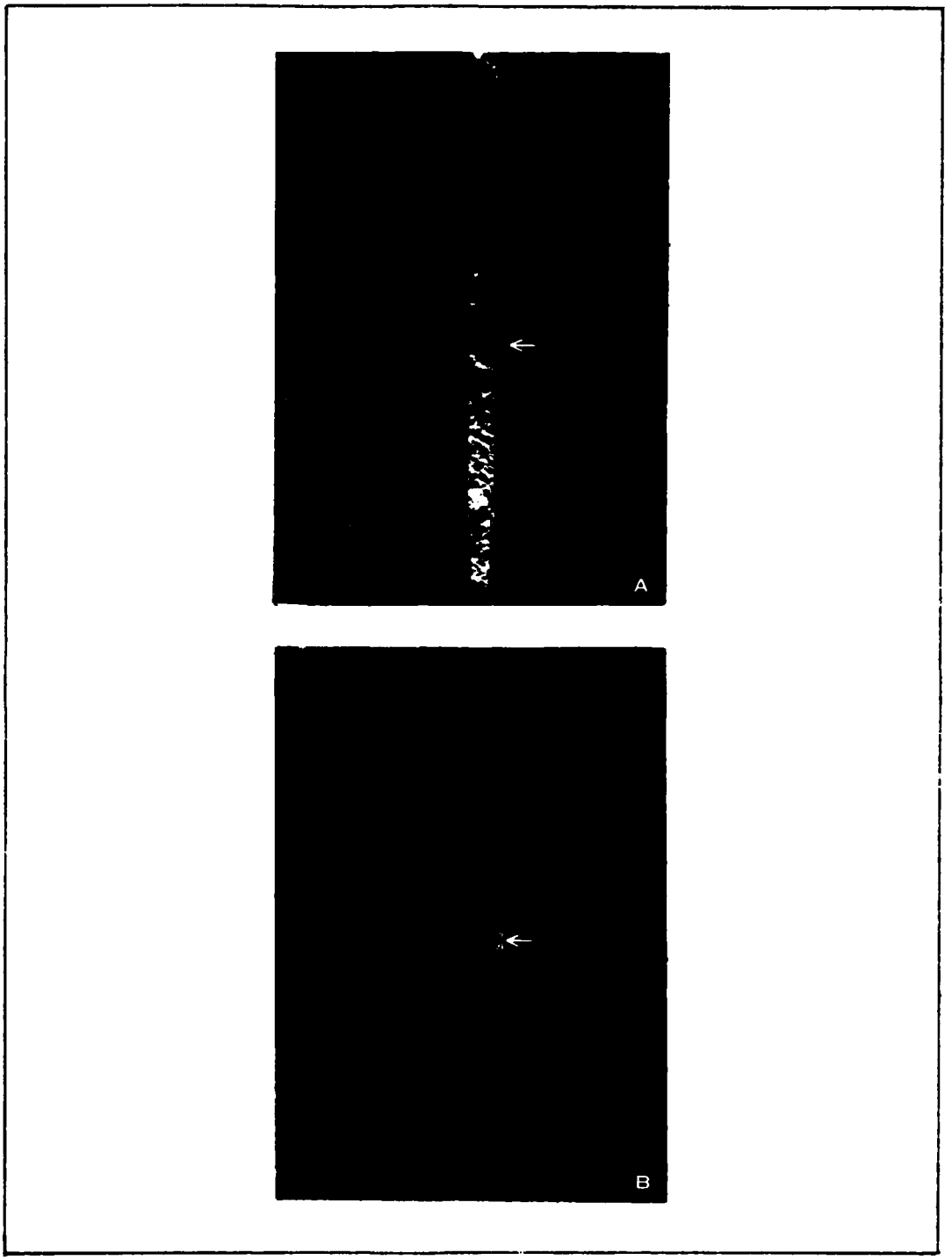

Fig 75. Schlieren Photographs of Combustor Flow

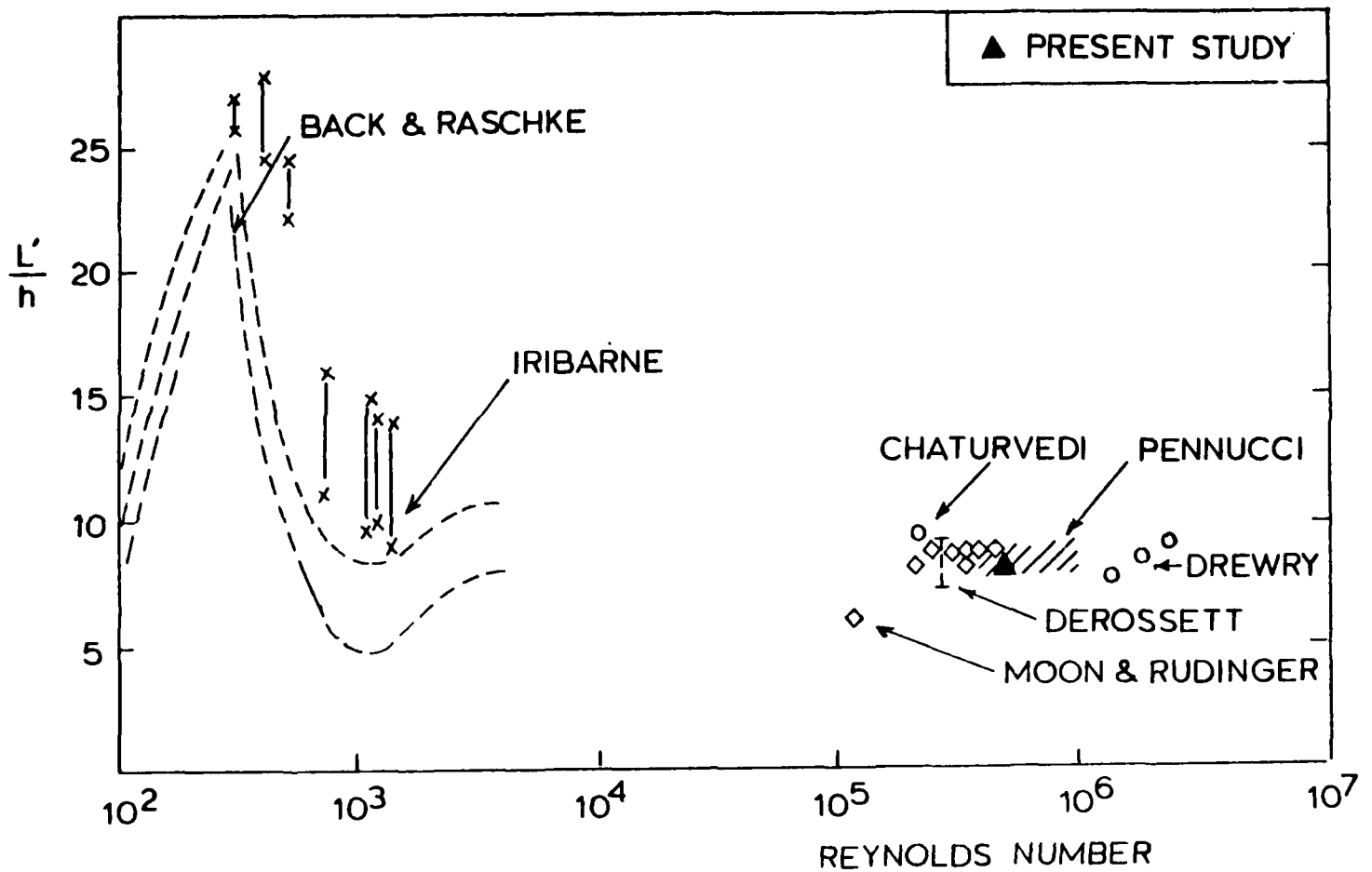

Fig 76. Recirculation Zone Length to Step Height as a Function of Reynold's Number (Ref 9)

While an absolute conclusion cannot be made from the limited amount of data, it is strongly suggested that schlieren photography can be used in distinguishing between the recirculating zone and the reattached flow. One drawback of the schlieren method is the fact that it is "looking" through three regimes of flow. There is the recirculation region on each glass face and the core flow in the center. However, there does appear a definite indication of the recirculation zone in the combustor. From continual observations, the injection of helium appeared to have no adverse effect on the geometry of the flow.

Conclusions

From the limited data taken, it strongly suggests that the recriculation zone can be visualized with the schlieren method and thusly the length of the zone may be determined. The influence of the helium injected into the flow is not completely known through this study, but by comparison with expected results the length of the recirculation zone is very well supported.

Recommendations

Based on the observations made during the schlieren testing, the fabrication of an all metal model with optical quality glass windows is recommended. Not only is there the possibility of gaining further information with flow visualization techniques, but a study with the laser velocimeter

system is very feasible. This is especially important when considering the results of the flow behind a disk. This system would allow the flow to be analyzed across the inside diameter of the combustor at various distances from the step face. The resulting data could then provide velocity and turbulence intensity profiles as well as flow directions and recirculation zone dimensions.

Appendix B. Data Reduction and Sample Calculations

Section IV gives a step by step procedure for determining flow direction. This is accomplished at the time data is recorded by observing changes in the autocorrelation function's frequency due to phase modulation. Initially, a relationship must be established between the function's frequency and the mode settings on the phase modulator drive unit in a known flow direction. If in a downstream flow, the function's frequency is found to increase when the phase modulator is turned from the off to the inverted mode (or to decrease when turned from the off to drive mode), which was the case in this study, a pattern is developed. Anywhere in the flow field where a similar relationship exists between function frequency and mode switching is indicative of positive downstream flow. Conversely, if the frequency of the curve is decreased when switching from the off to the inverted mode (or increased when switching from the off to the drive mode), the flow will be in the opposite or negative direction. The relationship between mode switching and flow direction should be reevaluated for any new laser velocimeter system set-up as it may be just the opposite if the equipment arrangement in relation to the flow field is changed.

Having initially determined the flow direction, the magnitude of the mean flow velocity and the turbulence intensity must be calculated according to the equations presented in Ref 18. Initially, the fringe spacing,

S , is computed with the relation

$$S = \frac{L}{D}\frac{\lambda}{\mu} \tag{11}$$

where L = focal length of lens

D = separation of two parallel laser beams as they enter the lens

μ = refractive index ≈ 1.0 for air

λ = wavelength, helium-neon laser light = $.6328 \times 10^{-6}$ meters (m)

The equations required in determining velocity and turbulence intensity values depend on whether or not the phase modulator is used.

Without Phase Modulation

The mean velocity is determined by

$$U = \frac{S}{(\text{Peak} - 3)(\text{Sample Time})} \tag{12}$$

where the peak is the channel number of the first maximum occurring on the autocorrelation function and sample time is the value in nanoseconds set on the digital correlator.

The turbulence intensity is calculated as follows. First a value for R must be computed with

$$R = \frac{g_2 - g_1}{g_2 - g_3} \tag{13}$$

where g_1 = value contained in the channel of the first minimum (Fig 77)

g_2 = value contained in the channel of the first maximum (Fig 77)

g_3 = value contained in the channel of the second minimum (Fig 77)

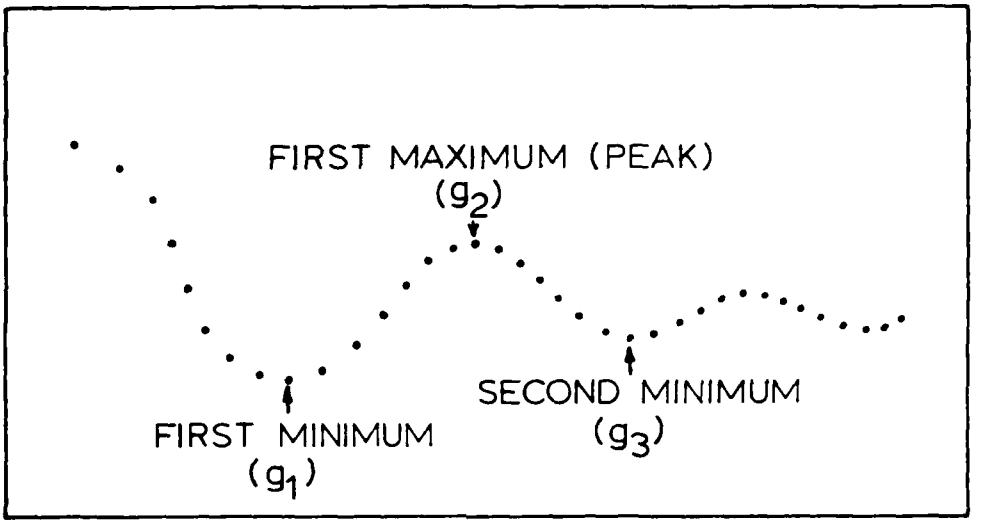

Fig 77. Autocorrelation Function

Turbulence intensity, η , is then computed as

$$\eta = \frac{1}{\pi} \{\tfrac{1}{2}(R-1) + \frac{1}{2N^2}\}^{\frac{1}{2}} \qquad (14)$$

where $N = \frac{r_o}{s}$

r_o = laser beam radius = 0.55mm

With Phase Modulation

When the phase modulator is in operation (either in the drive or inverted mode), the data reduction is different than without modulation (Ref 21). Now the autocorrelation curve

viewed on the oscilloscope does not represent the true flow velocity, but is the true flow velocity plus or minus the velocity induced by the phase modulator. This apparent velocity, U^* , is determined with same equation used before:

$$U^* = \frac{S}{(\text{Peak} - 3)(\text{Sample time})} \tag{15}$$

This velocity corresponds to a doppler frequency shift, f^*_d , found by

$$f_d^* = \frac{U^*}{S} = \frac{2U^*\sin\theta}{\lambda} \tag{16}$$

where $\theta = \tan^{-1}\left(\frac{1}{2}\frac{D}{L}\right)$

The true doppler frequency shift of the flow is then

$$f_d = f^*_d \pm |\Delta f| \tag{17}$$

where $|\Delta f|$ is the magnitude of the frequency shift applied to the phase modulator.

Whenever the frequency shift results in an increase in the observed frequency on the oscilloscope (fringe movements against the flow), the true doppler frequency shift is

$$f_d = f_d^* - |\Delta f|$$

Conversely, whenever a decrease in frequency occurs due to phase modulation

$$f_d = f_d^* + |\Delta f|$$

The true velocity of the flow is then

$$U = (S)(f_d) = \frac{f_d \lambda}{2 \sin\theta} \qquad (18)$$

From Ref 21 the turbulence intensity is now computed with

$$\eta = \frac{1}{\pi} \{ \tfrac{1}{2}(R-1) \frac{U}{U^*} + \frac{1}{2N^2} \}^{\frac{1}{2}} \qquad (19)$$

Sample Calculations

To illustrate how the above equations were applied, a sample calculation is provided using data excerpted from Table IX of Appendix C.

Y IN.	SAMPLE TIME 10^{-9} SEC	PEAK	FREQ KHZ	g_1	g_2	g_3
-0.75	100	16	0	22423573	22443731	22436989
-0.75	100	21	-204.43	10188384	10193086	10191143

The sign next to the frequency in the data table was used to indicate which mode the phase modulator was in and does not represent either an increase or decrease in the frequency. A positive sign indicates the drive mode and a negative sign indicates the inverted mode.

From the data shown above and the previously determined relationship between mode switching and function frequency for this set-up, the inverted mode has resulted in a decrease in the frequency of the display (the peak occurred at an earlier channel) indicating negative or reversed flow at this data point. The optical arrangement of the system being used in this study created the $L/D = 40.1$.

Therefore,

$$S = (40.1)(.6328 \times 10^{-6}\text{m}) = 2.5375 \times 10^{-5}\text{m}$$

The true mean velocity of the flow is

$$U = \frac{2.5375 \times 10^{-5}\text{m}}{(16 - 3)(100^{-9}\ \text{second})} = 19.519\ \frac{\text{m}}{\text{sec}}$$

$$= 64.02\ \frac{\text{ft}}{\text{sec}}$$

Turbulence intensity was found to be

$$\eta = 31.7\%$$

For the data obtained with phase modulation

$$U^* = \frac{2.5375 \times 10^{-5}\text{m}}{(21 - 3)(100 \times 10^{-9})} = 14.097\ \frac{\text{m}}{\text{sec}}$$

$$= 46.24\ \frac{\text{ft}}{\text{sec}}$$

$$f^*_d = \frac{U^*}{S} = \frac{14.097}{2.5375}\ \frac{\text{m/sec}}{\text{m}} = .5556 \times 10^6\ \text{HZ}$$

$$f_d = f_d^* + |\Delta f| = .5556 \times 10^6 + .2043 \times 10^6$$

$$= .7599 \times 10^6 \text{ HZ}$$

The true mean velocity of the flow is then

$$U = (f_d)(S) \approx (.7599 \times 10^6 \text{ HZ})(2.5375 \times 10^{-5} \text{m})$$

$$= 19.281 \frac{\text{m}}{\text{sec}}$$

$$= 63.24 \frac{\text{ft}}{\text{sec}}$$

The velocity found with the modulator should be the same as the velocity found without the modulator since the same point in the flow is being observed. This is indeed the case since the values are very close. Turbulence intensity was found to be 31.1% with the phase modulator.

Appendix C. Laser Velocimeter Data

TABLE II

Experimental Data, Free Jet, X/D = 12.0
(PATM: 29.96 in Hg; TATM: 71° F; Jet Mach Number: 0.35; L/D: 40.1)

Y IN.	SAMPLE TIME 10^{-9} SEC	PEAK	FREQ KHZ	g_1	g_2	g_3
-3.0	100	25	0	363619	375488	366235
-3.0	100	18	-201.45	1365541	1368088	1366137
-2.75	100	19	0	685023	690056	686343
-2.75	100	15	-201.3	4530947	4539540	4533387
-2.50	100	16	0	6645168	6672713	6656006
-2.50	100	13	-201.68	3086266	3098903	3091242
-2.25	100	13.5	0	4951276	4978383	4963252
-2.25	100	12	-201.51	1061421	1069402	1065114
-2.0	50	19.6	0	5188975	5238181	5214976
-2.0	50	17	-201.46	1519916	1535885	1528840
-1.75	50	16.8	0	1246411	1271399	1260706
-1.75	50	19	206.38	2336739	2372347	2356199
-1.50	50	15	0	1446927	1471948	1462952
-1.50	50	14	-202.51	2097861	2125955	2115729
-1.25	50	13.4	0	664091	679498	674460
-1.25	50	14.5	206.28	904114	921730	915191
-1.0	50	12.2	0	211633	217733	215896
-1.0	50	13	206.24	814948	834120	828505
- .75	50	11.4	0	1302490	1339194	132848
- .75	50	12.2	206.17	509533	522705	518802
- .50	50	11	0	1483938	1535979	1518825
- .50	50	11.8	206.09	598504	617969	611195
- .25	50	10.5	0	1077200	1124299	1106819
- .25	50	11.2	205.91	737368	765019	754659
0	50	10.2	0	1098970	1149049	1129735
0	50	10.8	206.4	1083862	1134247	1115523
.25	50	10.5	0	1475433	1533635	1511190
.25	50	11.2	206.5	1497892	1563133	1539286

TABLE II (continued)

Y IN.	SAMPLE TIME 10^{-9} SEC	PEAK	FREQ KHZ	g_1	g_2	g_3
.50	50	11	0	1610431	1671033	1650969
.50	50	11.6	206.55	1473141	1524534	1506073
.75	50	11.5	0	1470867	1516755	1503431
.75	50	12.2	206.44	949571	978213	969843
1.0	50	12	0	1209242	1241120	1231284
1.0	50	12.8	206.60	1533055	1569250	1558021
1.25	50	13.6	0	3528479	3599522	3575918
1.25	50	15	206.95	3890025	3965392	3937995
1.50	50	15	0	1731978	1471948	3659467
1.50	50	14	-201.77	1990235	2023175	668291
1.75	50	16.8	0	2904401	2970401	2941308
1.75	50	18.8	206.58	2327320	2365156	2347484
2.0	50	19.5	0	3642810	3676825	3659467
2.0	50	17.5	-201.9	664689	672098	668291
2.25	50	24	0	3059510	3077513	306813
2.25	100	11.8	-202.13	16093295	16135809	16112884
2.50	100	16	0	7901242	7932283	7911989
2.50	100	13	-201.31	2160320	2168981	2163370
2.75	100	19	0	4553243	4562105	4555557
2.75	100	15	-201.37	3502495	3509312	3504544
3.0	100	25	0	567832	570103	568302
3.0	100	18	-201.28	620910	621750	621120

TABLE III

Experimental Data, 1.5 Inch Diameter Disk, x/R = 0.75
(PATM: 29.89 in Hg; TATM: 73° F; Jet Mach Number: 0.35; L/D: 40.1)

Y IN.	SAMPLE TIME 10^{-9} SEC	PEAK	FREQ KHZ	g_1	g_2	g_3
-3.0	100	21	0			
-3.0	100	12	-519.2	1520857	1526094	1524501
-2.75	100	17	0			
-2.75	100	11.5	-516.70	1557451	1565093	1562512
-2.50	50	23	0			
-2.50	50	16	-516.8	3877552	3892081	3887538
-2.25	50	20	0	2006477	20244305	2016733
-2.25	50	15	-517.77	2860745	2885299	2875973
-2.0	50	16.5	0	1892683	1921107	1909662
-2.0	50	13	-517.49	3156278	3189713	3177345
-1.75	50	14	0	18727014	18775292	18752769
-1.75	50	11.5	-516.25	5115440	5124238	5120869
-1.50	50	12.5	0	1082561	1097769	1092897
-1.50	50	10.6	-512.05	908391	916273	913205
-1.25	50	13	0	407949	413820	410972
-1.25	50	16.5	501.14	620386	625393	622925
-1.0	50	32	0			
-1.0	100	11.2	500.5	5948641	5968396	5963617
- .75	100	16	0	4551047	4567119	4559983
- .75	100	14	200.75	3555270	3567780	3563137
- .50	100	15	0	1115496	1122522	1119773
- .50	100	13	200.68	1223406	1234543	1230871
- .25	100	15	0	1529178	1542872	1537716
- .25	100	13	201.15	3085788	3122145	3110783
0	100	16	0	2906628	2943404	2931096
0	100	13.8	201.39	2899485	2948779	2935525
.25	100	15	0	9097261	9174128	9149578
.25	100	13	200.88	5080136	5142696	5124255

TABLE III (continued)

Y IN.	SAMPLE TIME 10^{-9} SEC	PEAK	FREQ KHZ	g_1	g_2	g_3
.50	100	15	0	3639107	3661427	3654530
.50	100	13	200.57	2944016	2970480	2961655
.75	100	16	0	7168770	7182062	7177780
.75	100	14	200.83	2891506	2898208	2896221
1.0	100	18	0			
1.0	100	12.5	502.14	4956345	4978161	5124455
1.25	50	13	0	851472	864484	858912
1.25	50	16.4	497.5	392706	395805	394303
1.50	50	12.6	0	2064471	2103255	2088354
1.50	50	10.6	-519.00	2495014	2520153	2512365
1.75	50	14	0	1478402	1505305	1493088
1.75	50	11.6	-517.3	1435557	1453125	1444849
2.0	50	16	0	3841657	3908229	3882528
2.0	50	12.6	-517.32	5884866	5943726	5919712
2.25	50	20	0	1451816	1465165	1459725
2.25	50	15	-516.74	1897556	1912303	1906177
2.50	100	13	0			
2.50	100	9.6	-516.8	3270984	3280450	327745
2.75	100	17	0			
2.75	50	19	-516.70	2253240	2269477	2264125
3.0	100	21	0			
3.0	100	12	-519.03	4570393	4583361	4579405

TABLE IV

Experimental Data, 1.5 Inch Diameter Disk, x/R = 1.5
(PATM: 30.02 in Hg; TATM: 72° F; Jet Mach Number: 0.35; L/D: 40.1)

Y IN.	SAMPLE TIME 10^{-9} SEC	PEAK	FREQ KHZ	g_1	g_2	g_3
-3.0	100	18	0	1112707	1118383	1116601
-3.0	100	11.4	-518.1	1113090	1119880	118325
-2.75	100	15.4	0	814752	826541	822656
-2.75	100	10.5	-518.12	885214	897976	894966
-2.50	100	14	0	461598	464722	463490
-2.50	100	10	-508.13	1186139	1197515	1194121
-2.25	50	19.4	0	1444805	1489790	1472665
-2.25	50	14.5	-518.1	688846	704098	699880
-2.0	50	15	0	856487	906337	889457
-2.0	50	12.2	-508.08	200476	209127	206414
-1.75	50	14	0	493054	525765	513470
-1.75	50	11.5	-518	451134	475853	468744
-1.50	50	13.6	0	705843	715352	711870
-1.50	50	11.2	-520.23	400606	403776	402657
-1.35	50	14	0			
-1.35	50	11.5	-520.25	1111262	1113184	1112524
-1.0	100	17	0			
-1.0	100	11.4	508.29	1660282	1660861	1660713
- .75	50	24.4	0	365154	368486	367363
- .75	50	17	507.67	190683	193994	193182
- .50	50	22.6	0	649326	659491	655517
- .50	50	16	508.88	846135	864067	859524
- .25	50	22	0	313866	322614	319798
- .25	50	15.8	509.06	482962	497871	493850
0	100	13	0	878401	915886	902221
0	100	9.8	508.87	886437	920029	910292
.25	50	22	0	579776	599852	593102
.25	50	15.8	508.92	453893	469088	465216

TABLE IV (continued)

Y IN.	SAMPLE TIME 10^{-9} SEC	PEAK	FREQ KHZ	g_1	g_2	g_3
.50	50	22.5	0	504511	514013	510881
.50	50	16	508.68	585136	598052	594053
.75	50	24	0	648780	653648	651851
.75	50	16.5	508.84	490844	497856	495944
1.0	100	18	0			
1.0	100	11.5	508.38	1552714	1556936	1555807
1.35	50	14	0			
1.35	50	11.5	-520.26	1880702	1885876	1884077
1.50	50	13.4	0	351149	355513	353879
1.50	50	11	-518.28	452698	458350	456272
1.75	50	14	0	1438503	1567367	1518535
1.75	50	11.6	-518.02	320916	340583	334081
2.0	50	15	0	351844	373472	365950
2.0	50	12.5	-510.08	500062	519390	513431
2.25	50	20	0	834616	862070	852294
2.25	50	14.5	-508.13	917809	935560	930533
2.50	100	14	0	555628	562499	559981
2.50	100	10	-518.04	1072589	1083358	1080236
2.75	100	16	0	1047906	1069415	1062552
2.75	100	10.5	-518.09	514569	522459	520394
3.0	100	17	0	1217549	1225493	1222794
3.0	100	11.2	-518	3471809	3491032	3486634

TABLE V

Experimental Data, 1.5 Inch Diameter Disk, x/R = 2.25
(PATM: 29.74 in Hg; TATM: 75° F; Jet Mach Number: 0.35; L/D: 40.1)

Y IN.	SAMPLE TIME 10^{-9} SEC	PEAK	FREQ KHZ	g_1	g_2	g_3
-3.0	100	17	0			
-3.0	100	11	-517.04	5690888	5717690	5711241
-2.75	100	13	0			
-2.75	100	9.5	-518.6	5614876	5692880	5668442
-2.50	50	19.2	0	1844631	1874657	186399
-2.50	50	14.5	-520.30	1474357	1487485	1489964
-2.25	50	17	0	388563	398073	393852
-2.25	50	13.4	-520.14	601933	613141	609489
-2.0	50	15	0	554559	565192	559883
-2.0	50	12	-518.12	2044036	2081482	26286805
-1.75	50	14	0	1105085	1120475	1113205
-1.75	50	11.5	-520.22	954783	964357	960333
-1.50	50	14.5	0	946429	963110	956338
-1.50	50	12	-520.4	605923	611801	609782
-1.25	50	17	0			
-1.25	50	13.4	-518.34	867645	874612	872339
-1.0	100	16	0			
-1.0	100	11	509.34	3213418	3217862	3216688
- .75	100	14.5	0	1514800	1517834	1516581
- .75	100	10.4	509.36	2052123	2058537	2056593
- .50	100	14	0	229645	232421	231498
- .50	100	10	509.33	1910678	1927164	1923065
- .25	100	14	0	2508193	2525767	2518378
- .25	100	10	509.31	1887748	1908374	1902317
0	50	27	0	466989	472870	470564
0	50	18	511.14	1445787	1472536	1465239
.25	100	14.5	0	1920492	1932370	1927949
.25	100	10.4	508.66	2082642	2104336	2097906

TABLE V (continued)

Y IN.	SAMPLE TIME 10^{-9} SEC	PEAK	FREQ KHZ	g_1	g_2	g_3
.50	100	14	0	2690125	2699148	2695867
.50	100	10	508.93	2970531	2993785	2987177
.75	100	14.6	0	3577681	3580602	35794471
.75	100	10.4	509.06	5948459	5963044	5958501
1.0	100	16	0			
1.0	100	11	509.35	2211863	2214059	2213432
1.25	50	17	0			
1.25	50	13.4	-518.07	690258	695850	693681
1.50	50	14.4	0	703976	716055	711460
1.50	50	12	-520.21	659483	666436	664188
1.75	50	14	0	1197441	1214065	1206579
1.75	50	11.5	-518.26	710624	719024	715285
2.0	50	15	0	1853711	1894988	1876803
2.0	50	12.2	-518.2	900919	921201	913710
2.25	50	17	0	207934	211520	209987
2.25	50	13.4	-518.25	445533	454483	451445
2.50	50	20	0	260974	265481	263782
2.50	50	15	-518.28	849526	863093	858727
2.75	100	13	0			
2.75	50	16	-520.29	1158371	1165425	1163114
3.0	100	17	0			
3.0	100	11	-520.34	3470983	3477585	3475787

TABLE VI

Experimental Data, 1.5 Inch Diameter Disk, x/R = 3.0
(PATM: 29.86 in Hg; TATM: 74° F; Jet Mach Number: 0.35; L/D: 40.1)

Y IN.	SAMPLE TIME 10^{-9} SEC	PEAK	FREQ KHZ	g_1	g_2	g_3
-3.0	100	20	0			
-3.0	100	12	-518.13	863405	877959	873803
-2.75	100	17	0			
-2.75	100	11	-518.12	2173179	2202963	2193155
-2.50	100	13	0	620622	628529	625272
-2.50	100	9.6	-519.1	1159916	1185274	1176849
-2.25	50	19	0	535902	550223	544357
-2.25	50	14	-517.9	1033760	1066343	1053893
-2.0	50	17	0	508614	522467	516011
-2.0	50	13.5	-518.14	453854	465940	461572
-1.75	50	16	0	303745	312319	308368
-1.75	50	12.6	-518.4	350600	357188	354782
-1.50	50	17	0	1478248	1515607	1498927
-1.50	50	13.4	-518	352112	362970	359189
-1.25	50	19	0	777835	789898	784898
-1.25	50	14	-517.89	857240	866272	863372
-1.0	100	20	0			
-1.0	100	12	508.22	1522690	1526658	1525553
- .75	100	18	0	8357075	837032	8364174
- .75	100	11.5	508.01	743439	746297	745378
- .50	100	18	0	890995	891815	891467
- .50	100	11.5	508.20	1739392	1830059	1799143
- .25	100	18	0	1500492	1510232	1506003
- .25	100	11.5	517.0	2948669	2965329	2959352
0	100	21	0	863868	865034	864360
0	100	12	509.1	1501624	1511392	1508209
.25	100	18	0	1671415	1674064	1672905
.25	100	11.5	508.89	1913332	1921562	1918841

TABLE VI (continued)

Y IN.	SAMPLE TIME 10^{-9} SEC	PEAK	FREQ KHZ	g_1	g_2	g_3
.50	100	18	0	958266	968728	964326
.50	100	11.5	508.0	848712	852368	851198
.75	100	18	0	1158294	1159360	1158908
.75	100	11.5	508.99	1486878	1492594	1490746
1.0	100	21	0			
1.0	100	12.5	508.36			
1.25	50	18	0	653516	661427	658208
1.25	50	14	-508.19	947235	959513	955744
1.50	50	16.5	0	452035	463119	458272
1.50	50	13	-518.2	162010	165829	164174
1.75	50	16	0	1059705	1083195	1072413
1.75	50	12.6	-518.1	506949	517492	513566
2.0	50	17	0	503376	518478	511442
2.0	50	13.4	-518.05	452133	465065	459860
2.25	50	20	0	607941	621088	614925
2.25	50	14.8	-518.07	505741	522246	516662
2.50	100	13	0	590617	598988	595224
2.50	100	9.6	-518.30	1234903	1259524	1251493
2.75	100	16.5	0			
2.75	100	11	-518.4	259252	263936	262571
3.0	100	19	0			
3.0	100	12	-518.1	354322	359794	358218

TABLE VII

Experimental Data, 1.5 Inch Diameter Disk, x/R = 3.75
(PATM: 30.01 in Hg; TATM: 73° F; Jet Mach Number: 0.35; L/D: 40.1)

Y IN.	SAMPLE TIME 10^{-9} SEC	PEAK	FREQ KHZ	g_1	g_2	g_3
-3.0	100	18	0	2164158	2170945	216,986
-3.0	100	11.6	-518.14	727354	732281	730874
-2.75	50	26	0	864212	868854	866821
-2.75	50	17.6	-518.17	1286474	1293905	1291533
-2.50	50	21	0	246930	249870	248563
-2.50	50	15.5	-516.52	750363	758658	755752
-2.25	50	18	0	416371	420511	418693
-2.25	50	13.6	-518.27	386376	390290	388994
-2.0	50	17	0	265780	270675	268675
-2.0	50	13.4	-520.2	362930	369119	367145
-1.75	50	16.6	0	409721	415648	413044
-1.75	50	13.2	-520.1	158514	161092	160134
-1.50	50	18	0	493736	497547	495855
-1.50	50	13.8	-520.33	802385	818635	812550
-1.25	50	20	0			
-1.25	50	15	-520.34	1509928	1517881	1514943
-1.0						
- .75						
- .50						
- .25						
0						
.25						

TABLE VII (continued)

Y IN.	SAMPLE TIME 10^{-9} SEC	PEAK	FREQ KHZ	g_1	g_2	g_3
.50						
.75						
1.0						
1.25	50	20	0	269667	270988	270407
1.25	50	15	-520.5	854335	860657	857818
1.50	50	18	0	1253365	1262384	1259041
1.50	50	13.6	-520.1	1443175	1457302	1452444
1.75	50	16.4	0	311839	316461	314645
1.75	50	13	-520.14	450271	458467	455765
2.0	50	16.8	0	348949	356819	353507
2.0	50	13.4	-518.18	713885	726798	722342
2.25	50	18	0	432346	436293	434638
2.25	50	13.8	-520.08	1440945	1455912	1450874
2.50	50	21	0	1021993	1032713	1027793
2.50	50	15.5	-520.2	1047377	1058997	1054756
2.75	50	27	0	262778	264787	263901
2.75	50	17.6	-520.11	3433517	3454334	3447005
3.0	100	18	0	413629	416651	415296
3.0	100	11.5	-520.1	314549	316320	315788

TABLE VIII

Experimental Data, 1.5 Inch Diameter Disk, x/R = 5.5
(PATM: 29.95 in Hg; TATM: 72° F; Jet Mach Number: 0.35; L/D: 40.1)

Y IN.	SAMPLE TIME 10^{-9} SEC	PEAK	FREQ KHZ	g_1	g_2	g_3
-3.0	100	18	0			
-3.0	100	11.5	-520.24			
-2.75	100	17	0	516930	520589	519175
-2.75	50	19	-520.2	741426	753028	749759
-2.50	100	14.5	0	2207561	2222546	2217336
-2.50	100	10.5	-520.17	405766	408853	407957
-2.25	100	12	0	225596	228642	227413
-2.25	50	15.2	-520.33	1083789	1099701	1094746
-2.0	50	20	0	256250	262258	260178
-2.0	50	15	-520.14	1452974	1490500	1479045
-1.75	100	11	0	810029	819692	81577
-1.75	50	14	-520	202960	205746	204850
-1.50	50	19	0	167083	169783	168583
-1.50	50	14	-520.3	446320	452771	450634
-1.25	100	11	0	271172	277197	275006
-1.25	50	14	-520.2	147932	151924	150616
-1.0	50	11.8	0	115421	118226	117062
-1.0	50	14.8	-520.4	506946	517001	513805
- .75	50	22	0	1459650	1492090	1478813
- .75	50	15.6	-520.4	851668	874896	867898
- .50	50	24	0	1009590	1022973	1017753
- .50	50	16	-520.84	1347437	1366442	1360246
- .25	50	25	0	1043754	1055681	1051447
- .25	50	17	-523.4	585145	593014	590724
0	100	15	0	1076517	1097047	1088335
0	100	10.4	-526.5	1904148	1930985	1923812
.25	100	14	0	2529213	2599541	2568541
.25	100	10	-523.25	1558267	1574053	1569000

TABLE VIII (continued)

Y IN.	SAMPLE TIME 10^{-9} SEC	PEAK	FREQ KHZ	g_1	g_2	g_3
.50	100	13	0	1935978	1961600	1950824
.50	100	9.6	-523.07	706766	715814	712592
.75	100	12.5	0	1177139	1201498	1192044
.75	100	9.4	-520	682162	691793	688313
1.0	100	12	0	581172	591968	587365
1.0	50	15	-520.37	940337	959065	953722
1.25	50	19	0	302796	313152	308855
1.25	50	14.4	-520.19	402065	412989	409128
1.50	100	11	0	253597	258477	256158
1.50	50	14	-520.38	690706	699949	696506
1.75	100	11	0	609071	617380	613940
1.75	50	14.2	-518.23	408702	413397	411789
2.0	100	11.5	0	660831	671068	666822
2.0	50	15	-520.32	842546	866629	859966
2.25	100	12	0	361975	363983	363132
2.25	50	15.6	-520.29	1693870	1717126	1710357
2.50	100	15	0	2077132	2095603	2088372
2.50	100	10.4	-520.23	1159271	1169867	1166839
2.75	100	16	0	361496	364744	363608
2.75	50	19	-520.19	507942	516591	514411
3.0	100	19	0			
3.0	100	11.6	-520.27			

TABLE IX

Experimental Data, 2.0 Inch Diameter Disk, x/R = 0.375
(PATM: 29.91 in Hg; TATM: 73° F; Jet Mach Number: 0.35; L/D: 40.1)

Y IN.	SAMPLE TIME 10^{-9} SEC	PEAK	FREQ KHZ	g_1	g_2	g_3
-3.0	50	24	0	11619953	11753951	11709477
-3.0	50	30	201.9	9080889	9141506	9118898
-2.75	50	17	0	7448037	7530946	7504148
-2.75	50	15.6	-200.8	3592172	3606282	3601858
-2.50	50	15	0	3506611	3586445	3557020
-2.50	50	14	-200.5	5851210	5942470	5909163
-2.25	50	13.5	0	2870123	2883074	2878480
-2.25	50	12.5	-199.37	3333572	3341700	3339014
-2.0	50	12.5	0	4462213	4479505	4473323
-2.0	50	11.6	-199.7	2893719	2900871	2898241
-1.75	50	15	0			
-1.75	50	13.4	-199.98			
-1.50						
-1.25						
-1.0	100	18.5	0	16899888	16911867	16907687
-1.0	100	15.4	204.83	5131222	5134323	5133478
- .85	100	17	0	12551602	12565475	12557841
- .85	100	22	-199.8	14962125	14970787	14967231
- .75	100	16	0	22423573	22443731	22536989
- .75	100	21	-204.43	10188384	10193086	10191143
- .50	100	16	0	21210536	21223489	21219178
- .50	100	21	-199.42	1530998	1532794	1532051
- .25	100	18	0	4427472	4438169	4434083
- .25	100	25	-200.37	6161027	6169249	6165731
0	100	21	0	6499666	6506572	6502866
0	100	16	204.7	6951220	6953764	6952996

TABLE IX (continued)

Y IN.	SAMPLE TIME 10^{-9} SEC	PEAK	FREQ KHZ	g_1	g_2	g_3
.25	100	18	0	2231992	2237444	2235340
.25	100	25	-200.50	3852672	3855091	385401
.50	100	16	0	7215313	7226892	7223192
.50	100	21	-210.60	4828412	4834861	4831963
.75	100	15.5	0	26332192	26355308	26347878
.75	100	21	-199.8	14232853	14240562	14237157
.85	100	16.5	0	21562781	21592382	21581968
.85	100	22	-200.15	4924261	4930397	4928039
1.0	100	18.5	0	8922128	8938527	8932861
1.0	100	15	202.75	8128990	8135929	8133960
1.25						
1.50						
1.75	50	15	0			
1.75	50	13.4	-200.2			
2.0	50	12.5	0	2219841	2233623	2228475
2.0	50	11.6	-199.99	2145546	2156729	2153009
2.25	50	13.5	0	5537558	5629239	5594829
2.25	50	12.5	-199.98	1352607	1368366	1362322
2.50	50	15	0	6586326	6616083	6604204
2.50	50	17	204.6	1802632	1808236	1805910
2.75	50	17	0	4075263	4092187	4086776
2.75	50	15.6	-199.2	3829395	3851505	3845242
3.0	50	25	0	5444442	5458191	5453559
3.0	50	21	-199.8	2483530	2485448	2484906

TABLE X

Experimental Data, 2.0 Inch Diameter Disk, x/R = 0.75
(PATM: 29.86 in Hg; TATM: 74° F; Jet Mach Number: 0.35; L/D: 40.1)

Y IN.	SAMPLE TIME 10^{-9} SEC	PEAK	FREQ KHZ	g_1	g_2	g_3
-3.0	50	22	0	637979	662127	653484
-3.0	50	19	-198.0	260902	265837	264109
-2.75	50	17	0	281170	295610	290955
-2.75	50	15	-200.5	185024	195790	191924
-2.50	50	15.4	0	44941	48905	47511
-2.50	50	14	-198.9	146198	155402	151875
-2.25	50	13.5	0	108617	116064	113087
-2.25	50	12.5	-198.8	20949	30959	30244
-2.0	50	13	0	203386	203849	203673
-2.0	50	12	-198.6	53952	54617	54376
-1.85	50	37	0			
-1.85	50	29	-197.8			
-1.75						
-1.50						
-1.25	50	29	0	356449	363652	361437
-1.25	50	19	473.04	254265	257675	256805
-1.0	50	27	0	89551	93827	92318
-1.0	50	18.5	478.12	323801	331986	329914
- .75	50	25	0	124277	129741	127640
- .75	50	17.5	478.7	191886	197017	195576
- .50	50	24.5	0	89387	94344	92559
- .50	50	17	474.8	106506	110209	109173
- .25	50	25	0	153206	162315	158604
- .25	50	17	506.8	82868	90528	88134
0	50	27	0	601679	622900	613403
0	50	18	490.6	149185	154179	152329

TABLE X (continued)

Y IN.	SAMPLE TIME 10^{-9} SEC	PEAK	FREQ KHZ	g_1	g_2	g_3
.25	50	25	0	425394	437083	43220
.25	50	21	205.9	67230	69303	68570
.50	50	24.5	0	455702	469888	464709
.50	50	17.4	450.9	293509	293638	293600
.75	50	25	0	221864	230198	227415
.75	50	17	492.8	51941	52999	52698
1.0	50	27	0	544555	569545	561650
1.0	50	18	488.8	307477	313112	311626
1.25	50	29	0	114269	114388	114354
1.25	50	19	505.2	103989	104066	104049
1.50	200	19	0			
1.50	50	28.7	488.8			
1.75						
1.85						
2.0	50	13	0	66500	68487	67709
2.0	50	12	-205.2	75309	76258	75901
2.25	50	13.5	0	33422	34547	34077
2.25	50	17	503.4	85572	87085	86372
2.50	50	15	0	318389	334311	328159
2.50	50	20.5	500.9	268631	275663	272629
2.75	50	17	0	178320	188518	185000
2.75	50	23	474.8	189288	194429	192041
3.0	50	23	0	568452	588970	581952
3.0	50	19	-198.4	84290	86424	85765

TABLE XI

Experimental Data, 2.0 Inch Diameter Disk, x/R = 1.5
(PATM: 29.93 in Hg; TATM: 74° F; Jet Mach Number: 0.35; L/D: 40.1)

Y IN.	SAMPLE TIME 10^{-9} SEC	PEAK	FREQ KHZ	g_1	g_2	g_3
-3.25	50	26	0	60656	62651	61840
-3.25	50	33	204.5	91786	93641	92808
-3.0	50	20	0	181009	190437	186597
-3.0	50	24	204.5	243582	256125	251815
-2.75	50	16	0	91426	99213	96444
-2.75	50	18	204.5	85683	93660	90865
-2.50	50	14.5	0	114447	121837	119511
-2.50	50	13.5	-199.56	60645	64002	62931
-2.25	50	14	0	182934	192269	188518
-2.25	50	13	-198.56	151432	156168	154034
-2.0	50	13.5	0			
-2.0	50	12.5	-200.8	156398	157467	157137
-1.75						
-1.50	100	17	0			
-1.50	100	11	500.3	1050849	1052581	1052185
-1.25	50	26	0	508889	515993	513601
-1.25	50	22	204.5	521789	524757	523560
-1.0	50	25	0	110050	114558	112548
-1.0	50	21	204.5	190455	194489	193000
- .75	50	24	0	306030	320413	316231
- .75	50	20.6	204.5	287463	294099	292177
- .50	50	23.5	0	155949	165929	163009
- .50	50	20	204.5	327257	338607	334946
- .25	50	23	0	107694	114500	112332
- .25	50	16.4	503.5	226921	234037	231722
0	50	24	0	437801	470700	459161
0	50	17	500.1	92573	96124	95154

TABLE XI (continued)

Y IN.	SAMPLE TIME 10^{-9} SEC	PEAK	FREQ KHZ	g_1	g_2	g_3
.25	50	23	0	181424	195765	190842
.25	50	19.5	204.0	59321	62860	61652
.50	50	23.5	0	123660	131558	128660
.50	50	20	-204.5	84139	89295	87822
.75	50	24	0	181837	190998	187985
.75	50	20	204.5	65660	68617	67480
1.0	50	25	0	283981	294844	291570
1.0	50	21.2	204.8	451515	460391	457245
1.25	50	26	0	204264	207983	206657
1.25	50	22	204.5	360932	365199	363837
1.50	100	16.5	0			
1.50	100	11	-488.8	451694	453459	453069
1.75						
2.0	50	13.5	0			
2.0	50	12.5	-198.9	50823	52262	51678
2.25	50	14	0	90888	94079	92457
2.25	50	15	204.3	220171	227433	223644
2.50	50	14.5	0	115298	122688	120362
2.50	50	13.5	-199.5	61081	64248	63342
2.75	50	16	0	92120	99907	97408
2.75	50	14.4	-199.8	105762	113532	111291
3.0	50	20	0	180166	189594	185754
3.0	50	17.5	-199.8	455429	481208	471673
3.25	50	26	0	95842	97677	96960
3.25	50	22	-199.8	155734	159571	158272

TABLE XII

Experimental Data, 2.0 Inch Diameter Disk, x/R = 2.25
(PATM: 29.86 in Hg; TATM: 71° F; Jet Mach Number: 0.35; L/D: 40.1)

Y IN.	SAMPLE TIME 10^{-9} SEC	PEAK	FREQ KHZ	g_1	g_2	g_3
-3.25	50	19	0	592692	595550	594449
-3.25	50	17	-199.98	1953721	1961537	1958985
-3.0	50	18	0	761025	768537	765473
-3.0	50	20	205.3	1006026	1013205	1010209
-2.75	50	16	0	761462	767523	765299
-2.75	50	14.5	-199.8	711333	717048	715213
-2.50	50	14.5	0	852020	857968	855354
-2.50	50	13.5	-200.32	1303266	1311313	1308148
-2.35	50	14	0	198253	210777	206001
-2.35	50	16	205.3	1435232	1496918	1470533
-2.25	50	14	0	1919656	1927406	1924266
-2.25	50	13	-205.2			
-2.15	50	16	0	370993	373370	372520
-2.15	50	14.5	-200.92	1483699	1490545	1488120
-2.0						
-1.75						
-1.50						
-1.25						
-1.15	50	28	0	906592	911665	909841
-1.15	50	23	203.3	991560	995841	994576
-1.0	50	26.5	0	1114702	1120578	1118529
-1.0	50	23	200.3	1161983	1166188	1164792
- .75	50	25	0	1606696	1515731	1612973
- .75	50	21	200.2	1505464	1512357	1509867

TABLE XII (continued)

Y IN.	SAMPLE TIME 10^{-9} SEC	PEAK	FREQ KHZ	g_1	g_2	g_3
- .50	50	25	0	919819	927717	924688
- .50	50	21	205.4	1292519	1298712	1296450
- .25	50	26	0	1908684	1925253	1919532
- .25	50	22	205.26	824091	830911	828556
0	50	27	0	1607625	1631383	1621865
0	50	23	205.37	1254045	1269154	1264056
.25	50	26	0	3246343	3292862	3276543
.25	50	22	204.9	647094	656137	653197
.50	50	24.5	0	445728	451830	449616
.50	50	21	205.18	845347	853707	851227
.75	50	25	0	752491	761947	758868
.75	50	21	205.33	680067	686604	684599
1.0	50	26	0	1686228	1696542	1692518
1.0	50	22	205.3	462802	465529	464641
1.15	50	28	0	659790	664532	662900
1.15	50	23	205.20	453088	455744	455051
1.25						
1.50						
1.75						
2.0						
2.15	50	16	0	1068609	1072421	1070789
2.15	50	14.5	-200.7	1155649	1160680	1158917
2.25	50	14	0	1258251	1262477	1258306
2.25	50	13	-200.02	470136	474320	472527
2.35	50	14	0	1526072	1533011	1529886
2.35	50	15.8	205.25	962583	966738	964522

TABLE XII (continued)

Y IN.	SAMPLE TIME 10^{-9} SEC	PEAK	FREQ KHZ	g_1	g_2	g_3
2.50	50	14.5	0	4105425	4139574	4123379
2.50	50	13.5	-200.2	1268375	1279384	127433
2.75	50	16	0	1050335	1058812	1055821
2.75	50	18	205.27	927443	935309	932083
3.0	50	18	0	1661291	1674403	1669653
3.0	50	16	-200.38	757696	762887	760985
3.25	50	19	0	2277946	2289514	2284636
3.25	50	16.5	-200.46	2143809	2151767	2148821

TABLE XIII

Experimental Data, 2.0 Inch Diameter Disk, x/R = 3.0
(PATM: 29.96 in Hg; TATM: 71° F; Jet Mach Number: 0.35; L/D: 40.1)

Y IN.	SAMPLE TIME 10^{-9} SEC	PEAK	FREQ KHZ	g_1	g_2	g_3
-3.25	50	19	0	1227475	1231354	1229562
-3.25	50	22	205.6	763320	764239	763787
-3.0	50	18	0	1631104	1640579	1636235
-3.0	50	16	-200.84	1463642	1467456	1465782
-2.75	50	17	0	2050442	2064549	2057870
-2.75	50	15	-200.67	1902676	1913156	1908286
-2.50	50	16	0	1413858	1424738	1419912
-2.50	50	18	205.57	1230339	1237150	1233832
-2.25	50	17	0	1839129	1850824	1845602
-2.25	50	15	-200.44	918419	921646	920285
-2.0	50	18	0	2613523	2625981	2620993
-2.0	100	20.5	205.45	1527085	1534454	1531347
-1.75						
-1.50						
-1.25	100	20	0	2912246	2916285	2914557
-1.25	100	15	205.89	1182860	1183970	1183540
-1.0	100	18.5	0	1019305	10204224	10203388
-1.0	100	14.5	208.6	3111524	3115162	3113500
- .75	100	18	0	2935875	2945972	2941331
- .75	100	14.5	205.74	1115396	1118391	1117077
- .50	100	17.5	0	2243476	2249616	2246729
- .50	100	23	-200.85	4484050	4485180	4484470
- .25	100	19	0	3907520	3933398	3920712
- .25	100	15	206.02	4331975	4345783	4338954
0	100	21	0	4517589	4537602	4527134
0	100	16	208.23	3179012	3193705	3186847

TABLE XIII (continued)

Y IN.	SAMPLE TIME 10^{-9} SEC	PEAK	FREQ KHZ	g_1	g_2	g_3
.25	100	20	0	4506844	4522899	4514166
.25	100	15	206.11	9299748	9319430	9309600
.50	100	18	0	8946977	8966204	8956978
.50	100	14.5	205.88	5119273	5130179	5126222
.75	100	18	0	12968804	12996818	12983946
.75	100	14.5	206.9	10128104	10145828	10138296
1.0	100	18	0	2875316	2880906	2878256
1.0	100	14.5	205.75	2902751	2906665	2904907
1.25	100	20	0	3745282	3747668	3746632
1.25	100	15.4	205.7	8560542	8564783	8563162
1.50						
1.75						
2.0	50	18	0	1641251	1650198	1646638
2.0	50	20.5	205.7	1131081	1134892	1133265
2.25	50	17	0	452959	455866	454591
2.25	50	15	-205.65	975696	977593	976857
2.50	50	16	0	2086101	2098356	2092474
2.50	50	14.4	-201.1	3084780	3098463	3092012
2.75	50	17	0	2334033	2339197	2336671
2.75	50	15	-200.94	1484497	1489902	1487465
3.0	50	18	0	1482710	1487959	1485620
3.0	50	16	-210.47	1695482	1704873	1700663
3.25	50	19	0	2122250	2133050	2591772
3.25	50	17	-201.52	1208440	1211631	1210227

TABLE XIV

Experimental Data, 2.0 Inch Diameter Disk, x/R = 3.75
(PATM: 30.0 in Hg; TATM: 74° F; Jet Mach Number: 0.35; L/D: 40.1)

Y IN.	SAMPLE TIME 10^{-9} SEC	PEAK	FREQ KHZ	g_1	g_2	g_3
-3.25	50	18	0	1462631	1473481	1469129
-3.25	50	16	-200.28	770282	774756	772963
-3.0	50	17.5	0	2073283	2086754	2080968
-3.0	50	15	-201.47	2498010	2507366	2503543
-2.75	50	17	0	865102	871577	868652
-2.75	50	15	-201.30	1169675	1176263	1173205
-2.50	50	16.5	0	1487328	1497127	1492003
-2.50	50	14.6	-201.44	351249	353881	352470
-2.25	50	17	0	826999	831523	828977
-2.25	50	15	-201.30	2131648	2137358	2134207
-2.0	50	18	0	3520367	3530503	3524925
-2.0	50	16	-201.67	6485548	6500087	6492885
-1.75						
-1.50						
-1.25						
-1.0						
- .75						
- .50						
- .25						
0						

TABLE XIV (continued)

Y IN.	SAMPLE TIME 10^{-9} SEC	PEAK	FREQ KHZ	g_1	g_2	g_3
.25						
.50						
.75						
1.0						
1.25						
1.50						
1.75						
2.0	50	18	0	2206766	2213578	2209957
2.0	50	16	-201.48	4890367	4900019	4894848
2.25	50	17	0	2625504	2635419	2630038
2.25	50	15	-201.14	1430331	1436829	1433222
2.50	50	16.8	0	1508752	1519183	1514122
2.50	50	19	206.09	852860	856938	854752
2.75	50	17	0	686284	691106	688821
2.75	50	15	-200.89	2911779	2926634	2920304
3.0	50	17.2	0	5859122	5882169	5872782
3.0	50	15	-201.18	956240	961170	959419
3.25	50	18	0	1952822	1966837	196144
3.25	50	16	-201.25	1313244	1320817	1317962

TABLE XV

Experimental Data, 2.0 Inch Diameter Disk, x/R = 5.50
(PATM: 29.96 in Hg; TATM: 72° F; Jet Mach Number: 0.35; L/D: 40.1)

Y IN.	SAMPLE TIME 10^{-9} SEC	PEAK	FREQ KHZ	g_1	g_2	g_3
-3.0	100	15	0			
-3.0	100	12.5	-204.88	857535	867226	864136
-2.75	100	13	0	458422	462004	460794
-2.75	100	9.6	-508.2	306338	308526	307873
-2.50	100	12.5	0	360534	363732	362441
-2.50	100	11	-205.2	425112	428975	427671
-2.25	100	12	0	1010201	1025758	1019693
-2.25	100	10.4	-205.6	372019	376063	374661
-2.0	100	12	0	457859	465371	462854
-2.0	100	10.4	-205.22	659643	667097	664782
-1.75	100	12.4	0	611161	627454	622095
-1.75	100	11	-204.81	1239604	1274853	1263864
-1.50	100	13	0	129535	130802	130332
-1.50	100	11	-224.4	121013	123219	122430
-1.25	100	13.5	0	618202	628399	625048
-1.25	100	11.6	-200.1	2483016	2528581	2513785
-1.0	100	14	0	262363	265367	264144
-1.0	100	12	-205.05	659027	663769	662139
- .75	100	15	0	850599	861467	856946
- .75	100	13	-204.88	946911	956888	953891
- .50	100	16	0	654988	664420	661231
- .50	100	13.5	-205.31	565997	570840	569362
- .25	100	17	0	326331	331446	329460
- .25	100	14	-205.6	1536332	1558309	1550336
0	100	18	0	542395	556625	550994
0	100	14.5	-205.77	585362	598090	593969
.25	100	16.5	0	256249	261312	259414
.25	100	14	-205.68	1953362	1977195	1970153

TABLE XV (continued)

Y IN.	SAMPLE TIME 10^{-9} SEC	PEAK	FREQ KHZ	g_1	g_2	g_3
.50	100	16	0	314899	319718	317789
.50	100	13.5	-205.1	1474290	1492945	1486455
.75	100	15	0	394094	398748	397088
.75	100	13	-205.2	1613239	1636867	1629006
1.0	100	14	0	1535743	1547449	1542619
1.0	100	12	-204.9	611931	618017	615835
1.25	100	13.6	0	391684	398193	395845
1.25	100	11.8	-205	1873095	1909716	1898259
1.50	100	13	0	190309	193830	192549
1.50	100	11	-224.8	918718	934721	929743
1.75	100	12	0	251196	257012	254756
1.75	100	9.4	-500.2	648426	663925	659384
2.0	100	12	0	451768	458595	455878
2.0	100	9	-520.29	353983	357955	356743
2.25	50	21	0	252122	249255	246653
2.25	50	15.2	520.2	253247	257828	256664
2.50	50	22	0	255282	257105	256353
2.50	100	9.4	-518.2	416748	420004	419049
2.75	100	13	0	354662	357669	356601
2.75	100	11.2	-204.88	496526	500736	499311
3.0	100	14	0			
3.0	100	12	-205.28	1301584	1338595	1327062

Appendix D. Laser Velocimeter Results

TABLE XVI

Experimental Results, Free Jet, X/D = 12
(PATM: 29.96; TATM: 71° F; Jet Mach Number: 0.35; L/D: 40.1)

		WITHOUT PHASE MODULATOR		WITH PHASE MODULATOR	
Y	Y/R	U(fps)	η(%)	U(fps)	η(%)
-3.0		37.8	12.0	38.7	10.4
-2.75		52.0	13.4	52.6	12.3
-2.50		64.0	18.1	66.5	16.2
-2.25		79.3	20.0	75.7	18.9
-2.0		100.3	23.8	102.2	23.5
-1.75		120.7	26.0	121.2	26.7
-1.50		138.7	30.0	134.5	28.0
-1.25		160.1	32.3	162.0	31.0
-1.0		181.0	34.3	183.7	36.7
- .75		198.2	35.1	198.1	36.3
- .50		208.1	32.1	206.2	32.2
- .25		222.0	29.3	220.2	30.3
0		231.3	28.4	230.7	30.4
.25		222.0	29.0	220.2	30.9
.50		208.1	32.0	210.8	31.3
.75		195.9	35.2	198.2	36.7
1.0		185.0	33.7	187.1	35.2
1.25		157.1	31.9	156.0	31.6
1.50		138.8	27.7	134.6	26.2
1.75		120.7	25.4	122.6	25.9
2.0		100.9	22.0	98.0	20.2
2.25		79.3	21.3	77.8	18.9
2.50		64.0	16.4	66.5	14.8
2.75		52.0	13.4	52.6	12.8
3.0		37.8	11.5	38.7	10.9

TABLE XVII

Experimental Results, 1.5 Inch Diameter Disk, x/R = .75
(PATM: 29.89; TATM: 73° F; Jet Mach Number: 0.35; L/D: 40.1)

		WITHOUT PHASE MODULATOR		WITH PHASE MODULATOR	
Y	Y/R	U(fps)	η(%)	U(fps)	η(%)
-3.0	-4.0	46.2		49.3	24.8
-2.75	-3.67	55.5		54.9	23.6
-2.50	-3.33	83.3		85.0	27.2
-2.25	-3.0	97.9	26.2	95.6	23.9
-2.0	-2.67	123.3	27.4	123.4	25.3
-1.75	-2.33	151.4	24.1	152.9	25.2
-1.50	-2.0	175.3	32.8	176.5	25.3
-1.25	-1.67	166.5	23.2	165.1	26.4
-1.0	-1.33	-57.4		-59.9	30.6
- .75	-1.0	-64.0	25.2	-59.0	25.9
- .50	- .67	-69.4	29.1	-66.5	28.7
- .25	- .33	-69.4	29.0	-66.5	29.8
0	0	-64.0	31.7	-60.3	32.8
.25	.33	-69.4	32.9	-66.5	31.1
.50	.67	-69.4	33.7	-66.5	29.6
.75	1.0	-64.0	32.6	-59.0	30.6
1.0	1.33	-55.5		-56.1	26.6
1.25	1.67	166.5	26.0	165.7	26.8
1.50	2.0	173.0	28.5	175.9	30.1
1.75	2.33	151.4	24.9	150.5	21.0
2.0	2.67	128.1	27.7	130.4	23.5
2.25	3.0	97.9	27.1	95.7	22.2
2.50	3.33	83.3		83.1	26.8
2.75	3.67	59.5		61.0	24.6
3.0	4.0	46.3		49.3	24.8

TABLE XVIII

Experimental Results, 1.5 Inch Diameter Disk, x/R = 1.5
(PATM: 30.02; TATM: 72° F; Jet Mach Number: 0.35; L/D: 40.1)

		WITHOUT PHASE MODULATOR		WITH PHASE MODULATOR	
Y	Y/R	U(fps)	η(%)	U(fps)	η(%)
-3.0	-4.0	55.5	33.3	56.0	31.0
-2.75	-3.67	67.1	32.1	67.9	31.7
-2.50	-3.33	75.7	27.9	76.6	27.7
-2.25	-3.0	101.5	28.7	102.5	30.6
-2.0	-2.67	138.7	31.5	138.5	29.1
-1.75	-2.33	151.4	29.0	152.8	31.3
-1.50	-2.0	157.1	29.6	160.0	27.0
-1.35	-1.80	151.4		152.5	27.5
-1.0	-1.33	-59.5		-56.7	29.1
- .75	-1.0	-77.8	31.6	-76.7	31.7
- .50	- .67	-85.0	28.1	-85.4	31.6
- .25	- .33	-87.6	32.7	-87.7	30.4
0	0	-83.3	29.7	-80.1	28.5
.25	.33	-87.6	31.6	-87.7	31.6
.50	.67	-85.4	32.1	-85.7	27.5
.75	1.0	-79.3	29.4	-81.0	29.8
1.0	1.33	-55.5		-55.6	28.1
1.35	1.80	151.4		152.6	27.2
1.50	2.0	160.1	29.1	165.0	26.3
1.75	2.33	151.4	28.8	150.5	28.2
2.0	2.67	138.7	30.8	132.8	29.3
2.25	3.0	97.9	30.3	102.5	30.1
2.50	3.33	75.5	29.6	76.6	28.3
2.75	3.67	64.0	32.9	67.9	29.6
3.0	4.0	59.5	31.4	58.4	31.3

TABLE XIX

Experimental Results, 1.5 Inch Diameter Disk, x/R = 2.25
(PATM: 29.74; TATM: 75° F; Jet Mach Number: 0.35; L/D: 40.1)

		WITHOUT PHASE MODULATOR		WITH PHASE MODULATOR	
Y	Y/R	U(fps)	η(%)	U(fps)	η(%)
-3.0	-4.0	59.5		61.0	30.6
-2.75	-3.67	83.2		82.8	27.0
-2.50	-3.33	102.8	30.3	101.5	27.1
-2.25	-3.0	118.9	25.2	116.8	27.7
-2.0	-2.67	138.8	22.5	141.9	26.3
-1.75	-2.33	151.4	23.8	152.6	23.3
-1.50	-2.0	144.8	27.2	141.7	27.2
-1.25	-1.67	118.9		117.0	27.6
-1.0	-1.33	-64.0		-61.7	28.9
- .75	-1.0	-72.4	26.8	-70.1	26.9
- .50	- .67	-75.7	31.9	-76.5	31.4
- .25	- .33	-75.7	26.4	-76.5	28.0
0	0	-69.4	28.0	-68.4	28.9
.25	.33	-72.4	29.2	-70.2	27.4
.50	.67	-75.7	29.8	-76.5	28.6
.75	1.0	-71.8	27.8	-70.1	26.4
1.0	1.33	-64.0		-61.7	27.4
1.25	1.67	118.9		117.0	24.2
1.50	2.0	146.0	28.7	141.7	28.5
1.75	2.33	151.4	24.9	152.7	22.2
2.0	2.67	138.8	25.4	137.8	25.7
2.25	3.0	118.9	26.0	117.0	26.8
2.50	3.33	97.9	28.9	95.6	27.1
2.75	3.67	83.2		84.8	26.2
3.0	4.0	59.5		60.7	28.1

TABLE XX

Experimental Results, 1.5 Inch Diameter Disk, x/R = 3.0
(PATM: 29.86; TATM: 74° F; Jet Mach Number: 0.35; L/D: 40.1)

		WITHOUT PHASE MODULATOR		WITH PHASE MODULATOR	
Y	Y/R	U(fps)	η(%)	U(fps)	η(%)
-3.0	-4.0	49.0		49.3	26.0
-2.75	-3.67	59.5		60.9	24.6
-2.50	-3.33	83.3	26.9	82.9	25.9
-2.25	-3.0	104.1	27.0	108.2	24.2
-2.0	-2.67	118.9	24.1	115.4	25.5
-1.75	-2.33	128.1	24.3	130.3	25.7
-1.50	-2.0	118.9	25.1	117.0	26.3
-1.25	-1.67	104.1	26.8	108.2	27.7
-1.0	-1.33	-49.0		-50.2	26.7
- .75	-1.0	-55.5	24.2	-55.6	24.6
- .50	- .67	-55.5	26.2	-55.6	23.6
- .25	- .33	-55.5	25.7	-54.9	22.5
0	0	-46.2	19.2	-50.1	23.8
.25	.33	-55.5	25.5	-55.5	24.1
.50	.67	-55.5	26.4	-55.6	24.7
.75	1.0	-55.5	26.2	-55.6	24.5
1.0	1.33	-46.2		-45.3	
1.25	1.67	111.0	27.2	109.1	28.7
1.50	2.0	123.3	25.5	124.2	22.2
1.75	2.33	128.1	24.4	130.3	25.3
2.0	3.0	97.9	24.0	98.0	26.2
2.50	3.33	83.3	24.9	83.0	26.2
2.75	3.67	61.7		60.9	26.8
3.0	4.0	52.0		49.4	25.8

TABLE XXI

Experimental Results, 1.5 Inch Diameter Disk, x/R = 3.75
(PATM: 30.01; TATM: 73° F; Jet Mach Number: 0.35; L/D: 40.1)

		WITHOUT PHASE MODULATOR		WITH PHASE MODULATOR	
Y	Y/R	U(fps)	η(%)	U(fps)	η(%)
-3.0	-4.0	55.5	25.6	53.6	26.5
-2.75	-3.67	72.4	25.5	70.9	25.9
-2.50	-3.33	92.5	25.2	90.2	25.2
-2.25	-3.0	111.0	25.4	113.9	27.2
-2.0	-2.67	118.9	27.1	116.8	28.1
-1.75	-2.33	122.4	25.4	119.9	25.1
-1.50	-2.0	111.1	25.2	110.5	24.6
-1.25	-1.67	97.3		95.4	24.4
-1.0	-1.33				
- .75	-1.0				
- .50	- .67				
- .25	- .33				
0	0				
.25	.33				
.50	.67				
.75	1.0				
1.0	1.33				
1.25	1.67	97.9	25.4	95.4	20.7
1.50	2.0	111.0	26.3	113.8	26.5
1.75	2.33	124.3	28.0	123.2	27.6
2.0	2.67	120.7	26.4	117.0	26.5
2.25	3.0	111.0	26.5	110.9	26.8
2.50	3.33	92.5	24.4	89.9	24.4
2.75	3.67	69.4	25.3	70.7	24.0
3.0	4.0	55.5	25.0	54.6	25.6

TABLE XXII

Experimental Results, 1.5 Inch Diameter Disk, x/R = 5.5
(PATM: 29.95; TATM: 72° F; Jet Mach Number: 0.35; L/D: 40.1)

		WITHOUT PHASE MODULATOR		WITH PHASE MODULATOR	
Y	Y/R	U(fps)	η(%)	U(fps)	η(%)
-3.0	-4.0	55.5		54.6	
-2.75	-3.67	59.5	28.4	60.8	27.5
-2.50	-3.33	72.4	30.8	67.7	27.5
-2.25	-3.0	92.5	27.4	93.2	27.7
-2.0	-2.67	97.9	30.9	95.4	28.2
-1.75	-2.33	104.1	27.2	108.1	27.6
-1.50	-2.0	104.1	25.2	108.0	27.0
-1.25	-1.67	104.1	29.8	108.1	27.2
-1.0	-1.33	94.6	26.7	97.8	27.4
- .75	-1.0	87.6	27.0	88.9	28.1
- .50	- .67	83.3	25.9	84.7	26.3
- .25	- .33	75.7	30.3	75.4	28.0
0	0	69.4	26.2	68.7	29.1
.25	.33	75.7	25.4	75.4	26.1
.50	.67	83.3	26.4	82.5	24.5
.75	1.0	87.6	28.3	86.8	24.4
1.0	1.33	92.5	26.1	95.4	29.5
1.25	1.67	104.1	26.7	102.7	25.5
1.50	2.0	104.1	23.6	108.0	24.7
1.75	2.33	104.1	26.8	105.5	26.3
2.0	2.67	97.9	26.7	95.4	30.2
2.25	3.0	92.5	26.2	88.8	28.8
2.50	3.33	69.4	28.0	69.2	27.9
2.75	3.67	64.0	30.7	60.7	29.6
3.0	4.0	52.0		53.5	

TABLE XXIII

Experimental Results, 2.0 Inch Diameter Disk, x/R = .375
(PATM: 29.91; TATM: 73° F; Jet Mach Number: 0.35; L/D: 40.1)

		WITHOUT PHASE MODULATOR		WITH PHASE MODULATOR	
Y	Y/R	U(fps)	η(%)	U(fps)	η(%)
-3.0	-3.0	79.3	31.9	78.5	32.9
-2.75	-2.75	118.9	32.6	115.4	31.6
-2.50	-2.50	138.7	29.4	134.7	28.0
-2.25	-2.25	158.6	30.3	158.7	30.5
-2.0	-2.0	175.3	30.2	176.9	28.2
-1.75	-1.75	138.7		143.5	
-1.50	-1.50				
-1.25	-1.25				
-1.0	-1.0	-53.7	30.7	-50.1	31.8
- .85	- .85	-59.5	31.1	-60.4	31.7
- .75	- .75	-64.0	31.7	-63.3	31.4
- .50	- .50	-64.0	31.9	-62.8	31.2
- .25	- .25	-55.5	28.6	-54.5	31.2
0	0	-46.3	28.0	-47.0	29.3
.25	.25	-55.5	28.4	-54.5	30.1
.50	.50	-64.0	32.8	-63.8	29.3
.75	.75	-66.6	32.7	-62.9	29.5
.85	.85	-61.7	30.6	-60.5	33.5
1.0	1.0	-53.7	30.1	-52.5	31.1
1.25	1.25				
1.50	1.50				
1.75	1.75	138.7		143.4	
2.0	2.0	175.3	29.1	177.0	30.5
2.25	2.25	158.6	29.0	158.6	27.0
2.50	2.50	138.7	27.6	136.0	28.6
2.75	2.75	118.9	32.8	115.6	33.5
3.0	3.0	75.7	31.7	75.9	32.5

TABLE XXIV

Experimental Results, 2.0 Inch Diameter Disk, x/R = .75
(PATM: 29.86; TATM: 74° F; Jet Mach Number: 0.35; L/D: 40.1)

		WITHOUT PHASE MODULATOR		WITH PHASE MODULATOR	
Y	Y/R	U(fps)	η(%)	U(fps)	η(%)
-3.0	-3.0	87.6	30.1	86.9	28.1
-2.75	-2.75	118.9	32.6	122.1	28.2
-2.50	-2.50	134.3	30.6	134.8	26.9
-2.25	-2.25	158.6	27.6	258.7	27.7
-2.0	-2.0	166.5	28.7	168.5	28.5
-1.85	-1.85	49.0		47.6	
-1.75	-1.75				
-1.50	-1.50				
-1.25	-1.25	-64.0	33.8	-64.7	30.3
-1.0	-1.0	-69.4	30.5	-67.6	30.7
- .75	- .75	-75.7	28.5	-75.0	29.1
- .50	- .50	-77.4	30.0	-79.4	29.5
- .25	- .25	-75.7	27.1	-76.7	26.8
0	0	-69.4	25.0	-70.2	23.3
.25	.25	-75.7	26.7	-75.3	27.5
.50	.50	-77.4	29.7	-78.1	28.6
.75	.75	-75.6	31.8	-77.9	28.9
1.0	1.0	-69.4	33.1	-70.3	29.9
1.25	1.25	-64.0	30.9	-62.0	32.6
1.50	1.50	-26.0		-28.7	
1.75	1.75				
2.0	2.0	166.5	28.1	167.9	27.6
2.25	2.25	158.6	26.6	160.8	27.7
2.50	2.50	138.7	28.4	136.8	31.0
2.75	2.75	118.9	31.4	122.8	29.3
3.0	3.0	83.2	31.2	87.6	30.9

AD-A082 167 AIR FORCE INST OF TECH WRIGHT-PATTERSON AFB OH SCHOO--ETC F/G 20/4
A DIAGNOSTIC STUDY OF FLOW IN THE WAKE OF A CIRCULAR DISK USING--ETC(U)
MAR 80 S L MORRIS
UNCLASSIFIED AFIT/GAE/AA/79D-12 NL

3 OF 3

END
DATE FILMED
4-80
DTIC

TABLE XXVI

Experimental Results, 2.0 Inch Diameter Disk, x/R = 2.25
(PATM: 29.86; TATM: 71° F; Jet Mach Number: 0.35; L/D: 40.1)

		WITHOUT PHASE MODULATOR		WITH PHASE MODULATOR	
Y	Y/R	U(fps)	η(%)	U(fps)	η(%)
-3.25	-3.25	104.1	28.4	102.3	30.0
-3.0	-3.0	111.0	27.1	115.0	28.8
-2.75	-2.75	128.1	29.6	128.2	30.8
-2.50	-2.50	144.8	25.4	142.0	26.4
-2.35	-2.35	151.4	28.7	146.2	27.8
-2.25	-2.25	151.4	27.3	149.4	24.2
-2.15	-2.15	128.1	30.2	128.1	28.6
-2.0	-2.0				
-1.75	-1.75				
-1.50	-1.50				
-1.25	-1.25				
-1.15	-1.15	-66.6	30.0	-65.6	30.8
-1.0	-1.0	-70.8	30.8	-66.6	28.6
- .75	- .75	-75.7	29.1	-75.8	27.1
- .50	- .50	-75.7	28.5	-75.4	26.8
- .25	- .25	-72.4	31.0	-70.5	27.8
0	0	-69.4	27.5	-66.1	28.1
.25	.25	-72.4	30.6	-70.6	29.1
.50	.50	-77.4	29.8	-75.4	31.3
.75	.75	-75.7	32.4	-75.4	30.6
1.0	1.0	-72.4	28.1	-70.5	29.1
1.15	1.15	-66.6	31.1	-66.2	33.8
1.25	1.25				
1.50	1.50				
1.75	1.75				
2.0	2.0				
2.15	2.15	128.1	26.0	128.1	28.8

TABLE XXVI (continued)

Y	Y/R	WITHOUT PHASE MODULATOR U(fps)	WITHOUT PHASE MODULATOR η(%)	WITH PHASE MODULATOR U(fps)	WITH PHASE MODULATOR η(%)
2.25	2.25	151.4	25.8	149.9	24.7
2.35	2.35	151.4	24.9	147.2	22.4
2.50	2.50	144.7	23.7	141.9	23.1
2.75	2.75	128.1	30.5	128.1	29.0
3.0	3.0	111.0	29.9	111.4	27.6
3.25	3.25	104.0	26.4	206.6	27.3

TABLE XXVII

Experimental Results, 2.0 Inch Diameter Disk, x/R = 3.0
(PATM: 29.96; TATM: 71° F; Jet Mach Number: 0.35; L/D: 40.1)

		WITHOUT PHASE MODULATOR		WITH PHASE MODULATOR	
Y	Y/R	U(fps)	η(%)	U(fps)	η(%)
-3.25	-3.25	104.1	24.3	104.8	25.0
-3.0	-3.0	111.0	24.5	111.4	23.7
-2.75	-2.75	118.9	24.3	122.0	22.7
-2.50	-2.50	128.1	25.2	128.1	24.8
-2.25	-2.25	118.9	25.1	122.1	24.7
-2.0	-2.0	111.0	27.5	112.2	28.6
-1.75	-1.75				
-1.50	-1.50				
-1.25	-1.25	-49.0	26.0	-52.2	24.6
-1.0	-1.0	-53.7	23.6	-55.0	21.4
- .75	- .75	-55.5	24.4	-55.3	22.2
- .50	- .50	-57.4	23.9	-58.3	20.5
- .25	- .25	-52.0	22.9	-52.2	19.7
0	0	-46.2	21.5	-46.7	20.5
.25	.25	-49.0	20.6	-52.2	19.5
.50	.50	-55.5	23.4	-55.3	26.1
.75	.75	-55.5	24.4	-55.2	22.9
1.0	1.0	-55.5	23.7	-55.3	21.8
1.25	1.25	-49.0	25.7	-50.0	24.7
1.50	1.50				
1.75	1.75				
2.0	2.0	111.0	27.7	112.3	28.3
2.25	2.25	118.9	25.5	121.6	26.5
2.50	2.50	128.1	23.4	129.3	22.4
2.75	2.75	118.9	23.0	122.0	23.3
3.0	3.0	111.0	25.1	110.6	23.2
3.25	3.25	104.1	25.7	102.1	23.5

TABLE XXVIII

Experimental Results, 2.0 Inch Diameter Disk, x/R = 3.75
(PATM: 30.0; TATM: 74° F; Jet Mach Number: 0.35; L/D: 40.1)

		WITHOUT PHASE MODULATOR		WITH PHASE MODULATOR	
Y	Y/R	U(fps)	η(%)	U(fps)	η(%)
-3.25	-3.25	111.0	27.5	111.4	25.7
-3.0	-3.0	114.8	25.9	122.0	25.4
-2.75	-2.75	118.9	24.8	122.0	22.7
-2.50	-2.50	123.3	21.5	126.8	19.7
-2.25	-2.25	118.9	19.8	122.0	19.0
-2.0	-2.0	111.0	22.7	111.3	21.2
-1.75	-1.75				
-1.50	-1.50				
-1.25	-1.25				
-1.0	-1.0				
- .75	- .75				
- .50	- .50				
- .25	- .25				
0	0				
.25	.25				
.50	.50				
.75	.75				
1.0	1.0				
1.25	1.25				
1.50	1.50				
1.75	1.75				
2.0	2.0	111.0	21.1	111.3	19.5
2.25	2.25	118.9	20.7	122.0	18.9
2.50	2.50	120.7	23.2	121.2	22.6
2.75	2.75	118.9	23.7	122.0	24.5
3.0	3.0	117.3	27.2	122.0	28.4
3.25	3.25	111.0	28.4	111.3	27.0

TABLE XXIX

Experimental Results, 2.0 Inch Diameter Disk, x/R = 5.5
(PATM: 29.96; TATM: 72° F; Jet Mach Number: 0.35; L/D: 40.1)

		WITHOUT PHASE MODULATOR		WITH PHASE MODULATOR	
Y	Y/R	U(fps)	η(%)	U(fps)	η(%)
-3.0	-3.0	69.4		70.6	31.3
-2.75	-2.75	83.3	31.5	83.8	28.1
-2.50	-2.50	87.6	27.4	87.0	28.8
-2.25	-2.25	92.5	28.2	95.4	28.5
-2.0	-2.0	92.5	31.7	95.4	30.9
-1.75	-1.75	88.6	32.2	87.0	30.6
-1.50	-1.50	83.3	29.3	85.4	27.3
-1.25	-1.25	79.3	32.2	80.1	29.5
-1.0	-1.0	75.7	27.2	75.4	28.1
- .75	- .75	69.4	26.7	66.2	30.6
- .50	- .50	64.0	31.5	62.2	30.1
- .25	- .25	59.5	28.3	58.6	26.2
0	0	55.5	27.8	55.3	28.4
.25	.25	61.7	29.1	58.5	30.6
.50	.50	64.0	27.5	62.2	27.3
.75	.75	69.4	30.2	66.2	28.4
1.0	1.0	75.7	26.9	75.4	27.2
1.25	1.25	78.5	30.0	77.5	30.2
1.50	1.50	83.3	29.8	85.3	30.3
1.75	1.75	92.5	28.3	88.4	28.8
2.0	2.0	92.5	27.7	95.4	28.2
2.25	2.25	92.5	29.7	93.2	31.9
2.50	2.50	87.6	26.9	86.9	28.6
2.75	2.75	83.3	30.3	84.5	28.7
3.0	3.0	75.7		75.4	30.2

VITA

Captain Steven L. Morris was born in Dallas, Texas, in 1952. Upon graduation from high school in the Spring of 1971, he applied, and was subsequently accepted, to attend the United States Air Force Academy in Colorado Springs, Colorado. In the Spring of 1975, he graduated with a Bachelor's Degree in Engineering Sciences. Following graduation, he was stationed at Holloman Air Force Base, Alamogordo, New Mexico, where for the next two years he held the position of Group Test Engineer at the High Speed Test Track. In June of 1978, he entered the Graduate Aeronautical Engineering Program at the Air Force Institute of Technology.

Permanent Address: Route 1, Box 103
Trinidad, Texas 75163

This thesis was typed by Dee Babiarz.

UNCLASSIFIED

SECURITY CLASSIFICATION OF THIS PAGE (When Data Entered)

REPORT DOCUMENTATION PAGE		READ INSTRUCTIONS BEFORE COMPLETING FORM
1. REPORT NUMBER AFIT/GAE/AA/79D-12	2. GOVT ACCESSION NO.	3. RECIPIENT'S CATALOG NUMBER
4. TITLE (and Subtitle) A DIAGNOSTIC STUDY OF FLOW IN THE WAKE OF A CIRCULAR DISK USING A PHOTON CORRELATION LASER VELOCIMETER SYSTEM		5. TYPE OF REPORT & PERIOD COVERED MS Thesis 6. PERFORMING ORG. REPORT NUMBER
7. AUTHOR(s) Steven L. Morris Captain, USAF		8. CONTRACT OR GRANT NUMBER(s)
9. PERFORMING ORGANIZATION NAME AND ADDRESS Air Force Institute of Technology (AFIT/EN) Wright-Patterson AFB OH 45433		10. PROGRAM ELEMENT, PROJECT, TASK AREA & WORK UNIT NUMBERS
11. CONTROLLING OFFICE NAME AND ADDRESS		12. REPORT DATE March 1980 13. NUMBER OF PAGES 185
14. MONITORING AGENCY NAME & ADDRESS(if different from Controlling Office)		15. SECURITY CLASS. (of this report) Unclassified 15a. DECLASSIFICATION DOWNGRADING SCHEDULE

16. DISTRIBUTION STATEMENT (of this Report)

Approved for public release; distribution unlimited

17. DISTRIBUTION STATEMENT (of the abstract entered in Block 20, if different from Report)
Approved for public release IAW AFR 190-17

JOSEPH P. HIPPS, Major, USAF
Director of Public Affairs

18. SUPPLEMENTARY NOTES

19. KEY WORDS (Continue on reverse side if necessary and identify by block number)

Laser Velocimeter
Schlieren System
Mean Velocity
Turbulence Intensity
Circular Disk
Free Jet
Recirculation Zone
Reversed Flow Region

20. ABSTRACT (Continue on reverse side if necessary and identify by block number)

The present investigation involves a diagnostic study of flow in the wake of a circular disk utilizing schlieren photography and a photon correlation laser velocimeter system (LDV). The schlieren system was used to examine the basic flow pattern over a 2.0 inch diameter disk and to establish the bounds of the recirculation zone. In all tests, the flow originated from a 1.5 inch diameter axially symmetric free jet with an exit Mach number of 0.35. The disk was

DD FORM 1 JAN 73 1473 EDITION OF 1 NOV 65 IS OBSOLETE

UNCLASSIFIED

SECURITY CLASSIFICATION OF THIS PAGE (When Data Entered)

positioned in the flow 12 jet diameters downstream of the exit. Mean velocity and turbulence intensity profiles were measured at selected locations in the near wake region of the 2.0 and a 1.5 inch diameter disk with the LDV system. This was accomplished without particle seeding of the flow. A free jet survey was conducted for comparison with theoretical predictions to analyze the quality of the LDV data.

The schlieren system produced high quality photographs from which the dimensions of the recirculation zone were obtained. Mean velocity and turbulence intensity profiles were acquired at the varied stream-wise locations behind each disk with the LDV system. The laser velocimeter system, when used in conjunction with a phase modulator, clearly identified the flow direction. Bounds of the recirculation zone found from the LDV study agreed with the results of the schlieren study.